Performance Analysis of Network Coding Techniques and Resource Allocation Algorithms in Multiuser Wireless Systems

Yue Yan

Thesis submitted to the Faculty of the
Virginia Polytechnic Institute and State University
in partial fulfillment of the requirements for the degree of

Master of Science
in
Electrical Engineering

Claudio R. C. M. da Silva, Chair
Jeffrey H. Reed
Steven W. Ellingson

September 9, 2011
Blacksburg, Virginia

Keywords: Network coding, cognitive radio, resource allocation, channel estimation, time synchronization

Performance Analysis of Network Coding Techniques and Resource Allocation Algorithms in Multiuser Wireless Systems

Yue Yan

ABSTRACT

The following thesis consists of two main contributions to the fields of network coding and resource allocation.

The first is a quantitative analysis of the effects of channel estimation errors and time synchronization errors on the performance of different network coding algorithms. It is shown that the performance improvement gained by a relay-based network scheme is significant for small number of users and when the quality of the relay link is better than that of the direct link. However, it is shown that potential performance improvement resulting from the considered relay-based network coding scheme could be negated by channel estimation errors. To consider the effects of time synchronization errors, we study a digital network coding (DNC) system and a physical-layer network coding (PNC) system with non-coherent frequency shift keying (FSK) modulation. For each of these two systems, we investigate the effects of received E_b/N_0, unequal link quality, and time synchronization errors.

The second contribution is an analysis of the value and cost of cognition obtained by investigating three resource allocation algorithms with different levels of channel knowledge in the context of ad hoc networks. The performance (quantified in terms of "percentage of users reaching target data rate" and "average effective data rate") and cost ("power consumption" and "number of channel estimations") of these algorithms are analyzed. Results show that a resource allocation algorithm with a higher level of channel knowledge results in better performance, but greater cost in terms of number of channel estimations, as expected. In addition, a resource allocation algorithm with a higher level of channel knowledge converges quicker when channel adaptation are necessary. Both an ideal medium access control (MAC) protocol and a non-ideal MAC protocol (dedicated control channel) are considered.

Acknowledgments

First and foremost, my sincere appreciation goes to my academic advisor, Dr. Claudio da Silva for his professional guidance and advice throughout my study in Virginia Tech. I also would like to thank Dr. Jeffrey H. Reed and Dr. Steven W. Ellingson for serving on my committee and giving me suggestions.

Many a times, my conversation with my fellow researchers had been insightful in the methodology of research and furthering my knowledge of wireless communication. Many thanks go to William C. Headley, Daniel Jakubisin, Gautham Chavali, Qing Yang, An He, Xuetao Chen, Ying Wang, Bei Xie and Qian Liu for their time and helpful suggestions. I am grateful towards all my fellow researchers and the staff of the department of Electrical and Computer Engineering for making my stay at Virginia Tech a memorable one. Part of this work was supported by DISA. I wish to thank them for their support.

Finally, I want to thank my parents for their constant love, support and confidence in me.

Contents

List of Figures

List of Tables

Chapter 1

Introduction

This research is concerned with the effects of channel estimation errors and time synchronization errors on the performance of different network coding schemes and with the value and cost of cognition in the context of resource allocation for cognitive radio (CR) based ad hoc networks.

In the first part of this work, the performance of network coding schemes is considered. Network coding offers a new perspective on how to handle information from one user passing through other intermediate users to the destination in a network [1]-[10]. In traditional wireless communication networks, the collision of packets, which would introduce interference, is regarded as a harmful factor. Interference is usually avoided by careful receiver design and orthogonal transmission. On the other hand, network coding regards the interference as a capacity-boosting factor [1]. The main idea is that information, instead of packets, is transmitted through the communication link. This means that the packets can be allowed to conflict, as long as the information can be extracted at the destination. For this reason, network coding saves transmission time since it allows simultaneous non-orthogonal transmissions.

Although much work has been done on relay-based network coding schemes (see, among

others, [8], [9], and reference therein), to the best of the author's knowledge, the effect of channel estimation errors in a decode-and-forward relay-based network coding system with different numbers of users has not been discussed yet. In this work, the maximum likelihood detector for a decode-and-forward relay-based network coding system is derived for different numbers of users. Then the effects of imperfect channel estimation on the bit error rate (BER) performance are examined. It is shown that the gain provided by the proposed network coding scheme is significant for small number of users and when the quality of the relay link is better than that of the direct link, as expected. However, it is shown that potential performance improvement resulting from the proposed network coding scheme could be negated by channel estimation errors.

Although some work has been done on time synchronization errors in network coding schemes with BPSK and QPSK [11]-[13], the effects of time synchronization errors in a physical-layer network coding (PNC) system and digital network coding (DNC) system with FSK modulation has not been investigated yet. For this reason, the effect of timing errors on the BER performance in a DNC system with non-coherent FSK signals is analyzed in this work. Using this analysis as a benchmark, we also investigate the effect of timing errors on the BER performance in a PNC system with an optimal receiver for non-coherent FSK signals. The effect of various system parameters (received Eb/No and unequal link quality) on the BER performance of the two systems is considered, with particular emphasis on the effects of time synchronization errors.

In the second part of the work, the value and cost of cognition of three resource allocation algorithms with different levels of channel knowledge in a CR-based ad hoc network are investigated. CR is a radio that is aware of the spectrum environment, can learn about its environment, and adjust its transmission parameters for "highly reliable transmission and efficient utilization of the radio spectrum" [14]. Distributed resource allocation algorithms are considered due to the lack of infrastructure of ad hoc networks. In our work, we investigate the value and cost of cognition by studying resource allocation algorithms with different levels of channel knowledge. Three resource allocation algorithms are proposed, and the

trade-off between performance gain and cost is investigated. Both an ideal medium access control (MAC) protocol and a non-ideal MAC protocol (dedicated control channel [15]) are considered.

1.1 Previous Work

1.1.1 Network Coding

Network coding offers a new perspective on dealing with information passing through intermediate nodes in a network. Consider a network with several source nodes, destination nodes, and intermediate nodes. When the direct path between a source node and its destination is unavailable or lossy, the source node hands its packet(s) to a chain of intermediate nodes, where each intermediate node forwards the packet(s) to either another intermediate node or the destination. Typically, intermediate nodes store the packets and transmit copies. For all the packets an intermediate node receives (possibly from several different sources), the intermediate node will typically transmit them one by one, and there is no data processing of the packets by the intermediate node (except for possible error detection and correction).

In the case of network coding, intermediate nodes combine several packets together by coding, bringing potential throughput improvements to the network [1]. Ahlswede, Ning, Li, and Yeung proved that network coding achieves the max-flow min-cut[1] capacity in multicast systems and thus demonstrated the advantage of network coding over traditional store-and-forward transmission [1]. It has also been proved that linear network coding, in which an

[1]As discussed in [16], a flow network is a directed graph $G = (V, E)$, where V is the set of nodes and E is the set of edges. Each edge has a non-negative capacity and each edge carries a flow (a flow could be a transmitted signal in a wireless network, for example). The amount of flow on an edge cannot exceed its capacity. In optimization theory, the max-flow min-cut theorem states that in a flow network, the maximum amount of flow passing from the source to the destination is equal to the capacity of a minimum cut. A cut "...divides the nodes of the graph into two sets, A and B..." [16], where the source node is in A and the destination node is in B. A minimum cut is a cut with minimum capacity. The capacity of a cut is the sum of the capacity of a cut-set, which is a set of edges, and each edge in the cut-set has its two end points in A and B, individually.

output packet is a weighted sum of the input packets, is enough to achieve the max-flow min-cut capacity for a multicast problem [2]. It has been shown that when using linear network coding, as long as the receiver gets enough independent combined packets and knows the encoding matrix, each individual packet can be successfully decoded by solving a set of equations [3]-[5]. As a final example of fundamental results on network coding, random network coding [3], in which intermediate network nodes independently and randomly choose code coefficients to perform linear mapping from inputs to outputs, was shown to achieve the max-flow min-cut capacity "with probability exponentially approaching 1 with the code length" [5].

1.1.2 Network Coding in Wireless Communication

The performance improvement of network coding in wired networks is often very limited. As mentioned by Liu, Goeckel and Towsley, "for networks with bidirectional links that can be modeled as an arbitrary undirected graph, ... the throughput improvement is upper bounded by a factor of two for the single source multicast case, and upper bounded by one (no benefit) for the single source unicast or broadcast case. In addition, it is thought that there is no throughput benefit for the multi-pair unicast case..." [17]. For this reason, most research on network coding focuses on wireless networks. In wireless systems, a transmitted signal may reach several nodes and a node may receive several signals simultaneously. The fact that several signals would reach a node at the same time would cause multiple access interference, which, at least in principle, is harmful to the system performance. Traditionally, wireless networks avoid or reduce this interference by transmission scheduling and receiver design. Network coding can be applied to this situation to turn the broadcast nature of wireless networks to an advantage. Rather than avoiding interference, network coding manages the interference strategically at the physical layer to increase network capacity.

DNC [10], PNC [6] and analog network coding (ANC) [7] are the three main kinds of network coding schemes. For ease of presentation, a two-way exchange channel [6], [18], [19] is used

to illustrate these network coding schemes. In this model, two nodes (S_1 and S_2) exchange their information (x_1 and x_2, and x_1, $x_2 \in \{0, 1\}$) through a intervening relay node R, as shown in Fig. 1.1. These three nodes are half-duplex, which means they either transmit or receive at any given time.

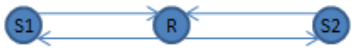

Figure 1.1: A two-way exchange channel. S_1 and S_2 are two source nodes which are out of reachable transmission range with each other. These two nodes exchange their information with the help of the relay node R.

If no network coding is used, four time slots are required to complete the transmission as indicated in Table 1.1. In the first time slot, S_1 transmits x_1 to R. In the second time slot, R forwards $\hat{x}_1$ to S_2, where $\hat{x}_1$ is an estimate of x_1. In the third time slot, S_2 transmits x_2 to R. In the fourth time slot, R forwards $\hat{x}_2$ to S_1, where $\hat{x}_2$ is an estimate of x_2.

Table 1.1 shows that the total transmission time can be reduced by means of network coding. In DNC schemes, senders transmit in sequence, and routers broadcast the mixed version of the signals. That is, in the first time slot, S_1 transmits x_1 to R. In the second time slot, S_2 transmits x_2 to R. Finally in the third time slot, R transmits $x_R = XOR(\hat{x}_1, \hat{x}_2)$ to S_1 and S_2, where XOR is the exclusive-or function. When S_1 receives $\hat{x}_R$, which is an estimate of x_R, it can extract x_2 from x_R because it knows x_1. The estimated $\tilde{x}_2$ at S_1 is equal to $XOR(x_1, \hat{x}_R)$. An equivalent procedure is used by S_2 to decode x_1. Since it takes three time slots to complete the transmission for DNC, it has a time saving of 25% compared to the transmission time, which is four time slots, of no network coding transmission scheme.

The total transmission time can be further reduced by allowing concurrent transmissions of senders, as is the case in PNC and ANC.

PNC schemes use "...demodulation-mapping and the corresponding modulation-mapping criteria, respectively, to decode and re-generate signal for the relay nodes, such that each terminal can obtain the information for itself by some nonlinear operation..." [20]. In this scheme, S_1 and S_2 transmit x_1 and x_2 to R in the first time slot. Suppose the modulated

Table 1.1: Transmission time scheduling with or without network coding (DNC/PNC/ANC) in a two-way exchange channel.

Scheme	*1st time slot*	*2nd time slot*	*3rd time slot*	*4th time slot*
No network coding	S_1 transmit	R transmit	S_2 transmit	R transmit
DNC	S_1 transmit	S_2 transmit	R transmit	N/A
PNC	S_1,S_2 transmit	R transmit	N/A	N/A
ANC	S_1,S_2 transmit	R transmit	N/A	N/A

signals from S_1 and S_2 are $X_1(t)$ and $X_2(t)$ respectively, where $X_1(t)$ and $X_2(t)$ use the same modulation scheme. R receives the sum of the two signals, which is $Y_R(t) = hX_1(t)+gX_2(t)+n_R(t)$. The parameters h and g are the channel gains between S_1 and R and between S_2 and R, respectively, and $n_R(t)$ is a noise process. x_R is decoded at R based on the received signal $Y_R(t)$, where x_R is an estimate of $XOR(x_1, x_2)$[2]. In the second time slot, R transmits $X_R(t)$ to S_1 and S_2, where $X_R(t)$ is the modulated signal of x_R. When S_1 receives $hX_R(t) + n_1(t)$, where $n_1(t)$ is a noise process, it estimates x_2 based on the knowledge of x_1. The estimated x_2 is equal to $XOR(x_1, \hat{x}_R)$, where $\hat{x_R}$ is the estimated x_R decoded from $hX_R(t) + n_1(t)$. An equivalent procedure is used by S_2.

In ANC schemes, "...relay nodes do some linear operations to the received mixed analog signals from both terminals and then broadcast them back to the terminals. Each terminal node can subtract the backward self-interference signal from itself and obtain the signal from the other one..." [20]. In this scheme, S_1 and S_2 transmit x_1 and x_2 to R in the first time slot. R receives the sum of two signals $X_1(t)$ and $X_2(t)$, which is $Y_R(t) = hX_1(t)+gX_2(t)+n_R(t)$, where h, g and $n_R(t)$ are the same as defined in PNC schemes. In the second time slot, R forwards $X'_R(t)$ to S_1 and S_2, where $X'_R(t)$ is the algebraic sum of the analog signals, and $X'_R(t) = Y_R(t)$. In ANC schemes, no decoding and encoding are performed at R. When S_1 receives $hY_R(t) + n_1(t)$, it subtracts the signal it has initially transmitted. Then the estimated x_2 is obtained from $hY_R(t) + n_1(t) - h^2X_1(t) = hgX_2(t) + hn_R(t) + n_1(t)$ at S_1.

[2]Readers interested in more details on the receiver design and deriving decision rules are referred to Chapter 3 and [6].

Therefore, an additional noise component $hn_R(t)$ is introduced in the received information at S_1 compared with PNC. An equivalent procedure is used by S_2. The transmission of PNC and ANC completes within two time slots, with a time saving of 50% compared to no network coding transmission scheme and saves 33% compared to DNC. The ANC scheme is not considered in this thesis.

In the previously discussed network coding schemes, only one pair of users is considered and it is assumed that the two nodes are out of the reachable transmission range of each other. However, network coding can also be applied to a relay-based network where there is direct link between a source node and a destination node (see, among others, [8], [9], and reference therein). Although some work has been done on relay-based network coding schemes, to the best of the author's knowledge, the effect of imperfect channel estimation in a decode-and-forward relay-based network coding system with different numbers of users has not been discussed yet. In Chapter 2, we describe the transmission scheme and derive the optimal decision rule of a maximum-likelihood detector for multiple users. Note that for one pair of users, Gacanin and Adachi presented the BER performance of imperfect channel estimation with a amplify-and-forward relay node [21]. In addition, Yasami and Abedi presented the throughput analysis of a PNC system with channel estimation error for one pair of users [22]. The effect of imperfect channel estimation in a decode-and-forward relay-based network coding system with different numbers of users is analyzed in Chapter 2. The effect of unequal link quality is also considered.

When PNC was first proposed, both perfect symbol-level time synchronization and perfect phase estimation were assumed [6]. The effects of phase estimation error and time synchronization error in a PNC system of BPSK and QPSK modulated signals were first investigated in [11], and the robustness of PNC with BPSK and QPSK modulation to these errors was studied in [11]. In addition, for asynchronous PNC with BPSK and QPSK signals, the effects of symbol misalignment were analyzed in [12], [13]. However, these papers have only considered BPSK and QPSK. The effects of phase estimation errors and time synchronization errors in a PNC system with FSK modulation has not been investigated yet.

Non-coherent detection is considered in this work because "...the phase tracking required for coherent detection is impractical..." [23] in DNC and PNC systems. Current work focusing on network coding systems with non-coherent FSK signals includes [7], [23]-[26]. Also, non-coherent relay decoders for MSK systems using analog network coding (ANC) were proposed in [7], [24]. Non-coherent receivers for CPFSK in DNC and PNC systems were proposed in [25], [26]. Reference [23] addressed the decision region of a relay receiver in a PNC system with BFSK modulation. However, none of these papers discussed the effect of time synchronization error in a PNC system with FSK modulation. The analysis of the effects of time synchronization error of non-coherent FSK signals in DNC and PNC systems is a contribution of this work.

1.1.3 Resource Allocation Algorithms in OFDMA CR-based ad hoc Networks

CR is a radio that is aware of the spectrum environment, can learn from its environment, and adjust its transmission parameters for reliable transmission and efficient utilization of the radio spectrum [14]. The term "cognitive radio" was first introduced by Mitola in 1999 [27]. For a comprehensive review of the history of CR, the reader is referred to [28] and [14]. When used in an opportunistic/dynamic spectrum access scenario [29], CRs are able to "...determine which portions of the spectrum are available and detect the presence of licensed users when a user operates in a licensed band", "...select the best available channel", "...coordinate access to this channel with other users", and "...vacate the channel when a licensed user is detected" [30]. As a cognitive radio has the capability to select the best available channels, the next challenge is to efficiently allocate resources. In this work, we are interested in the value and cost of cognition of different resource allocation algorithms.

In this thesis, we consider distributed resource allocation for CR-based ad hoc networks. A survey on distributed resource allocation algorithms suitable for ad hoc networks is provided in [31]. In this scenario, given the variety of spectrum opportunities with different bandwidth

and channel states, CRs first select channels and then perform power allocation. CRs select transmission channels by using a "pricing" function, which can be the channel "quality" (quantified in terms of signal-to-noise-plus-interference-ratio) [32]-[34], interference temperature [35]-[37], or some other pricing factor [38]-[40]. After the channels are selected, power is allocated with the goal of meeting the SINR requirement while minimizing interference to possible PUs. In [41], a distributed algorithm was proposed for allocating power and bits in multiuser OFDM-based wireless systems. Grace, Tozer, and Burr proposed that each link increase its power by using a function of the ratio of its initial observed interference and some predetermined interference threshold [35]. The subcarriers are allowed to be simultaneously shared by multiple users, and both the iterative water-filling algorithm and equal power allocation are considered. With a waterfilling power allocation algorithm [42]-[45], more power is allocated to better channels with low noise levels, so that the sum of data rates in channels is maximized [46]. It is shown in [47] that a water-filling algorithm can reach the optimal allocation of power for a single user with a fixed allocation of subcarriers.

1.2 Outline

In Chapter 2, a network coding system based on a decode-and-forward relay is proposed. Specifically, the BER performance of a relay-based network coding system with perfect and imperfect channel estimation is studied for different numbers of users. We found that potential performance improvement resulting from the proposed network coding scheme could be negated by increasing number of users, poor relay link quality, and the effect of channel estimation errors.

In Chapter 3, we first derive the theoretical BER of a DNC system with an optimal non-coherent receiver for FSK modulated signals. The BER performance of a PNC system with an optimal non-coherent receiver for FSK signals is also studied via simulation. For each of these systems, we investigate the effects of received E_b/N_0, unequal link quality, and time

synchronization errors on the system performance.

In Chapter 4, the value and cost of cognition of three different resource allocation algorithms is investigated in the context of ad hoc networks. The performance (quantified in terms of "percentage of users reaching target data rate" and "average effective data rate") and cost ("power consumption" and "number of channel estimations") of these algorithms are analyzed. Results show that a resource allocation algorithm with a higher level of channel knowledge results in better performance gain and fewer channel adaptations, but greater cost in terms of number of channel estimations. Further, a resource allocation algorithm with a higher level of channel knowledge converges quicker when channel adaptations are necessary. Both an ideal MAC protocol and a non-ideal MAC protocol (DCC) are considered.

Finally, conclusions are drawn in Chapter 5.

Chapter 2

Performance Analysis of Relay-based Network Coding with Perfect and Imperfect Channel Estimation

2.1 Introduction

This chapter is concerned with the performance of a relay-based network coding scheme with perfect and imperfect channel estimation. Although much work has been done on relay-based network coding schemes (see, among others, [8], [9], and reference therein), to the best of the author's knowledge, the effect of imperfect channel estimation in such schemes has not been discussed yet. Note that for one pair of users, Gacanin and Adachi presented the BER performance of imperfect channel estimation in [21] by assuming a amplify-and-forward relay scheme. In addition, Yasami and Abedi presented a throughput analysis of a PNC system with channel estimation error for one pair of users [22]. In this chapter, the considered network coding scheme is investigated for different numbers of users. More specifically, we first present the transmission scheme and then derive the optimal decision

rule of a maximum-likelihood detector. In addition, the effects of channel estimation errors and unequal link quality of the direct and relay links are studied. It is shown that the relay link contributes less when the number of users increases, and therefore the BER performance of the considered network coding scheme approaches that of the direct link as the number of users increases (in the absence of channel estimation errors).

This chapter is organized as follows. The system model is described in Section 2.2. In Section 2.3, the maximum-likelihood detector for the proposed network coding scheme with perfect channel knowledge is derived. In Section 2.4, the performance of the proposed network coding scheme with imperfect channel knowledge is investigated. Simulation results are discussed in Section 2.5. Finally, conclusions are provided in Section 2.6.

2.2 System Model

A three-node model with only one source node S, one destination node D, and one relay node R is shown in Fig. 2.1(a). Fig. 2.1(b) illustrates a two-user network coding model with two source nodes S_1 and S_2, two destination nodes D_1 and D_2, and one relay node R. When there are M users in the system, the system model is shown in Fig. 2.1(c). The source nodes are denoted by $S_1, S_2...S_M$; the destination nodes are denoted by $D_1, D_2...D_M$; and the relay node is denoted by R.

The transmission consists of two phases: in the first one, in a time multiplexed manner, the source nodes broadcast their information to the destination nodes and the relay node; in the second phase, the relay node forwards the coded information to the destination nodes. Maximum-likelihood detection [48] is employed at the relay and at the destination.

The transmitted signal $s(t)$ by a source node or the relay node is written as

$$s(t) = \sum_{k=-\infty}^{\infty} d[k]\sqrt{2E_b}p(t - kT)cos(w_c t) \tag{2.1}$$

where w_c is the carrier angular frequency in rad/s, $d[k] \in \{-1, 1\}$ is the binary data, T is the symbol duration, E_b is symbol energy, and $p(t)$ is the real-valued pulse shape with unit power, which satisfies the Nyquist ISI criterion.

The received signal $r(t)$ at the relay node or any destination node (in both phase one and phase two), is given by

$$r(t) = h\ s(t) + n(t) \tag{2.2}$$

where h is the channel gain, assumed to be time-invariant. Perfect phase and time estimation is assumed. In (2.2), $n(t)$ is the noise component, which is taken to be a zero-mean Gaussian random process with two-sided spectral density $\frac{N_0}{2}$ W/Hz.

After downconverting and passing the resulting signal through a synchronous conventional *correlation receiver*, the output $y(n)$ is the signal sampled at the time instance $nT + T$ (ignoring double frequency components), which is given by

$$\begin{aligned}
&y(n) = \textstyle\int_{-\infty}^{\infty} r(t)cos(w_c t)f(t - nT)dt \\
&= \textstyle\int_{-\infty}^{\infty} (h\ s(t) + n(t))\, cos(w_c t)f(t - nT)dt \\
&= \textstyle\int_{-\infty}^{\infty} h\ s(t)cos(w_c t)\sqrt{2E_b}p(t - nT)dt + \int_{-\infty}^{\infty} n(t)cos(w_c t)f(t - nT)dt \\
&= \textstyle\int_{-\infty}^{\infty} h\left(\sum_{k=-\infty}^{\infty} d[k](\sqrt{2E_b})^2 p(t - kT)p(t - nT)cos^2(w_c t)\right) dt \\
&+ \textstyle\int_{-\infty}^{\infty} n(t)cos(w_c t)f(t - nT)dt \\
&= hE_b \textstyle\sum_{k=-\infty}^{\infty} d[k]\left(\int_{-\infty}^{\infty} p(t - kT)p(t - nT)dt\right) + \int_{-\infty}^{\infty} n(t)cos(w_c t)f(t - nT)dt \\
&= hE_b d[n]\left(\textstyle\int_{-\infty}^{\infty} p(t - nT)p(t - nT)dt\right) + \int_{-\infty}^{\infty} n(t)cos(w_c t)f(t - nT)dt \\
&= hE_b d[n] + N,
\end{aligned} \tag{2.3}$$

where $N = \int_{-\infty}^{\infty} n(t)cos(w_c t)f(nT - t)dt$ and $f(t) = \sqrt{\frac{2E_b}{T}}p(t)$. N is a zero mean Gaussian random variable with variance $\frac{E_b N_0}{2}$.

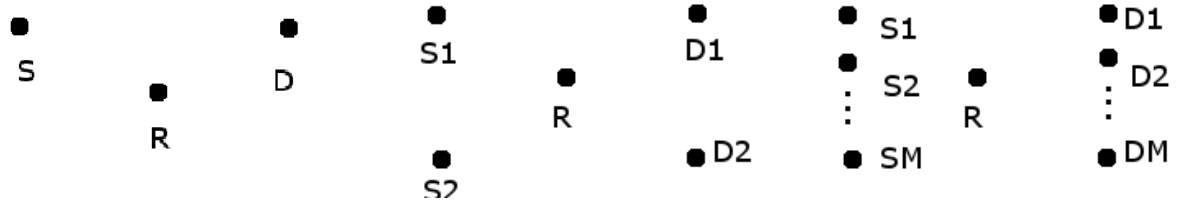

(a) One user model (b) Two-user model (c) M-user model

Figure 2.1: The system model of a relay-based network coding system.

2.2.1 One-user System Model

In the one-user system model, the channel gains are denoted by

h_{SD}	the channel gain between the source node S and the destination node D
h_{SR}	the channel gain between the source node S and the relay node R
h_{RD}	the channel gain between the relay node R and the destination node D

In the first time slot, S transmits x to R and D. D receives the information and R decodes the received information as $\tilde{x}$, where $\tilde{x}$ is an estimate of x. In the second time slot, R transmits $\tilde{x}$ to D. Using (2.3), the receiver output $y_D(1)$ at D and $y_R(1)$ at R in the first time slot, and the receiver output $y_D(2)$ at D in the second time slot, are given by

$$y_D(1) = h_{SD}E_b x + n_{SD}, \tag{2.4}$$

$$y_R(1) = h_{SR}E_b x + n_{SR}, \tag{2.5}$$

and

$$y_D(2) = h_{RD}E_b \tilde{x} + n_{RD}, \tag{2.6}$$

where $n_{SD} = \int_{-\infty}^{\infty} f(t)cos(w_c t)n_{SD}(t)dt$, $n_{SR} = \int_{-\infty}^{\infty} f(t)cos(w_c t)n_{SR}(t)dt$ and $n_{RD} = \int_{-\infty}^{\infty} f(t)cos(w_c t)n_{RD}(t)dt$ are independent Gaussian variables with zero mean and variance $\sigma^2 = \frac{N_0 E_b}{2}$.

2.2.2 *M*-user System Model

In the M-user system model ($M > 1$), the channel gains are denoted as:

h_{S1D1}	the channel gain between the source node S_1 and the destination node D_1
h_{S1R}	the channel gain between the source node S_1 and the relay node R
h_{S2D1}	the channel gain between the source node S_2 and the destination node D_1
h_{S2R}	the channel gain between the source node S_2 and the relay node R
...	
h_{SMD1}	the channel gain between the source node S_M and the destination node D_1
h_{SMR}	the channel gain between the source node S_M and the relay node R
h_{RD1}	the channel gain between the relay node R and the destination node D_1

Only the transmission of S_1 is discussed here as the performance of the other users can be obtained in the same way. In this case, the transmission is completed in $M+1$ time slots. In the i-th time slot, S_i broadcasts its information x_i to D_1 and R, where i=1,2,...M. R decodes the information as $\tilde{x_i}$. x_i is the bit transmitted by the i-th user, and $\tilde{x_i}$ is an estimate of x_i. In the $M+1$ time slot, R transmits $\tilde{x}$ to D_1, where $\tilde{x} = \tilde{x_1} \oplus \tilde{x_2} \oplus ... \oplus \tilde{x_M}$.

The receiver output $y_{D1}(k), y_R(k)$ at D_1 and R in the k-th time slot, where k=1,2...$M+1$, are given by

$$\begin{cases} y_{D1}(1) = h_{S1D1}E_b x_1 + n_{S1D1} \\ y_R(1) = h_{S1R}E_b x_1 + n_{S1R} \\ y_{D1}(2) = h_{S2D1}E_b x_2 + n_{S2D1} \\ y_R(2) = h_{S2R}E_b x_2 + n_{S2R} \\ ... \\ y_{D1}(i) = h_{SiD1}E_b x_i + n_{SiD1} \\ y_R(i) = h_{SiR}E_b x_i + n_{SiR} \\ ... \\ y_{D1}(M+1) = h_{RD1}E_b \tilde{x} + n_{RD1} \end{cases} \tag{2.7}$$

where $n_{SiD1} = \int_{-\infty}^{\infty} f(t)cos(w_c t)n_{SiD1}(t)dt$, $n_{SiR} = \int_{-\infty}^{\infty} f(t)cos(w_c t)n_{SiR}(t)dt$ and $n_{RD1} = \int_{-\infty}^{\infty} f(t)cos(w_c t)n_{RD1}(t)dt$ are independent Gaussian variables with zero mean and variance

$\sigma^2 = \frac{N_0 E_b}{2}$.

2.3 Detection with Perfect Channel Estimation

2.3.1 BER of the Direct Link and the Relay Link

The BER for direct transmission can be obtained by using (2.4). If x=1 is transmitted, $y_D(1)$ is a Gaussian distributed variable with mean $h_{SD}E_b$ and variance $\sigma^2 = \frac{N_0 E_b}{2}$. If x=-1 is transmitted, $y_D(1)$ is a Gaussian distributed variable with mean $-h_{SD}E_b$ and variance $\sigma^2 = \frac{N_0 E_b}{2}$. Based on the maximum-likelihood detection of BPSK, the optimal decision rule is $y_D(1) \underset{x=-1}{\overset{x=1}{\gtrless}} 0$, and the BER for the direct link $S \to D$ is $P_{eSD} = Q\left(h_{SD}\sqrt{\frac{2E_b}{N_0}}\right)$.

The BER for the relay link $S \to R \to D$ can be obtained by examining the BER of $S \to R$ and $R \to D$ link, and is given by

$$P_{eSRD} = P_{eSR}(1 - P_{eRD}) + P_{eRD}(1 - P_{eSR}), \tag{2.8}$$

where P_{eSR} and P_{eRD} are the BER of $S \to R$ and $R \to D$ link, respectively, with $P_{eSR} = Q\left(h_{SR}\sqrt{\frac{2E_b}{N_0}}\right)$ and $P_{eRD} = Q\left(h_{RD}\sqrt{\frac{2E_b}{N_0}}\right)$.

2.3.2 One-user System with Perfect Channel Estimation

In the relay-based network coding system, x is transmitted via both the direct link and the relay link, and both $y_D(1)$ and $y_D(2)$ are received at D as in (2.4) and (2.6). The decision rule of the maximum-likelihood detector, assuming that the symbols are equally likely, is

given by

$$\begin{aligned} & P(x=1|y_D(1),y_D(2)) \underset{x=-1}{\overset{x=1}{\gtrless}} P(x=-1|y_D(1),y_D(2)) \\ \Longrightarrow & \tfrac{p(y_D(1),y_D(2)|x=1)P(x=1)}{p(y_D(1),y_D(2))} \underset{x=-1}{\overset{x=1}{\gtrless}} \tfrac{p(y_D(1),y_D(2)|x=-1)P(x=-1)}{p(y_D(1),y_D(2))} \\ \Longrightarrow & p(y_D(1),y_D(2)|x=1) \underset{x=-1}{\overset{x=1}{\gtrless}} p(y_D(1),y_D(2)|x=-1). \end{aligned} \tag{2.9}$$

As shown in (2.4) and (2.6), since n_{SD} and n_{RD} are two independent random variables, $y_D(1)$ and $y_D(2)$ are conditionally independent given x. Therefore, the decision rule can be expressed as

$$\begin{aligned} & p(y_D(1)|x=1)p(y_D(2)|x=1) \underset{x=-1}{\overset{x=1}{\gtrless}} p(y_D(1)|x=-1)p(y_D(2)|x=-1) \\ \Longrightarrow & \tfrac{p(y_D(1)|x=1)p(y_D(2)|x=1)}{p(y_D(1)|x=-1)p(y_D(2)|x=-1)} \underset{x=-1}{\overset{x=1}{\gtrless}} 1. \end{aligned} \tag{2.10}$$

In (2.10), the densities $p(y_D(1)|x=1)$ and $p(y_D(1)|x=-1)$ can be written as

$$p(y_D(1)|x=1) = \frac{1}{\sqrt{2\pi}\sigma} exp\left(-\frac{(y_D(1)-h_{SD}E_b)^2}{2\sigma^2}\right) \tag{2.11}$$

and

$$p(y_D(1)|x=-1) = \frac{1}{\sqrt{2\pi}\sigma} exp\left(-\frac{(y_D(1)+h_{SD}E_b)^2}{2\sigma^2}\right). \tag{2.12}$$

Using the Total Probability Theorem, the density $p(y_D(2)|x=1)$ can be expressed as

$$\begin{aligned} & p(y_D(2)|x=1) \\ & = p(y_D(2)|\tilde{x}=1,x=1)P(\tilde{x}=1|x=1) + p(y_D(2)|\tilde{x}=-1,x=1)P(\tilde{x}=-1|x=1) \\ & = p(y_D(2)|\tilde{x}=1)P(\tilde{x}=1|x=1) + p(y_D(2)|\tilde{x}=-1)P(\tilde{x}=-1|x=1) \\ & = (1-P_{eSR})\tfrac{1}{\sqrt{2\pi}\sigma} exp\left(-\tfrac{(y_D(2)-h_{RD}E_b)^2}{2\sigma^2}\right) + P_{eSR}\tfrac{1}{\sqrt{2\pi}\sigma} exp\left(-\tfrac{(y_D(2)+h_{RD}E_b)^2}{2\sigma^2}\right) \end{aligned} \tag{2.13}$$

and similarly,

$$p(y_D(2)|x=-1) = P_{eSR}\frac{1}{\sqrt{2\pi}\sigma}exp(-\frac{(y_D(2)-h_{RD}E_b)^2}{2\sigma^2}) + (1-P_{eSR})\frac{1}{\sqrt{2\pi}\sigma}exp(-\frac{(y_D(2)+h_{RD}E_b)^2}{2\sigma^2}). \tag{2.14}$$

In (2.13) and (2.14), $P_{eSR} = Q(h_{SR}\sqrt{\frac{2E_b}{N_0}})$.

Therefore, the decision rule for the one-user case is given by

$$L \underset{x=-1}{\overset{x=1}{\gtrless}} 1, \tag{2.15}$$

where

$$L = \frac{e^{-\frac{(y_D(1)-h_{SD}E_b)^2}{2\sigma^2}}[(1-P_{eSR})e^{-\frac{(y_D(2)-h_{RD}E_b)^2}{2\sigma^2}} + P_{eSR}e^{-\frac{(y_D(2)+h_{RD}E_b)^2}{2\sigma^2}}]}{e^{-\frac{(y_D(1)+h_{SD}E_b)^2}{2\sigma^2}}[P_{eSR}e^{-\frac{(y_D(2)-h_{RD}E_b)^2}{2\sigma^2}} + (1-P_{eSR})e^{-\frac{(y_D(2)+h_{RD}E_b)^2}{2\sigma^2}}]}. \tag{2.16}$$

2.3.3 Two-user System with Perfect Channel Estimation

In the two-user system model, S_1 transmits x_1 to D_1 and S_2 transmits x_2 to D_1, where x_1 and x_2 are binary data bits from S_1 and S_2 ($x_1, x_2 \in \{1, -1\}$). Only the BER of the transmission of x_1 is discussed here. The BER for the transmission of x_2 (from S_2 to D_2) can be obtained in the same way. Since only the transmission of the first user S_1 is discussed, the subscript D_1 is simplified as D. Using maximum-likelihood detection, given the equal-probability transmission of the two symbols, the decision rule for the two-user system model is

$$\begin{aligned} & P(x_1=1|y_D(1),y_D(2),y_D(3)) \underset{x_1=-1}{\overset{x_1=1}{\gtrless}} P(x_1=-1|y_D(1),y_D(2),y_D(3)) \\ \Longrightarrow & \frac{p(y_D(1),y_D(2),y_D(3)|x_1=1)P(x_1=1)}{p(y_D(1),y_D(2),y_D(3))} \underset{x_1=-1}{\overset{x_1=1}{\gtrless}} \frac{p(y_D(1),y_D(2),y_D(3)|x_1=-1)P(x_1=-1)}{p(y_D(1),y_D(2),y_D(3))} \\ \Longrightarrow & p(y_D(1),y_D(2),y_D(3)|x_1=1) \underset{x_1=-1}{\overset{x_1=1}{\gtrless}} p(y_D(1),y_D(2),y_D(3)|x_1=-1). \end{aligned} \tag{2.17}$$

Since x_1 and x_2 are independent random variables, the density $p(y_D(1), y_D(2), y_D(3)|x_1 = 1)$

in (2.17) can be simplified by using the Total Probability Theorem as follows:

$$\begin{aligned}
&p(y_D(1), y_D(2), y_D(3)|x_1 = 1) \\
&= p(y_D(1), y_D(2), y_D(3)|x_1 = 1, x_2 = 1)P(x_2 = 1|x_1 = 1) \\
&+p(y_D(1), y_D(2), y_D(3)|x_1 = 1, x_2 = -1)P(x_2 = -1|x_1 = 1) \\
&= p(y_D(1), y_D(2), y_D(3)|x_1 = 1, x_2 = 1)P(x_2 = 1) \\
&+p(y_D(1), y_D(2), y_D(3)|x_1 = 1, x_2 = -1)P(x_2 = -1) \\
&= p(y_D(1), y_D(2), y_D(3)|x_1 = 1, x_2 = 1)\tfrac{1}{2} + p(y_D(1), y_D(2), y_D(3)|x_1 = 1, x_2 = -1)\tfrac{1}{2} \\
&= \tfrac{1}{2}P4 + \tfrac{1}{2}P1,
\end{aligned} \tag{2.18}$$

and similarly, the density $p(y_D(1), y_D(2), y_D(3)|x_1 = -1)$ in (2.17) can be shown to be equal to

$$p(y_D(1), y_D(2), y_D(3)|x_1 = -1) = \frac{1}{2}P2 + \frac{1}{2}P3, \tag{2.19}$$

where in (2.18) and (2.19),

$$\begin{cases}
P1 = p(y_D(1), y_D(2), y_D(3)|x_1 = 1, x_2 = -1) \\
P2 = p(y_D(1), y_D(2), y_D(3)|x_1 = -1, x_2 = 1) \\
P3 = p(y_D(1), y_D(2), y_D(3)|x_1 = -1, x_2 = -1) \\
P4 = p(y_D(1), y_D(2), y_D(3)|x_1 = 1, x_2 = 1).
\end{cases} \tag{2.20}$$

Therefore, the decision rule for the two-user case is

$$P4 + P1 \underset{x=-1}{\overset{x=1}{\gtrless}} P2 + P3. \tag{2.21}$$

Similar to the one user case, $y_D(1), y_D(2), y_D(3)$ are conditionally independent variables given

x_1 and x_2. Therefore, $p(y_D(1), y_D(2), y_D(3)|x_1, x_2)$ in (2.20) can be written as:

$$\begin{aligned} & p(y_D(1), y_D(2), y_D(3)|x_1, x_2) \\ & = p(y_D(1)|x_1, x_2)p(y_D(2)|x_1, x_2)p(y_D(3)|x_1, x_2) \\ & = p(y_D(1)|x_1)p(y_D(2)|x_2)p(y_D(3)|x_1, x_2). \end{aligned} \tag{2.22}$$

The conditional density functions in (2.20) can be further simplified. Taking P4 as an example, we have

$$\begin{aligned} & P4 = p(y_D(1), y_D(2), y_D(3)|x_1 = 1, x_2 = 1) \\ & = p(y_D(1)|x_1 = 1)p(y_D(2)|x_2 = 1)p(y_D(3)|x_1 = 1, x_2 = 1) \\ & = \tfrac{1}{\sqrt{2\pi}\sigma} e^{-\frac{(y_D(1)-h_{S1D}E_b)^2}{2\sigma^2}} \tfrac{1}{\sqrt{2\pi}\sigma} e^{-\frac{(y_D(2)-h_{S2D}E_b)^2}{2\sigma^2}} p(y_D(3)|x_1 = 1, x_2 = 1), \end{aligned} \tag{2.23}$$

where

$$\begin{aligned} & p(y_D(3)|x_1 = 1, x_2 = 1) \\ & = p(y_D(3)|\tilde{x} = 1, x_1 = 1, x_2 = 1)P(\tilde{x} = 1|x_1 = 1, x_2 = 1) \\ & + p(y_D(3)|\tilde{x} = -1, x_1 = 1, x_2 = 1)P(\tilde{x} = -1|x_1 = 1, x_2 = 1) \\ & = p(y_D(3)|\tilde{x} = 1)P(\tilde{x} = 1|x_1 = 1, x_2 = 1) \\ & + p(y_D(3)|\tilde{x} = -1)P(\tilde{x} = -1|x_1 = 1, x_2 = 1). \end{aligned} \tag{2.24}$$

In order to further simplify (2.24), Table 2.1 is used. This table shows the mapping between $\tilde{x_1}, \tilde{x_2}$ and $\tilde{x}$. As mentioned in the system model, $\tilde{x} = \tilde{x_1} \oplus \tilde{x_2}$.

Table 2.1: The truth table of $\tilde{x_1}, \tilde{x_2}$ and $\tilde{x}$

$\tilde{x_1}$	$\tilde{b_1}$	$\tilde{x_2}$	$\tilde{b_2}$	$\tilde{b_1} \bigoplus \tilde{b_2}$	$\tilde{x}$
-1	1	-1	1	0	1
-1	1	1	0	1	-1
1	0	-1	1	1	-1
1	0	1	0	0	1

Therefore, (2.24) can be expressed as

$$
\begin{aligned}
&p(y_D(3)|x_1=1,x_2=1)\\
&=p(y_D(3)|\tilde{x}=1)P(\tilde{x}=1|x_1=1,x_2=1)+p(y_D(3)|\tilde{x}=-1)P(\tilde{x}=-1|x_1=1,x_2=1)\\
&=p(y_D(3)|\tilde{x}=1)[P(\tilde{x_1}=-1,\tilde{x_2}=-1|x_1=1,x_2=1)\\
&+P(\tilde{x_1}=1,\tilde{x_2}=1|x_1=1,x_2=1)]\\
&+p(y_D(3)|\tilde{x}=-1)[P(\tilde{x_1}=-1,\tilde{x_2}=1|x_1=1,x_2=1)\\
&+P(\tilde{x_1}=1,\tilde{x_2}=-1|x_1=1,x_2=1)]\\
&=\tfrac{1}{\sqrt{2\pi}\sigma}exp\left(-\tfrac{(y_D(3)-h_{RD}E_b)^2}{2\sigma^2}\right)[P(\tilde{x_1}=-1,\tilde{x_2}=-1|x_1=1,x_2=1)\\
&+P(\tilde{x_1}=1,\tilde{x_2}=1|x_1=1,x_2=1)]\\
&+\tfrac{1}{\sqrt{2\pi}\sigma}exp\left(-\tfrac{(y_D(3)+h_{RD}E_b)^2}{2\sigma^2}\right)[P(\tilde{x_1}=-1,\tilde{x_2}=1|x_1=1,x_2=1)\\
&+P(\tilde{x_1}=1,\tilde{x_2}=-1|x_1=1,x_2=1)].
\end{aligned}
\tag{2.25}
$$

Since $\tilde{x_1}$ is independent of x_2 and $\tilde{x_2}$ is independent of x_1, the probability $P(\tilde{x_1}=1,\tilde{x_2}=1|x_1=1,x_2=1)$ in (2.25) is given by

$$
\begin{aligned}
&P(\tilde{x_1}=1,\tilde{x_2}=1|x_1=1,x_2=1)\\
&=P(\tilde{x_1}=1|x_1=1)P(\tilde{x_2}=1|x_2=1)=(1-P_{eS1R})(1-P_{eS2R}),
\end{aligned}
\tag{2.26}
$$

where $P_{eS1R}=Q(h_{S1R}\sqrt{\frac{2E_b}{N_0}})$ and $P_{eS2R}=Q(h_{S2R}\sqrt{\frac{2E_b}{N_0}})$.

Similarly, in (2.25) the probabilities $P(\tilde{x_1}=-1,\tilde{x_2}=-1|x_1=1,x_2=1)$, $P(\tilde{x_1}=1,\tilde{x_2}=$

$-1|x_1 = 1, x_2 = 1)$, and $P(\tilde{x_1} = -1, \tilde{x_2} = 1|x_1 = 1, x_2 = 1)$ can be written as

$$\begin{aligned}
&P(\tilde{x_1} = -1, \tilde{x_2} = -1|x_1 = 1, x_2 = 1) \\
&= P(\tilde{x_1} = -1|x_1 = 1)P(\tilde{x_2} = -1|x_2 = 1) = P_{eS1R}P_{eS2R} \\
&P(\tilde{x_1} = 1, \tilde{x_2} = -1|x_1 = 1, x_2 = 1) \\
&= P(\tilde{x_1} = 1|x_1 = 1)P(\tilde{x_2} = -1|x_2 = 1) = (1 - P_{eS1R})P_{eS2R} \\
&P(\tilde{x_1} = -1, \tilde{x_2} = 1|x_1 = 1, x_2 = 1) \\
&= P(\tilde{x_1} = -1|x_1 = 1)P(\tilde{x_2} = 1|x_2 = 1) = P_{eS1R}(1 - P_{eS2R}).
\end{aligned} \tag{2.27}$$

Using (2.26) and (2.27), (2.25) can be written as

$$\begin{aligned}
&p(y_D(3)|x_1 = 1, x_2 = 1) \\
&= \tfrac{1}{\sqrt{2\pi}\sigma} exp\left(-\tfrac{(y_D(3) - h_{RD}E_b)^2}{2\sigma^2}\right)(P_{eS1R}P_{eS2R} + (1 - P_{eS1R})(1 - P_{eS2R})) \\
&+ \tfrac{1}{\sqrt{2\pi}\sigma} exp\left(-\tfrac{(y_D(3) + h_{RD}E_b)^2}{2\sigma^2}\right)(P_{eS1R}(1 - P_{eS2R}) + (1 - P_{eS1R})P_{eS2R}).
\end{aligned} \tag{2.28}$$

Therefore, by using (2.23) and (2.28), the density P4 is obtained. The other three variables $P1$, $P2$ and $P3$ can be obtained in the same way:

$$\begin{aligned}
&P1 = p(y_D(1), y_D(2), y_D(3)|x_1 = 1, x_2 = -1) \\
&= \tfrac{1}{\sqrt{2\pi}\sigma} exp\left(-\tfrac{(y_D(1) - h_{S1D}E_b)^2}{2\sigma^2}\right) \tfrac{1}{\sqrt{2\pi}\sigma} exp\left(-\tfrac{(y_D(2) + h_{S2D}E_b)^2}{2\sigma^2}\right) p(y_D(3)|x_1 = 1, x_2 = -1)
\end{aligned} \tag{2.29}$$

in which

$$\begin{aligned}
&p(y_D(3)|x_1 = 1, x_2 = -1) \\
&= p(y_D(3)|\tilde{x} = 1)(P(\tilde{x_1} = -1|x_1 = 1)P(\tilde{x_2} = -1|x_2 = -1) \\
&+ P(\tilde{x_1} = 1|x_1 = 1)P(\tilde{x_2} = 1|x_2 = -1)) \\
&+ p(y_D(3)|\tilde{x} = -1)(P(\tilde{x_1} = -1|x_1 = 1)P(\tilde{x_2} = 1|x_2 = -1) \\
&+ P(\tilde{x_1} = 1|x_1 = 1)P(\tilde{x_2} = -1|x_2 = -1)) \\
&= \tfrac{1}{\sqrt{2\pi}\sigma} exp\left(-\tfrac{(y_D(3) - h_{RD}E_b)^2}{2\sigma^2}\right)[P_{eS1R}(1 - P_{eS2R}) + (1 - P_{eS1R})P_{eS2R}] \\
&+ \tfrac{1}{\sqrt{2\pi}\sigma} exp\left(-\tfrac{(y_D(3) + h_{RD}E_b)^2}{2\sigma^2}\right)[P_{eS1R}P_{eS2R} + (1 - P_{eS1R})(1 - P_{eS2R})],
\end{aligned} \tag{2.30}$$

$$P2 = p(y_D(1), y_D(2), y_D(3)|x_1 = -1, x_2 = 1)$$
$$= \frac{1}{\sqrt{2\pi}\sigma} exp\left(-\frac{(y_D(1)+h_{S1D}E_b)^2}{2\sigma^2}\right) \frac{1}{\sqrt{2\pi}\sigma} exp\left(-\frac{(y_D(2)-h_{S2D}E_b)^2}{2\sigma^2}\right) p(y_D(3)|x_1 = -1, x_2 = 1) \tag{2.31}$$

in which

$$\begin{aligned}
&p(y_D(3)|x_1 = -1, x_2 = 1) \\
&= p(y_D(3)|\tilde{x} = 1)(P(\tilde{x_1} = -1|x_1 = -1)P(\tilde{x_2} = -1|x_2 = 1) \\
&+P(\tilde{x_1} = 1|x_1 = -1)P(\tilde{x_2} = 1|x_2 = 1)) \\
&+p(y_D(3)|\tilde{x} = -1)(P(\tilde{x_1} = -1|x_1 = -1)P(\tilde{x_2} = 1|x_2 = 1) \\
&+P(\tilde{x_1} = 1|x_1 = -1)P(\tilde{x_2} = -1|x_2 = 1)) \\
&= \frac{1}{\sqrt{2\pi}\sigma} exp(-\frac{(y_D(3)-h_{RD}E_b)^2}{2\sigma^2})[(1 - P_{eS1R})P_{eS2R} + P_{eS1R}(1 - P_{eS2R})] \\
&+\frac{1}{\sqrt{2\pi}\sigma} exp(-\frac{(y_D(3)+h_{RD}E_b)^2}{2\sigma^2})[(1 - P_{eS1R})(1 - P_{eS2R}) + P_{eS1R}P_{eS2R}],
\end{aligned} \tag{2.32}$$

and

$$P3 = p(y_D(1), y_D(2), y_D(3)|x_1 = -1, x_2 = -1)$$
$$= \frac{1}{\sqrt{2\pi}\sigma} exp(-\frac{(y_D(1)+h_{S1D}E_b)^2}{2\sigma^2}) \frac{1}{\sqrt{2\pi}\sigma} exp(-\frac{(y_D(2)+h_{S2D}E_b)^2}{2\sigma^2}) p(y_D(3)|x_1 = -1, x_2 = -1) \tag{2.33}$$

in which

$$\begin{aligned}
&p(y_D(3)|x_1 = -1, x_2 = -1) \\
&= p(y_D(3)|\tilde{x} = 1)(P(\tilde{x_1} = -1|x_1 = -1)P(\tilde{x_2} = -1|x_2 = -1) \\
&+P(\tilde{x_1} = 1|x_1 = -1)P(\tilde{x_2} = 1|x_2 = -1)) \\
&+p(y_D(3)|\tilde{x} = -1)(P(\tilde{x_1} = -1|x_1 = -1)P(\tilde{x_2} = 1|x_2 = -1) \\
&+P(\tilde{x_1} = 1|x_1 = -1)P(\tilde{x_2} = -1|x_2 = -1)) \\
&= \frac{1}{\sqrt{2\pi}\sigma} exp\left(-\frac{(y_D(3)-h_{RD}E_b)^2}{2\sigma^2}\right)[(1 - P_{eS1R})(1 - P_{eS2R}) + P_{eS1R}P_{eS2R}] \\
&+\frac{1}{\sqrt{2\pi}\sigma} exp\left(-\frac{(y_D(3)+h_{RD}E_b)^2}{2\sigma^2}\right)[(1 - P_{eS1R})P_{eS2R} + P_{eS1R}(1 - P_{eS2R})].
\end{aligned} \tag{2.34}$$

2.3.4 M-user Detection with Perfect Channel Estimation

In the M-user system model, D_1 receives x_1, x_2,...,x_M in different time instances ($x_1, x_2, ..., x_M \in \{-1, 1\}$). Only the BER of the transmission of x_1 is discussed here, and the BER performance of the transmission of other users can be obtained in the same way. Since only the transmission of the first user S_1 is discussed, the subscript of D_1 is simplified as D. Based on the maximum-likelihood detection and the equal-probability transmission of all the symbols, the decision rule for the M-user system model is given by

$$\begin{aligned}
&P(x_1 = 1|y_D(1), y_D(2), ..., y_D(M), y_D(M+1)) \underset{x_1=-1}{\overset{x_1=1}{\gtrless}} \\
&P(x_1 = -1|y_D(1), y_D(2), ..., y_D(M), y_D(M+1)) \\
&\Longrightarrow \frac{p(y_D(1),y_D(2),...,y_D(M),y_D(M+1)|x_1=1)P(x_1=1)}{p(y_D(1),y_D(2),...,y_D(M),y_D(M+1))} \underset{x_1=-1}{\overset{x_1=1}{\gtrless}} \\
&\frac{p(y_D(1),y_D(2),...,y_D(M),y_D(M+1)|x_1=-1)P(x_1=-1)}{p(y_D(1),y_D(2),...,y_D(M),y_D(M+1))} \\
&\Longrightarrow p(y_D(1), y_D(2), ..., y_D(M), y_D(M+1)|x_1 = 1) \underset{x_1=-1}{\overset{x_1=1}{\gtrless}} \\
&p(y_D(1), y_D(2), ..., y_D(M), y_D(M+1)|x_1 = -1).
\end{aligned} \tag{2.35}$$

The decision rule can be simplified using the procedure given in Section 2.3.3 for two user case.

2.4 Maximum Likelihood Detection with Imperfect Channel Estimation

In Section 2.3, the maximum-likelihood detector was assumed to have perfect knowledge of the channel gains. However, in practice, knowledge of the channel gains is obtained by an estimation process and thus the channel gain estimates used are noisy. In this section, the effect of imperfect channel estimation on the performance of the considered network coding

schemes is addressed.

In this work, the error in the channel gain estimates is modeled as a zero mean Gaussian variable α [49]-[52]. Because the estimation error tends to be smaller for higher received E_b/N_0 values, the variance of α is set to be proportional to the received E_b/N_0 value. Specifically, α is assumed to have a variance of $\frac{\Delta}{E_b/N_0}$, where Δ is a deterministic value greater than 0. The estimate $\hat{h}$ of the channel gain h is written as

$$\hat{h} = h + \alpha. \tag{2.36}$$

The maximum likelihood detection of the one-user case is shown in (2.15) and (2.16). With imperfect channel estimation, the decision rule becomes

$$L = \frac{e^{-\frac{(y_D(1)-h\hat{_{SD}}E_b)^2}{2\sigma^2}}[(1-P\hat{_{eSR}})e^{-\frac{(y_D(2)-h\hat{_{RD}}E_b)^2}{2\sigma^2}} + P\hat{_{eSR}}e^{-\frac{(y_D(2)+h\hat{_{RD}}E_b)^2}{2\sigma^2}}]}{e^{-\frac{(y_D(1)+h\hat{_{SD}}E_b)^2}{2\sigma^2}}[P\hat{_{eSR}}e^{-\frac{(y_D(2)-h\hat{_{RD}}E_b)^2}{2\sigma^2}} + (1-P\hat{_{eSR}})e^{-\frac{(y_D(2)+h\hat{_{RD}}E_b)^2}{2\sigma^2}}]} \tag{2.37}$$

where $h\hat{_{SD}} = h_{SD} + \alpha_{esd}$ and $h\hat{_{RD}} = h_{RD} + \alpha_{erd}$, and α_{esd} and α_{erd} are independent.

In a system model with more than one user, the maximum-likelihood detector is the same as in the perfect channel estimation case except that the channel gains are substituted with imperfect estimates as in (2.36). For example, in a two-use case, the channel gains h_{S1D}, h_{S2D} and h_{RD} in (2.23), (2.28)-(2.34) are substituted with

$$\begin{aligned} h\hat{_{S1D}} &= h_{S1D} + \alpha_{es1d} \\ h\hat{_{S2D}} &= h_{S2D} + \alpha_{es2d} \\ h\hat{_{RD}} &= h_{RD} + \alpha_{erd} \end{aligned} \tag{2.38}$$

where α_{es1d},α_{es2d}, and α_{erd} are independent.

2.5 Simulation Results

Due to the complexity of determining the probability density function (pdf) of the decision variable, the BER of the considered network coding schemes is evaluated via simulation. In the numerical results presented in this section, the channel gains are set to have different values for all the users. This is done by randomly choosing channel gains for different users and the channel gain is assumed to be uniformly distributed between 0.9 to 1.1.

The system performance is evaluated under two different scenarios: the first scenario is when the received $\frac{E_b}{N_0}$ of the relay link is better than that of the direct link, and the second one is when the received $\frac{E_b}{N_0}$ of the relay link is worse than that of the direct link.

In the first part of the results, the BER performance of the network coding scheme when the channel estimates are perfect is analyzed. The BER of a given user when $M = 2, 3, 4, 5, 10$ is compared to the one-user ($M = 1$) case. Figs. 2.2 and 2.3 shows the BER performance. In Fig. 2.2(a), the relay link is 3 dB better than the direct link, which means $\left(\frac{E_b}{N_0}\right)_{SR} = \left(\frac{E_b}{N_0}\right)_{RD} = \left(\frac{E_b}{N_0}\right)_{SD} + 3$ dB. In Fig. 2.2(b), the relay link is 3 dB worse than the direct link, which means $\left(\frac{E_b}{N_0}\right)_{SR} = \left(\frac{E_b}{N_0}\right)_{RD} = \left(\frac{E_b}{N_0}\right)_{SD} - 3$ dB. In Fig. 2.3(a), the relay link is 10 dB better than the direct link. In Fig. 2.3(b), the relay link is 10 dB worse than the direct link.

As shown in the system model, the receiver has two "copies" of the information. One is received by using the direct path and the other is from the relay path. By making use of both copies when decoding, as shown in the decision rules given in Section 2.3.2 and 2.3.3, the considered scheme provides higher reliability compared to direct transmission. This is expected because additional information is available to the receiver with the use of the relay. This result is independent on whether the relay link is better or worse than the direct link. Therefore, for the perfect channel estimation case, the network coding scheme considered here always outperforms the case in which only the direct transmission is available. However, the performance improvement observed might be not significant in certain scenarios, as shown next.

For the one-user case, the considered network coding scheme greatly outperforms that of the direct transmission and the relay path when the relay link is better than the direct link, as shown in Figs. 2.2(a) and 2.3(a). For a number of users greater than one, the considered network coding scheme also outperforms the direct transmission when the relay link is better than the direct link. For example, in a two-user case, at $\left(\frac{E_b}{N_0}\right)_{SD} = 5$ dB, the BER is $2*10^{-4}$ when the relay link is 3 dB better than the direct link in Fig. 2.2(a), and the BER is $1.5*10^{-4}$ when the relay link is 10 dB better than the direct link in Fig. 2.3(a). Compared with the BER for the direct link in a two-user case at $\left(\frac{E_b}{N_0}\right)_{SD} = 5$ dB is $6*10^{-3}$, the direct link case is significantly worse than the cases with network coding. It is shown in these figures that network coding provides noticeable performance gain for the cases in which the number of users is as high as 5.

In Figs. 2.2(b) and 2.3(b), the relay link is worse than the direct link. For any number of users in the network, the BER performance of the considered network coding scheme always outperforms the direct transmission and the relay path. For example, when $\left(\frac{E_b}{N_0}\right)_{SD} = 5$ dB, the BER is $3.5*10^{-3}$ in Fig.2.2(b) when the number of users is 3 and the relay link is 3 dB worse than the direct link. Compared with the BER for the direct link in a three-user case at $\left(\frac{E_b}{N_0}\right)_{SD} = 5$ dB, which is $6*10^{-3}$, it is shown that the BER performance of the considered network coding scheme is better than the direct link and the relay path even when the relay link is worse than the direct link.

The situation when more users enter the network is studied, and it is found that the relay link contributes less when the number of users increases, as expected. As illustrated in Figs. 2.2(a) and 2.3(a), the ten-user case curve is the closest curve to the direct transmission curve. It is concluded that as the number of users approaches positive infinity, the proposed scheme has approximately the same BER performance as the direct transmission.

In Fig. 2.2(b), the BER is very close to the direct link curve for any number of users in the network since the relay link is worse than the direct link. In Fig. 2.3(b), the BER curve of the proposed scheme for any number of users is almost the same as that of the direct link

when the relay link is worse than the direct link. This is due to the fact that the information obtained from the relay path in this case is noisier than the one received from the direct path. Thus, the information received from the relay is of little or no value.

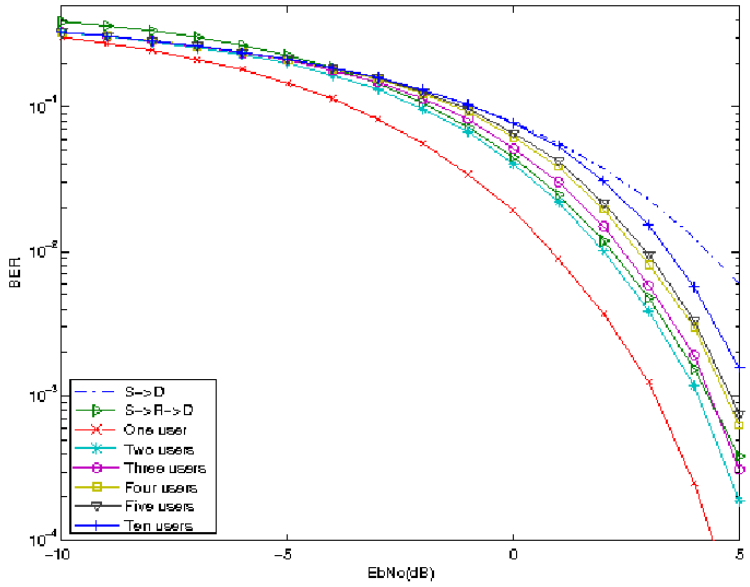

(a) relay link is 3 dB better than the direct link

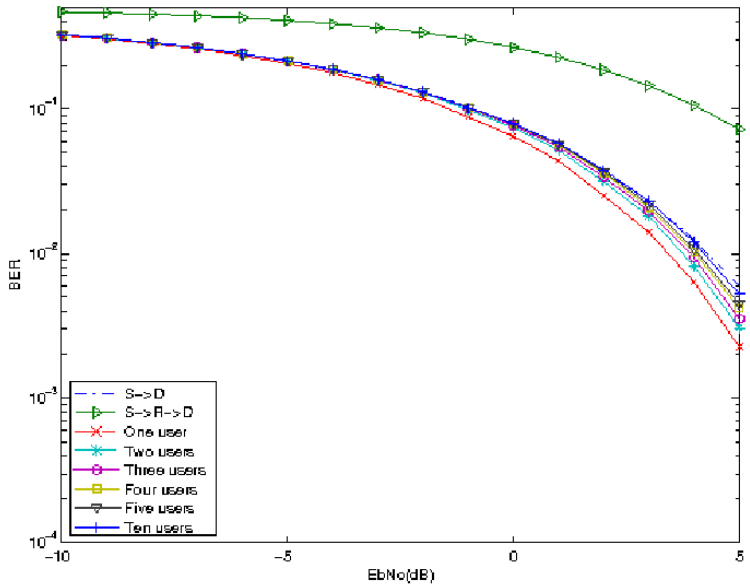

(b) relay link is 3 dB worse than the direct link

Figure 2.2: The BER performance with perfect channel knowledge. The x-label is the received $\left(\frac{E_b}{N_0}\right)_{S_1D_1}$ of the direct link.

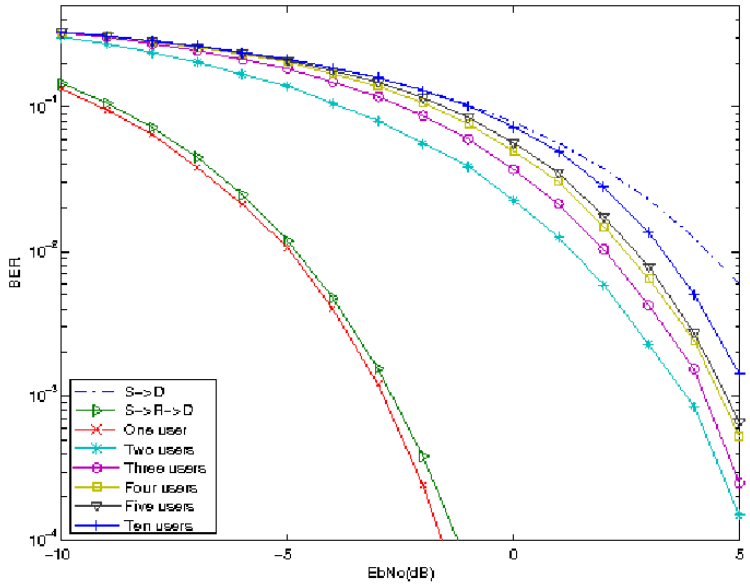

(a) relay link is 10 dB better than the direct link

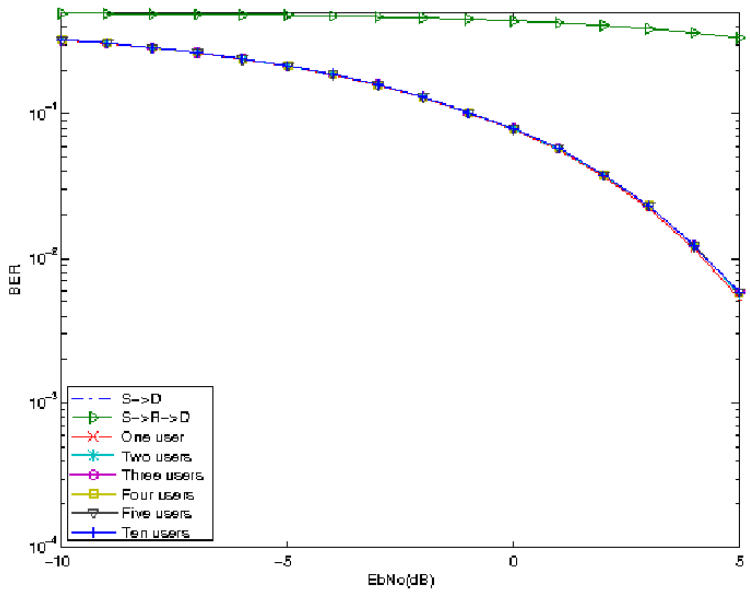

(b) relay link is 10 dB worse than the direct link

Figure 2.3: The BER performance with perfect channel knowledge. The x-label is the received $\left(\frac{E_b}{N_0}\right)_{S_1D_1}$ of the direct link.

The performance of the considered scheme with imperfect channel estimation is analyzed in Figs. 2.4-2.6. The random variables shown in (2.36) are used as the estimated channel gains in the decision rule. Figs. 2.4-2.6 shows the BER performance with imperfect channel knowledge with different values of Δ. In Figs. 2.4(a), 2.5(a) and 2.6(a), the relay link is 5 dB better than the direct link. In Figs. 2.4(b), 2.5(b) and 2.6(b), the relay link is 5 dB worse than the direct link.

The effect of both small and large channel estimation errors is investigated. In Fig. 2.4, the random variable in (2.36) has a small range with $\Delta = 0.1$. In Fig. 2.5, the estimation error is greater with $\Delta = 1$. In Fig. 2.6, the estimation error is even greater with $\Delta = 10$.

The BER performance when the channel estimation is imperfect is compared to the case when channel estimation is perfect. In Fig. 2.4, the curves of imperfect channel estimation with small estimation error closely approximate that of perfect channel estimation case.

In Fig. 2.5, when larger estimation error is introduced, the imperfect channel estimation cases show significantly worse performance compared to that of perfect channel estimation cases. For example in Fig. 2.5(a), the three-user imperfect channel estimation case needs 1.5 dB more to achieve a BER of 10^{-3} compared with the three-user perfect channel estimation case. In low SNR regime ($\frac{E_b}{N_0} < 2$ dB), the three-user imperfect channel estimation case has worse BER performance even than the direct link case. The same behavior is observed for the five-user imperfect channel estimation case when $\frac{E_b}{N_0} < 3.5$ dB. Additionally, in Fig. 2.5, the reduced performance gain becomes smaller in high SNR regime since the estimation error is set to be inversely proportional to the SNR.

In Fig. 2.6, the performance of imperfect channel estimation is significantly reduced compared to that with perfect channel estimation. All the imperfect channel estimation cases (one-user, three-user, five-user) have significantly worse performance than either the direct link or the relay link. For example, in Fig. 2.6(a), the five-user imperfect channel estimation case needs 10 dB more to achieve a BER of 10^{-3} compared with the five-user perfect channel estimation case. Since the estimation error, instead of thermal noise, dominates the detection errors,

all the three numbers of users have almost the same significant performance degradation.

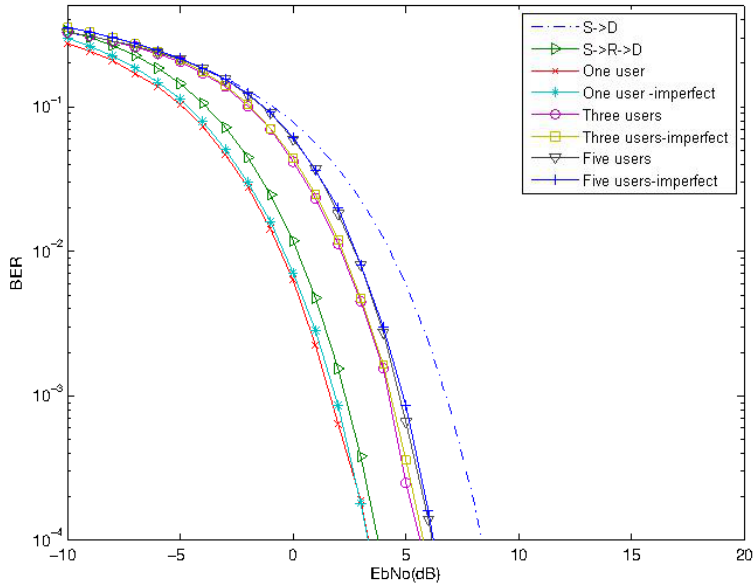

(a) relay link is 5 dB better than the direct link

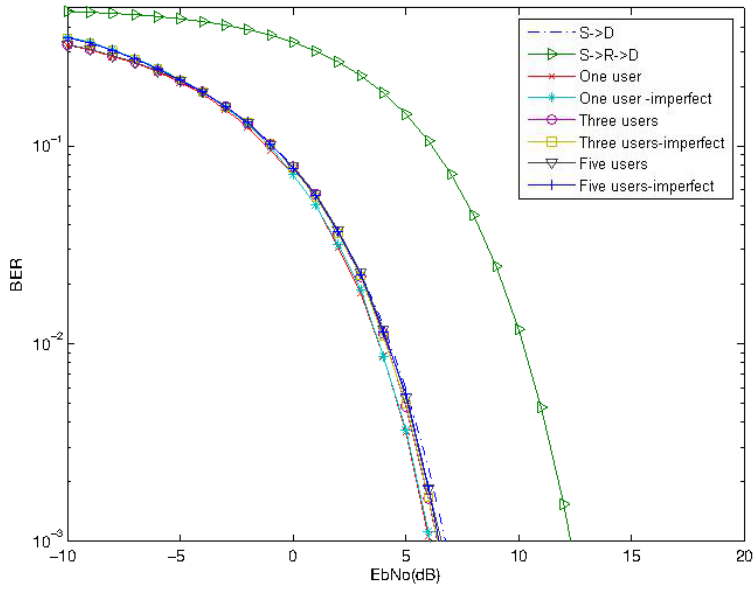

(b) relay link is 5 dB worse than the direct link

Figure 2.4: The BER performance with imperfect channel knowledge. The x-label is the received $\left(\frac{E_b}{N_0}\right)_{S_i D_i}$ of the direct link. The curves with label 'One user-imperfect', 'Three users-imperfect' and 'Five users-imperfect' are the curves for imperfect channel estimation. $\Delta = 0.1$.

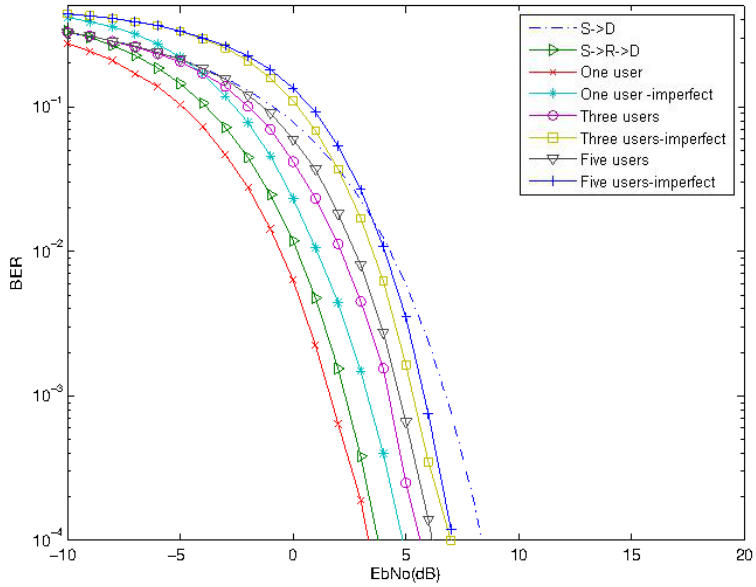

(a) relay link is 5 dB better than the direct link

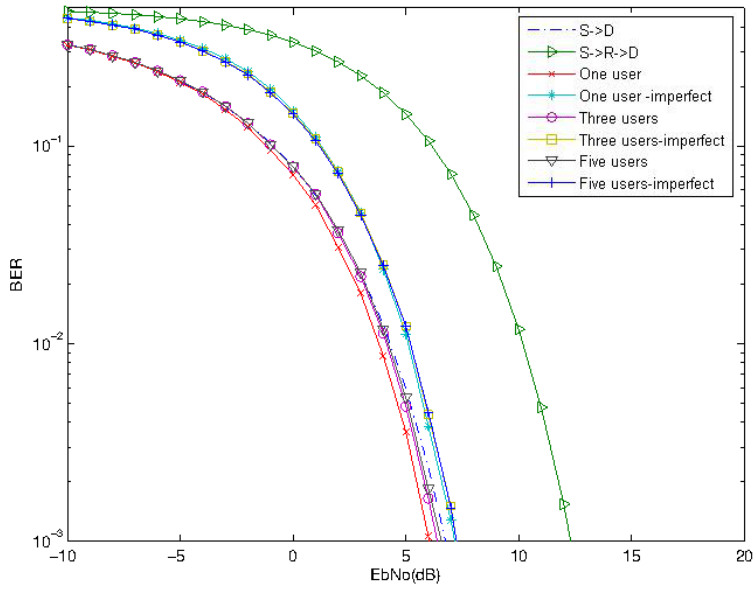

(b) relay link is 5 dB worse than the direct link

Figure 2.5: The BER performance with imperfect channel knowledge. The x-label is the received $\left(\frac{E_b}{N_0}\right)_{S_i D_i}$ of the direct link. The curves with label 'One user-imperfect', 'Three users-imperfect' and 'Five users-imperfect' are the curves for imperfect channel estimation. $\Delta = 1$.

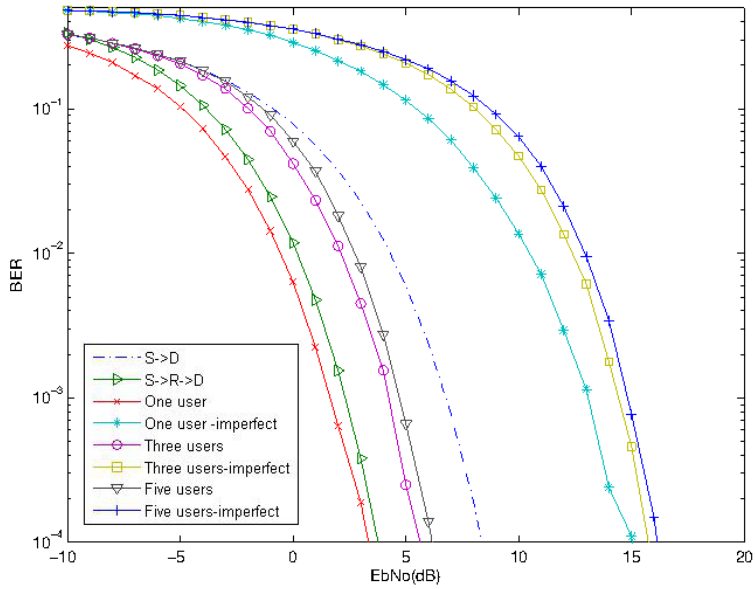

(a) relay link is 5 dB better than the direct link

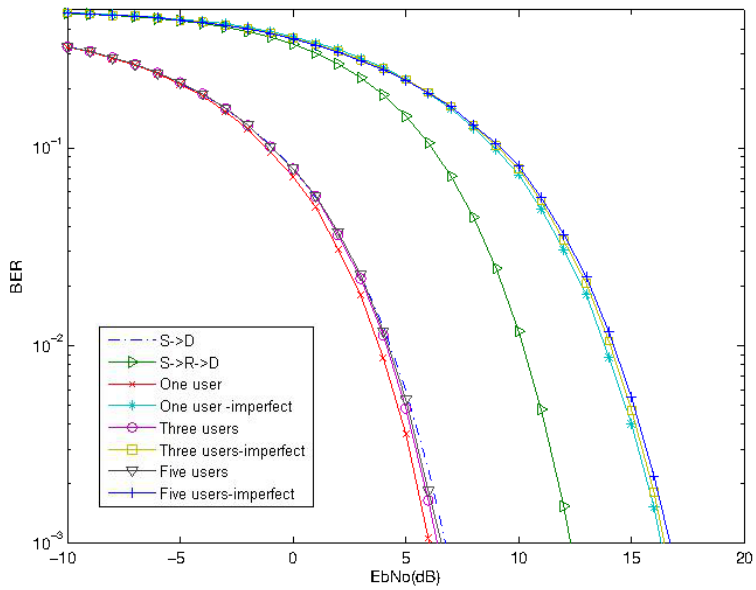

(b) relay link is 5 dB worse than the direct link

Figure 2.6: The BER performance with imperfect channel knowledge. The x-label is the received $\left(\frac{E_b}{N_0}\right)_{S_i D_i}$ of the direct link. The curves with label 'One user-imperfect', 'Three users-imperfect' and 'Five users-imperfect' are the curves for imperfect channel estimation. $\Delta = 10$.

2.6 Conclusions

In this chapter, the application of network coding techniques based on the use of a single relay to improve multi-user transmission was considered. In the proposed scheme, the relay node brings additional information to the destinations in order to improve the BER performance. The effect of perfect and imperfect channel estimation on BER performance was analyzed. From this work, several results were observed:

- The considered relay-based network coding scheme can bring BER improvement as compared with direct transmission because detection based on both the direct path and the relay path has redundancy.
- When the number of users increases, the gain achieved with the use of the considered network coding scheme is reduced. This is because the relay node transmits the *XOR* signal (that is, partial information) of all received signals. As the number of users increases in the network, the relay path contributes less to the destination even if the relay path has a higher SNR than the direct path. In this case, when the number of users goes to infinity, the performance of the considered network coding scheme is the same as the direct transmission (assuming perfect channel estimation).
- The BER performance of the considered network coding scheme system can be significantly degraded with large channel estimation errors. In some cases, the performance can be even worse than that of the direct transmission.

Chapter 3

Performance Analysis of Network Coding in FSK Systems with Time Synchronization Errors

3.1 Introduction

The effects of phase estimation errors and time synchronization errors in a physical-layer network coding (PNC) system were first investigated in [11] for BPSK and QPSK signals. In addition, for asynchronous PNC with BPSK and QPSK signals, the effects of symbol misalignment were analyzed in [12], [13]. However, the performance loss due to time synchronization errors in PNC and digital network coding (DNC) systems with FSK modulation has not been investigated yet.

Non-coherent detection is considered in this work because "...the phase tracking required for coherent detection is impractical..." [23] in DNC and PNC systems. Recent work focusing on network coding systems with non-coherent FSK signals includes [7], [23]-[26]. Non-coherent receivers for CPFSK in DNC and PNC systems were proposed in [25], [26]. In addition, the

decision region of a PNC system with BFSK modulation was addressed in [23].

The main goal of this chapter is to understand the effect of various system parameters (time synchronization errors, received E_b/N_0, and unequal link quality) on the BER performance of DNC and PNC systems. First, we derive the BER of a DNC system with an optimal detector for non-coherent FSK modulation. Then, we investigate the BER of a PNC system with an optimal detector for non-coherent FSK modulation. The BER performance of the optimal PNC system is investigated via simulation due to the complexity of determining the pdf of the corresponding decision variable.

Throughout this chapter, $I_0(.)$ is the zero order modified Bessel function of the first kind.

3.2 System Model

In this section, we introduce the system model used in this chapter. In this work, the BER of DNC and PNC schemes in a two-way exchange channel, which was described in Chapter 1, is investigated by setting the transmitted signal to be binary non-coherent FSK signals. In this model, two nodes (S_1 and S_2) exchange information (bits x_1 and x_2) through an intervening relay node R, as shown in Fig. 1.1.

The BFSK signal transmitted by node $S_i (i = 1, 2)$ or R is defined as

$$s(t) = \sqrt{\tfrac{2}{T}} \sum_0^{N-1} \cos(2\pi(\Delta f(a[n] + 1) + f_c)t) g(t - nT), \tag{3.1}$$

where $a[n] \in \{0, 1\}$ represents the n-th binary bit information transmitted by node $S_i (i = 1, 2)$ or R, T is the symbol interval, N is the number of symbol transmitted during one time slot, f_c is the carrier frequency, and $g(t)$ is the signal pulse, which is nonzero only during 0 to T and is assumed to be rectangular for ease of analysis. Also, it is assumed that $s(t)$ has unit power. To ensure that binary FSK are orthogonal under non-coherent detection, "...the minimum frequency separation required for orthogonality of the signals is $\Delta f = \frac{1}{T}$ ..." [48].

Therefore, it is assumed that $\Delta f = \frac{1}{T}$. It is worth noting that in situations where bandwidth efficiency is more important than power efficiency, FSK modulation is not well-suited [53].

3.2.1 Transmission of FSK Signals in a DNC System

In a DNC system, the received signals $r_1^{DNC}(t)$ from S_1 at R in the first time slot and $r_2^{DNC}(t)$ from S_2 at R in the second time slot are given by

$$\begin{aligned} r_1^{DNC}(t) &= A_{a1}s_1(t-\xi_1) + n_1(t) \\ r_2^{DNC}(t) &= A_{a2}s_2(t-\xi_2) + n_2(t), \end{aligned} \tag{3.2}$$

where A_{ai} is the symmetric channel gain from source S_i to R (i=1,2), which is assumed to be known. $n_1(t)$ and $n_2(t)$ are two independent Gaussian noise processes with two-sided power spectral density $\frac{N_0}{2}$. ξ_1 and ξ_2 are the time synchronization errors, assumed to be uniformly distributed between 0 and D_1 and 0 and D_2, respectively, where $D_1(0 < D_1 < T)$ and $D_2(0 < D_2 < T)$ are the maximum time synchronization errors. The information component of the two signals, which is $s_1(t)$ in the first time slot and $s_2(t)$ in the second time slot, can be written as

$$s_1(t-\xi_1) = \sqrt{\frac{2}{T}} \sum_{n=0}^{N-1} \cos\left(\frac{2\pi(a_1[n]+1)(t-\xi_1)}{T} + 2\pi f_c t + \phi_1\right) g(t-\xi_1-nT) \tag{3.3}$$

and

$$s_2(t-\xi_2) = \sqrt{\frac{2}{T}} \sum_{n=1}^{N} \cos\left(\frac{2\pi(a_2[n]+1)(t-\xi_2)}{T} + 2\pi f_c t + \phi_2\right) g(t-\xi_2-nT), \tag{3.4}$$

where $\phi_i = -2\pi f_c \xi_i$ $(i = 1, 2)$ is an unknown phase shift assumed to be uniformly distributed between 0 and 2π.

The relay node R receives $r_1^{DNC}(t)$ from S_1 in the first time slot and obtains $\widehat{a_1}[n]$, which is an estimate of $a_1[n]$. R receives $r_2^{DNC}(t)$ from S_2 in the second time slot and obtains

$\widehat{a_2}[n]$, which is an estimate of $a_2[n]$. In the third time slot, R broadcasts $r^{DNC}(t)$ to S_1 and S_2, which is a modulated signal containing $\widehat{d}[n] = XOR(\widehat{a_1}[n], \widehat{a_2}[n])$. The received signal $y_1^{DNC}(t)$ at S_1 and the received signal $y_2^{DNC}(t)$ at S_2 are written as

$$y_1^{DNC}(t) = A_{a1} r^{DNC}(t - \xi_{r1}) + n_{r1}(t) \tag{3.5}$$

and

$$y_2^{DNC}(t) = A_{a2} r^{DNC}(t - \xi_{r2}) + n_{r2}(t), \tag{3.6}$$

respectively, where ξ_{r1} and ξ_{r2} are the time synchronization errors, which are assumed to be uniformly distributed between 0 and D_{r1} and 0 and D_{r2}, respectively, where $D_{r1}(0 < D_{r1} < T)$ and $D_{r2}(0 < D_{r2} < T)$ are the maximum time synchronization errors. Also in (3.5) and (3.6), $n_{r1}(t)$ and $n_{r2}(t)$ are two Gaussian noise processes with two-sided power spectral density $\frac{N_0}{2}$, and

$$r^{DNC}(t - \xi_{r1}) = \sqrt{\frac{2}{T}} \sum_{n=0}^{N-1} \cos\left(\frac{2\pi(\widehat{d}[n] + 1)(t - \xi_{r1})}{T} + 2\pi f_c t + \phi_{r1} \right) g(t - \xi_{r1} - nT) \tag{3.7}$$

and

$$r^{DNC}(t - \xi_{r2}) = \sqrt{\frac{2}{T}} \sum_{n=0}^{N-1} \cos\left(\frac{2\pi(\widehat{d}[n] + 1)(t - \xi_{r2})}{T} + 2\pi f_c t + \phi_{r2} \right) g(t - \xi_{r2} - nT), \tag{3.8}$$

where $\phi_{ri} = -2\pi f_c \xi_{ri} (i = 1, 2)$ is an unknown phase shift which is uniformly distributed between 0 and 2π.

Finally, the source node S_1 receives $y_1^{DNC}(t)$ and obtains $\widetilde{d_1}[n]$, which is an estimate of $\widehat{d}[n]$. Therefore, the information transmitted via the link $S_2 \rightarrow R \rightarrow S_1$ is decoded as $\widetilde{a_2}[n] = XOR(\widetilde{d_1}[n], a_1[n])$, where $\widetilde{a_2}[n]$ is an estimate of $a_2[n]$. The source node S_2 decodes $y_2^{DNC}(t)$ using an equivalent procedure.

3.2.2 Transmission of FSK Signals in a PNC System

We consider the same transmission and detection schemes for a PNC system described in Chapter 1 by setting the transmitted signal to be non-coherent FSK. In a PNC system, the received signal in the first time slot is the sum of the signals from S_1 and S_2,

$$r_{12}^{PNC}(t) = A_{a1}s_1(t-\xi_1) + A_{a2}s_2(t-\xi_2) + n(t), \tag{3.9}$$

where $s_1(t-\xi_1)$ and $s_2(t-\xi_2)$ are defined in (3.3) and (3.8), respectively, and $n(t)$ is a Gaussian noise process with two-sided power spectral density $\frac{N_0}{2}$.

The relay node receives $r_{12}^{PNC}(t)$ and decodes to obtain $\widehat{a}[n]$ $(n = 0, 1, 2, ..., N-1)$, which is an estimate of $XOR(a_1[n], a_2[n])$ $(n = 0, 1, 2, ..., N-1)$. The detector is described in detail in Section 3.3. In the second time slot, the signal $y_1^{PNC}(t)$ received at S_1 and the signal $y_2^{PNC}(t)$ received at S_2 are written as

$$y_1^{PNC}(t) = A_{a1}r^{PNC}(t-\xi_{r1}) + n_{r1}(t) \tag{3.10}$$

and

$$y_2^{PNC}(t) = A_{a2}r^{PNC}(t-\xi_{r2}) + n_{r2}(t), \tag{3.11}$$

respectively, where ξ_{r1} and ξ_{r2} are the time synchronization errors, which are assumed to be uniformly distributed between 0 and D_{r1} and 0 and D_{r2}, respectively, where $D_{r1}(0 < D_{r1} < T)$ and $D_{r2}(0 < D_{r2} < T)$ are the maximum time synchronization errors. Also, in (3.10) and (3.11), $n_{r1}(t)$ and $n_{r2}(t)$ are two Gaussian noise processes with two-sided power spectral density $\frac{N_0}{2}$, and

$$r^{PNC}(t-\xi_{r1}) = \sqrt{\frac{2}{T}}\sum_{n=0}^{N-1}\cos\left(\frac{2\pi(\widehat{a}[n]+1)(t-\xi_{r1})}{T} + 2\pi f_c t + \phi_{r1}\right) g(t-\xi_{r1}-nT) \tag{3.12}$$

and

$$r^{PNC}(t-\xi_{r2}) = \sqrt{\frac{2}{T}}\sum_{n=0}^{N-1}\cos\left(\frac{2\pi(\widehat{a}[n]+1)(t-\xi_{r2})}{T}+2\pi f_c t+\phi_{r2}\right)g(t-\xi_{r2}-nT), \quad (3.13)$$

where $\phi_{ri} = -2\pi f_c \xi_{ri}$ $(i = 1, 2)$ is an unknown phase shift which is uniformly distributed between 0 and 2π.

Finally, the source node S_1 receives $y_1^{PNC}(t)$ and obtains $\widetilde{a}[n]$, which is an estimate of $\widehat{a}[n]$. Therefore, the information transmitted via the link $S_2 \rightarrow R \rightarrow S_1$ is decoded as $\widetilde{a_2}[n] = XOR(\widetilde{a}[n], a_1[n])$, where $\widetilde{a_2}[n]$ is an estimate of $a_2[n]$. The source node S_2 decodes using an equivalent procedure.

3.3 Non-coherent Detection of FSK signals in a DNC system

In this section, we discuss the non-coherent detection of FSK signals in a DNC system with time synchronization errors. The main goal is to understand the effect of various system parameters [1] on the BER performance of non-coherent detection of FSK signals in a DNC system and to develop benchmark principles that will help in analyzing the BER performance of the more complex PNC system in subsequent sections.

We begin our study by first deriving the theoretical BER of non-coherent detection of FSK signals in the considered DNC system with time synchronization errors. Due to the symmetry of the communication flows in the two opposite directions, only the BER performance of S_1 is discussed. The results are also applicable to that of S_2.

As described in the system model, the transmission of FSK signals in a DNC system consists of three phases: the transmission from S_1 to R in the first time slot, the transmission from

[1] These parameters are time synchronization error, received E_b/N_0, and unequal link quality, and details on these parameters will be provided later in this section.

S_2 to R in the second time slot, and the transmission from R to S_1 (and S_2) in the third time slot. Therefore, a bit error would occur at S_1 if the following one of the four events happens:

1. A bit error occurs in the link from S_1 to R in the first time slot, no bit error occurs in the link from S_2 to R in the second time slot, and no bit error occurs in the link from R to S_1 in the third time slot.

2. No bit error occurs in the link from S_1 to R in the first time slot, a bit error occurs in the link from S_2 to R in the second time slot, and no bit error occurs in the link from R to S_1 in the third time slot.

3. No bit error occurs in the link from S_1 to R in the first time slot, no bit error occurs in the link from S_2 to R in the second time slot, and a bit error occurs in the link from R to S_1 in the third time slot.

4. A bit error occurs in the link from S_1 to R in the first time slot, a bit error occurs in the link from S_2 to R in the second time slot, and a bit error occurs in the link from R to S_1 in the third time slot.

Therefore, the BER at S_1, after the third time slot transmission is complete, is given by

$$Pe_{S_1} = Pe_{rs1}(1 - Pe_r) + (1 - Pe_{rs1})Pe_r, \tag{3.14}$$

where Pe_{rs1} is the BER at S_1 of data transmission from R to S_1 in the third time slot, Pe_r is the BER at R after $\hat{d}[n] = XOR(\hat{a_1}[n], \hat{a_2}[n])$ is decoded (after two time slot transmissions), and Pe_r is given by

$$Pe_r = Pe_{s1r}(1 - Pe_{s2r}) + (1 - Pe_{s1r})Pe_{s2r}, \tag{3.15}$$

where Pe_{s1r} and Pe_{s2r} are the BER at R of data transmission from S_1 to R in the first time slot and from S_2 to R in the second time slot, respectively.

The optimal receiver for binary non-coherent orthogonal FSK signals [48] is used by S_1 and R. As shown in Fig. 3.1, the optimal detector observes two random variables y^U and y^L at time instant $nT + T$ and bases its decision on these variables.

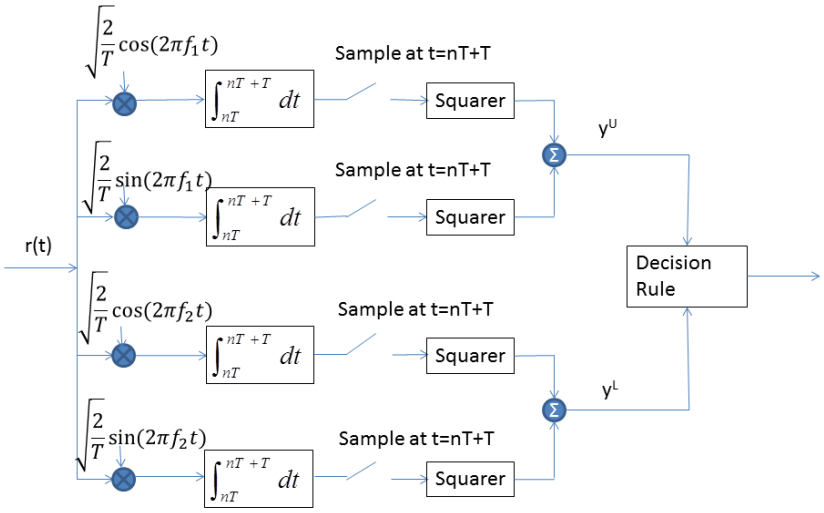

Figure 3.1: Non-coherent receiver of binary orthogonal FSK signals in a DNC system. $f_1 = f_c + \frac{1}{T}$ and $f_2 = f_c + \frac{2}{T}$.

The decision rule in Figure. 3.1 is

$$y^U \underset{a_1[n]=1}{\overset{a_1[n]=0}{\gtrless}} y^L, \tag{3.16}$$

where

$$y^U = \left(\int_{nT}^{nT+T} r(t)\sqrt{\frac{2}{T}}\cos(2\pi f_1 t)dt\right)^2 + \left(\int_{nT}^{nT+T} r(t)\sqrt{\frac{2}{T}}\sin(2\pi f_1 t)dt\right)^2 \tag{3.17}$$

and

$$y^L = \left(\int_{nT}^{nT+T} r(t)\sqrt{\frac{2}{T}}\cos(2\pi f_2 t)dt\right)^2 + \left(\int_{nT}^{nT+T} r(t)\sqrt{\frac{2}{T}}\sin(2\pi f_2 t)dt\right)^2, \tag{3.18}$$

and $r(t)$ is given by (3.2).

The output y^U at time instance $nT+T$ on the upper branch of the detector is equal to

$$y^U = (A_{a1}x_c^u + N_c^u)^2 + (A_{a1}x_s^u + N_s^u)^2, \tag{3.19}$$

where

$$\begin{aligned}
x_c^u &= \int_{nT}^{nT+T} s_1^{DNC}(t-\xi_1)\sqrt{\tfrac{2}{T}}\cos(2\pi f_1 t)dt \\
&= \int_{nT}^{nT+\xi_1} s_1^{DNC}(t-\xi_1)\sqrt{\tfrac{2}{T}}\cos(2\pi f_1 t)dt + \int_{nT+\xi_1}^{nT+T} s_1^{DNC}(t-\xi_1)\sqrt{\tfrac{2}{T}}\cos(2\pi f_1 t)dt \\
&= \int_{nT}^{nT+\xi_1} \sqrt{\tfrac{2}{T}}\cos(2\pi f_c t + \tfrac{2\pi}{T}(a_1[n-1]+1)(t-\xi_1)+\phi_1)\sqrt{\tfrac{2}{T}}\cos(2\pi f_1 t)dt \\
&+ \int_{nT+\xi_1}^{nT+T} \sqrt{\tfrac{2}{T}}\cos(2\pi f_c t + \tfrac{2\pi}{T}(a_1[n]+1)(t-\xi_1)+\phi_1)\sqrt{\tfrac{2}{T}}\cos(2\pi f_1 t)dt \\
&= \tfrac{1}{T}\int_{nT}^{nT+\xi_1}(\cos(2\pi 2 f_c t + \tfrac{2\pi}{T}(a_1[n-1]+1)(t-\xi_1) + \tfrac{2\pi t}{T} + \phi_1) \\
&+ \cos(2\pi \tfrac{1}{T}a_1[n-1](t-\xi_1) - \tfrac{2\pi\xi_1}{T} + \phi_1))dt \\
&+ \tfrac{1}{T}\int_{nT+\xi_1}^{nT+T}(\cos(2\pi 2 f_c t + \tfrac{2\pi}{T}(a_1[n]+1)(t-\xi_1) + \tfrac{2\pi t}{T} + \phi_1) \\
&+ \cos(2\pi \tfrac{1}{T}a_1[n](t-\xi_1) - \tfrac{2\pi\xi_1}{T} + \phi_1))dt,
\end{aligned} \tag{3.20}$$

and due to the high frequency component $2f_c$ in $\cos(2\pi 2 f_c t + \frac{2\pi}{T}(a_1[n-1]+1)(t-\xi_1) + \frac{2\pi t}{T} + \phi_1)$ and $\cos(2\pi 2 f_c t + \frac{2\pi}{T}(a_1[n]+1)(t-\xi_1) + \frac{2\pi t}{T} + \phi_1)$, the integration $\frac{1}{T}\int_{nT}^{nT+\xi_1}\cos(2\pi 2 f_c t + \frac{2\pi}{T}(a_1[n-1]+1)(t-\xi_1) + \frac{2\pi t}{T} + \phi_1)dt$ and $\frac{1}{T}\int_{nT+\xi_1}^{nT+T}\cos(2\pi 2 f_c t + \frac{2\pi}{T}(a_1[n]+1)(t-\xi_1) + \frac{2\pi t}{T} + \phi_1)dt$ are approximated as zero. Therefore, x_c^u equals to

$$x_c^u = \tfrac{1}{T}\int_{nT}^{nT+\xi_1}\cos(2\pi a_1[n-1]\tfrac{t-\xi_1}{T} - \tfrac{2\pi\xi_1}{T} + \phi_1)dt + \tfrac{1}{T}\int_{nT+\xi_1}^{nT+T}\cos(2\pi a_1[n]\tfrac{t-\xi_1}{T} - \tfrac{2\pi\xi_1}{T} + \phi_1)dt, \tag{3.21}$$

and similarly, x_s^u in (3.19) equals to

$$\begin{aligned}
x_s^u &= \int_{nT}^{nT+T} s_1^{DNC}(t-\xi_1)\sqrt{\tfrac{2}{T}}\sin(2\pi f_1 t)dt \\
&= \int_{nT}^{nT+\xi_1} s_1^{DNC}(t-\xi_1)\sqrt{\tfrac{2}{T}}\sin(2\pi f_1 t)dt + \int_{nT+\xi_1}^{nT+T} s_1^{DNC}(t-\xi_1)\sqrt{\tfrac{2}{T}}\sin(2\pi f_1 t)dt \\
&= \tfrac{1}{T}\int_{nT}^{nT+\xi_1}\sin(-2\pi a_1[n-1]\tfrac{t-\xi_1}{T} + \tfrac{2\pi\xi_1}{T} - \phi_1)dt \\
&+ \tfrac{1}{T}\int_{nT+\xi_1}^{nT+T}\sin(-2\pi a_1[n]\tfrac{t-\xi_1}{T} + \tfrac{2\pi\xi_1}{T} - \phi_1)dt.
\end{aligned} \tag{3.22}$$

Also, N_c^u and N_s^u in (3.19) are given by

$$N_c^u = \int_{nT}^{nT+T} n_1(t)\sqrt{\frac{2}{T}}\cos(2\pi f_1 t)dt, \tag{3.23}$$

and

$$N_s^u = \int_{nT}^{nT+T} n_1(t)\sqrt{\frac{2}{T}}\sin(2\pi f_1 t)dt. \tag{3.24}$$

N_c^u and N_s^u are two independent zero mean Gaussian variables with variance $\frac{N_0}{2}$.

The output y^L at time instance $nT+T$ on the lower branch of the detector is equal to

$$y^L = \left(A_{a1}x_c^l + N_c^l\right)^2 + \left(A_{a1}x_s^l + N_s^l\right)^2, \tag{3.25}$$

where

$$\begin{aligned} x_c^l &= \textstyle\int_{nT}^{nT+T} s_1^{DNC}(t-\xi_1)\sqrt{\frac{2}{T}}\cos(2\pi f_2 t)dt \\ &= \textstyle\int_{nT}^{nT+\xi_1} s_1^{DNC}(t-\xi_1)\sqrt{\frac{2}{T}}\cos(2\pi f_2 t)dt + \int_{nT+\xi_1}^{nT+T} s_1^{DNC}(t-\xi_1)\sqrt{\frac{2}{T}}\cos(2\pi f_2 t)dt \\ &= \textstyle\frac{1}{T}\int_{nT}^{nT+\xi_1}\cos(2\pi a_1[n-1]\frac{t-\xi_1}{T} - \frac{2\pi t}{T} - \frac{2\pi\xi_1}{T} + \phi_1)dt \\ &+ \textstyle\frac{1}{T}\int_{nT+\xi_1}^{nT+T}\cos(2\pi a_1[n]\frac{t-\xi_1}{T} - \frac{2\pi t}{T} - \frac{2\pi\xi_1}{T} + \phi_1)dt, \end{aligned} \tag{3.26}$$

$$\begin{aligned} x_s^l &= \textstyle\int_{nT}^{nT+T} s_1^{DNC}(t-\xi_1)\sqrt{\frac{2}{T}}\sin(2\pi f_2 t)dt \\ &= \textstyle\int_{nT}^{nT+\xi_1} s_1^{DNC}(t-\xi_1)\sqrt{\frac{2}{T}}\sin(2\pi f_2 t)dt + \int_{nT+\xi_1}^{nT+T} s_1^{DNC}(t-\xi_1)\sqrt{\frac{2}{T}}\sin(2\pi f_2 t)dt \\ &= \textstyle\frac{1}{T}\int_{nT}^{nT+\xi_1}\sin(-2\pi a_1[n-1]\frac{t-\xi_1}{T} + \frac{2\pi t}{T} + \frac{2\pi\xi_1}{T} - \phi_1)dt \\ &+ \textstyle\frac{1}{T}\int_{nT+\xi_1}^{nT+T}\sin(-2\pi a_1[n]\frac{t-\xi_1}{T} + \frac{2\pi t}{T} + \frac{2\pi\xi_1}{T} - \phi_1)dt, \end{aligned} \tag{3.27}$$

$$N_c^l = \int_{nT}^{nT+T} n_1(t)\sqrt{\frac{2}{T}}\cos(2\pi f_2 t)dt, \tag{3.28}$$

and

$$N_s^l = \int_{nT}^{nT+T} n_1(t)\sqrt{\frac{2}{T}}\sin(2\pi f_2 t)dt. \tag{3.29}$$

N_c^l and N_s^l are two independent zero mean Gaussian variables with variance $\frac{N_0}{2}$.

As x_c^u, x_s^u, x_c^l and x_s^l are functions of $a_1[n-1]$, $a_1[n]$, ξ_1 and ϕ_1, they are written in the

form of $x_c^u(a_1[n-1], a_1[n], \xi_1, \phi_1)$, $x_s^u(a_1[n-1], a_1[n], \xi_1, \phi_1)$, $x_c^l(a_1[n-1], a_1[n], \xi_1, \phi_1)$ and $x_s^l(a_1[n-1], a_1[n], \xi_1, \phi_1)$.

Since N_c^u and N_s^u are independent Gaussian variables, $\frac{y^U}{N_0/2}$ is a noncentral chi-square distribution with two degrees of freedom given $a_1[n-1]$, $a_1[n]$, and ξ_1. For the same reason, $\frac{y^L}{N_0/2}$ is also a noncentral chi-square distribution with two degrees of freedom given $a_1[n-1]$, $a_1[n]$, and ξ_1.

The probability of error Pe_{s1r} of data transmission from S_1 to R can be written as

$$\begin{aligned} Pe_{s1r} &= P(y^U < y^L | a_1[n-1]=0, a_1[n]=0) P(a_1[n]=0) P(a_1[n-1]=0) \\ &+ P(y^U < y^L | a_1[n-1]=1, a_1[n]=0) P(a_1[n]=0) P(a_1[n-1]=1) \\ &+ P(y^U > y^L | a_1[n-1]=1, a_1[n]=1) P(a_1[n]=1) P(a_1[n-1]=1) \\ &+ P(y^U > y^L | a_1[n-1]=0, a_1[n]=1) P(a_1[n]=1) P(a_1[n-1]=0), \end{aligned} \tag{3.30}$$

where $P(a_1[n-1]=1) = P(a_1[n-1]=0) = P(a_1[n]=1) = P(a_1[n]=0) = \frac{1}{2}$.

The probability $P(y^U < y^L | a_1[n-1]=0, a_1[n]=0)$ in (3.30) can be written as [48]

$$\begin{aligned} &P(y^U < y^L | a_1[n-1]=0, a_1[n]=0) \\ &= P(Y < X | a_1[n-1]=0, a_1[n]=0) \\ &= \tfrac{1}{D} \int_0^D \int_0^\infty P(Y < X | X=x, a_1[n-1]=0, a_1[n]=0) f_X(x) dx d\xi_1 \\ &= \tfrac{1}{D} \int_0^D \int_0^\infty \left(\int_0^x f_Y(y) dy \right) f_X(x) dx d\xi_1, \end{aligned} \tag{3.31}$$

where $X = \frac{y^L}{N_0/2}$ and $Y = \frac{y^U}{N_0/2}$. The pdf of X can be shown to be equal to

$$f_X(x) = \tfrac{1}{2} e^{-\frac{x+\lambda_L(0,0,\xi_1)}{2}} I_0\left(\sqrt{\lambda_L(0,0,\xi_1) x} \right), \tag{3.32}$$

where

$$\lambda_L(0,0,\xi_1) = \tfrac{2}{N_0} A_{a1}^2 [(x_c^l(0,0,\xi_1))^2 + (x_s^l(0,0,\xi_1))^2] = 0. \tag{3.33}$$

Also, the pdf of Y is given by

$$f_Y(y) = \tfrac{1}{2} e^{-\frac{y+\lambda_U(0,0,\xi_1)}{2}} I_0\left(\sqrt{\lambda_U(0,0,\xi_1) y}\right), \tag{3.34}$$

where

$$\lambda_U(0,0,\xi_1) = \tfrac{2}{N_0} A_{a1}^2 [(x_c^u(0,0,\xi_1))^2 + (x_s^u(0,0,\xi_1))^2] = \tfrac{2}{N_0} A_{a1}^2. \tag{3.35}$$

The probability $P(y^U < y^L | a_1[n-1] = 1, a_1[n] = 0)$ can be obtained in the same way with

$$\begin{aligned} \lambda_L(1,0,\xi_1) &= \tfrac{2}{N_0} A_{a1}^2 [(x_c^l(1,0,\xi_1))^2 + (x_s^l(1,0,\xi_1))^2] \\ &= \tfrac{2}{N_0} A_{a1}^2 (\tfrac{1}{2\pi^2 T^2} (T^2 + 2\pi^2 \xi_1^2 - T^2 \cos(\tfrac{2\pi\xi_1}{T}) - 2\pi T \xi_1 \sin(\tfrac{2\pi\xi_1}{T}))) \end{aligned} \tag{3.36}$$

and

$$\begin{aligned} &\lambda_U(1,0,\xi_1) = \tfrac{2}{N_0} A_{a1}^2 [(x_c^u(1,0,\xi_1))^2 + (x_s^u(1,0,\xi_1))^2] \\ &= \tfrac{2}{N_0} A_{a1}^2 (\tfrac{1}{2\pi^2 T^2} (T^2 + 2\pi^2 T^2 - 4\pi^2 T \xi_1 + 2\pi^2 \xi_1^2 - T^2 \cos(\tfrac{2\pi\xi_1}{T}) + 2\pi T (T - \xi_1) \sin(\tfrac{2\pi\xi_1}{T})). \end{aligned} \tag{3.37}$$

The probability $P(y^L < y^U | a_1[n-1] = 1, a_1[n] = 1)$ can be obtained in the same way with

$$\lambda_L(1,1,\xi_1) = \tfrac{2}{N_0} A_{a1}^2 [(x_c^l(1,1,\xi_1))^2 + (x_s^l(1,1,\xi_1))^2] = \tfrac{2}{N_0} A_{a1}^2 \tag{3.38}$$

and

$$\lambda_U(1,1,\xi_1) = \tfrac{2}{N_0} A_{a1}^2 [(x_c^u(1,1,\xi_1))^2 + (x_s^u(1,1,\xi_1))^2] = 0. \tag{3.39}$$

The probability $P(y^L < y^U | a_1[n-1] = 0, a_1[n] = 1)$ can be obtained in the same way with

$$\begin{aligned} &\lambda_L(0,1,\xi_1) = \tfrac{2}{N_0} A_{a1}^2 [(x_c^l(0,1,\xi_1))^2 + (x_s^l(0,1,\xi_1))^2] \\ &= \tfrac{2}{N_0} A_{a1}^2 (\tfrac{1}{2\pi^2 T^2} (T^2 + 2\pi^2 T^2 - 4\pi^2 T \xi_1 + 2\pi^2 \xi_1^2 - T^2 \cos(\tfrac{2\pi\xi_1}{T}) + 2\pi T (T - \xi_1) \sin(\tfrac{2\pi\xi_1}{T})) \end{aligned} \tag{3.40}$$

and

$$\begin{aligned}\lambda_U(0,1,\xi_1) &= \tfrac{2}{N_0}A_{a1}^2[(x_c^u(0,1,\xi_1))^2 + (x_s^u(0,1,\xi_1))^2] \\ &= \tfrac{2}{N_0}A_{a1}^2(\tfrac{1}{2\pi^2T^2}(T^2 + 2\pi^2\xi_1^2 - T^2\cos(\tfrac{2\pi\xi_1}{T}) - 2\pi T\xi_1\sin(\tfrac{2\pi\xi_1}{T}))).\end{aligned} \tag{3.41}$$

3.4 The Effects of System Parameters in a DNC System with Non-coherent FSK Signals and Timing Errors

To gain insight into the BER performance of a DNC system with non-coherent FSK signals and time synchronization errors, we consider the following three system parameters: ranges of timing errors, received E_b/N_0 values, and unequal link quality. Without loss of generality, it is assumed that $T = 1$.

3.4.1 Effect of Timing Errors

We first consider the effect of timing errors in a DNC system with non-coherent FSK signals. The other two system parameters are fixed and are discussed later. Same E_b/N_0 values are assumed for all links.

The BER performance of a DNC system with time synchronization error for different values of D_1, D_2 and D_{r1} are shown in Figs. 3.2-3.7. The received E_b/N_0 values from S_1 to R, from S_2 to R, and from R to S_1 are taken to be 10 dB. Based on these figures, we note the following:

- When any of D_1, D_2 or D_{r1} increases, the BER performance of the considered DNC system is degraded, as expected. For example, in Fig. 3.4, when $D_{r1} = 0.4$, the BER value is greater than 10^{-2}. The BER is approximately $4 * 10^{-3}$ with perfect synchronization (i.e. $D_1 = 0$, $D_2 = 0$ and $D_{r1} = 0$).

- The BER performance of the considered DNC system becomes significantly worse when time synchronization error is greater than 0.5 (i.e. $D_1 > 0.5$, $D_2 > 0.5$ or $D_{r1} > 0.5$). For example, as shown in Fig. 3.5- 3.7, the BER for any combination of values of D_1 and D_2 is greater than 10^{-2}.

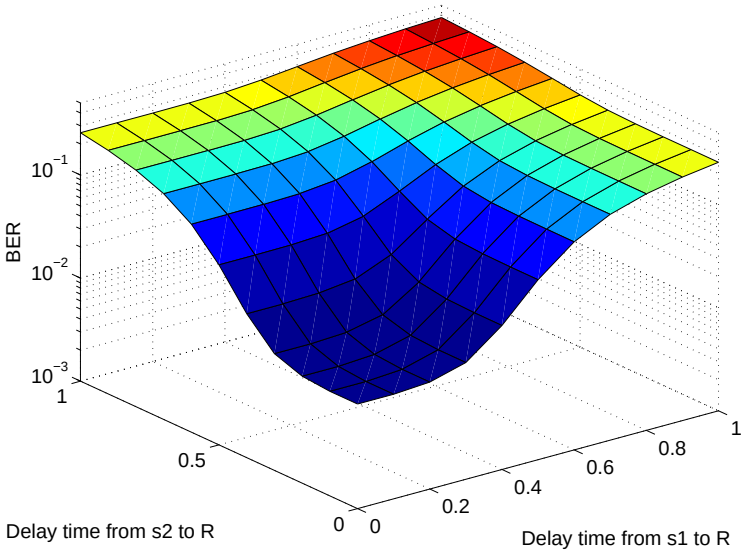

Figure 3.2: BER at S_1 in a DNC system with time synchronization error for different values of D_1 (x-axis) and D_2 (y-axis). ($D_{r1} = 0$, $A_{a1} = 1$, $A_{a2} = 1$, $E_b/N_0 = 10$ dB)

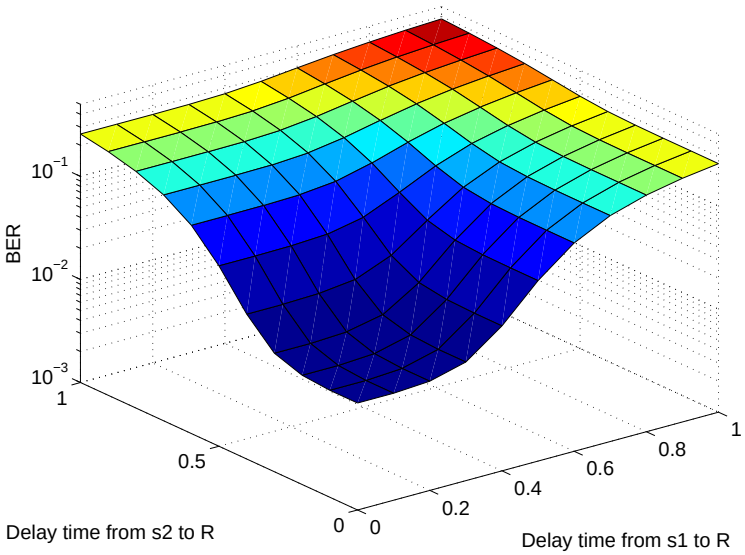

Figure 3.3: BER at S_1 in a DNC system with time synchronization error for different values of D_1 (x-axis) and D_2 (y-axis). ($D_{r1} = 0.2$, $A_{a1} = 1$, $A_{a2} = 1$, $E_b/N_0 = 10$ dB)

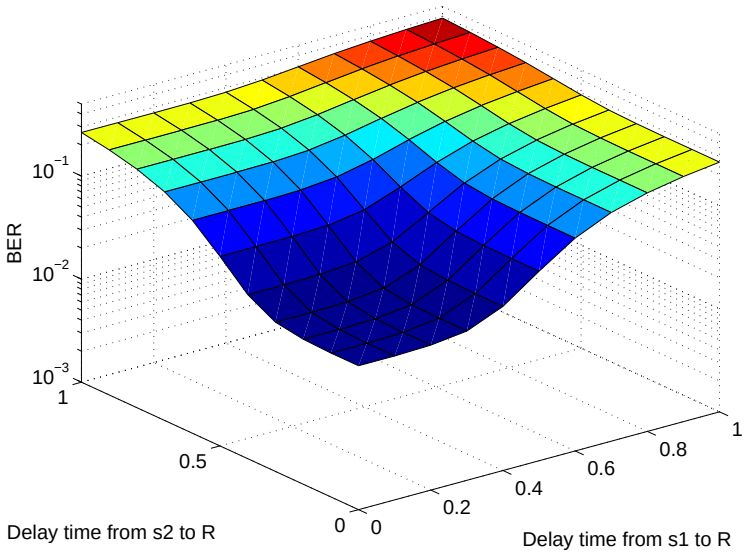

Figure 3.4: BER at S_1 in a DNC system with time synchronization error for different values of D_1 (x-axis) and D_2 (y-axis). ($D_{r1} = 0.4$, $A_{a1} = 1$, $A_{a2} = 1$, $E_b/N_0 = 10$ dB)

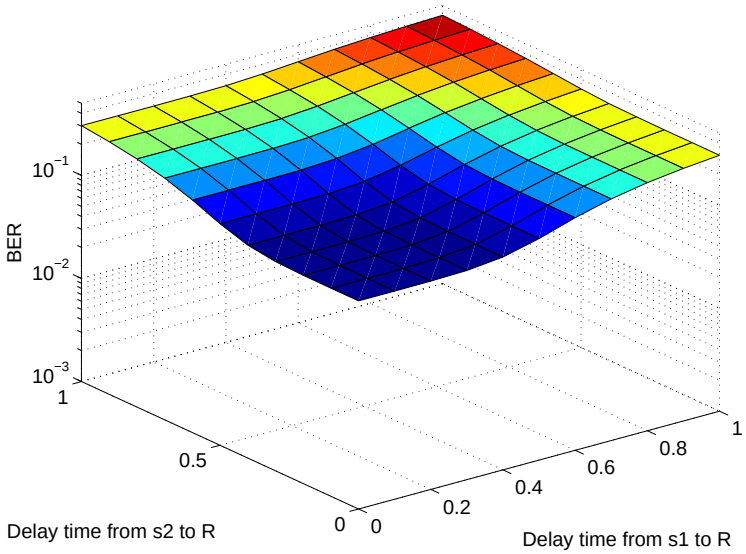

Figure 3.5: BER at S_1 in a DNC system with time synchronization error for different values of D_1 (x-axis) and D_2 (y-axis). ($D_{r1} = 0.6$, $A_{a1} = 1$, $A_{a2} = 1$, $E_b/N_0 = 10$ dB)

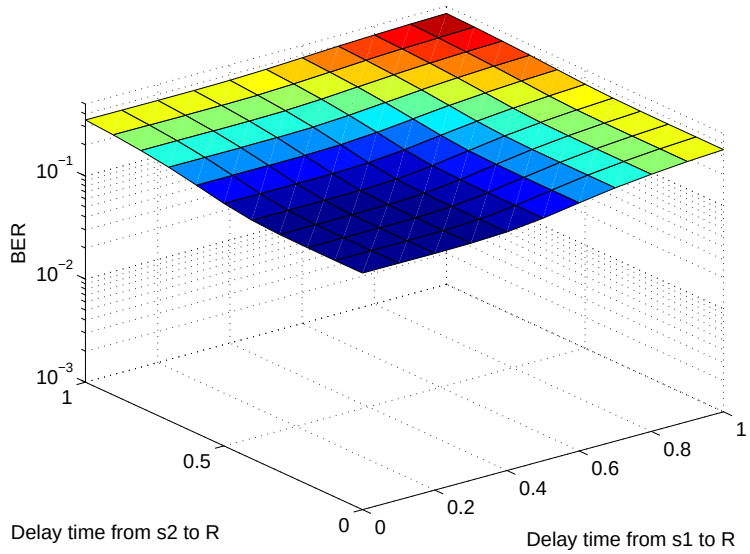

Figure 3.6: BER at S_1 in a DNC system with time synchronization error for different values of D_1 (x-axis) and D_2 (y-axis). ($D_{r1} = 0.8$, $A_{a1} = 1$, $A_{a2} = 1$, $E_b/N_0 = 10$ dB)

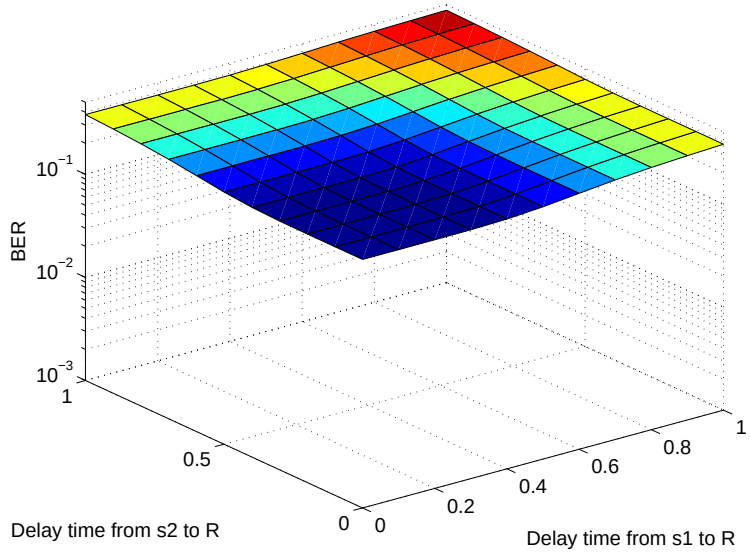

Figure 3.7: BER at S_1 in a DNC system with time synchronization error for different values of D_1 (x-axis) and D_2 (y-axis). ($D_{r1} = 1.0$, $A_{a1} = 1$, $A_{a2} = 1$, $E_b/N_0 = 10$ dB)

3.4.2 Effect of Received E_b/N_0

In order to characterize the effects of the received E_b/N_0, the received E_b/N_0 is varied from -4 dB to 14 dB. In this subsection, the received E_b/N_0 is assumed to be equal for all links.

The BER performance for different values of E_b/N_0, D_1, and D_2 in a DNC system with time synchronization error is shown in Figs. 3.8-3.10. In Fig. 3.8, it is assumed that $D_{r1} = 0$. In Fig. 3.9, it is assumed that $D_{r1} = 0.2$. In Fig. 3.10, it is assumed that $D_{r1} = 0.8$.

Based on these figures, we note that the performance degradation of the DNC system due to time synchronization errors can be significant. For example, as shown in Fig. 3.9, to achieve a BER of 10^{-3}, the required E_b/N_0 is 13 dB when $D_1 = 0$, $D_2 = 0$, and $D_{r1} = 0.2$. While in Fig. 3.10, to achieve a BER of 10^{-3}, the required E_b/N_0 is greater than 14 dB when $D_1 = 0$, $D_2 = 0$, and $D_{r1} = 0.8$.

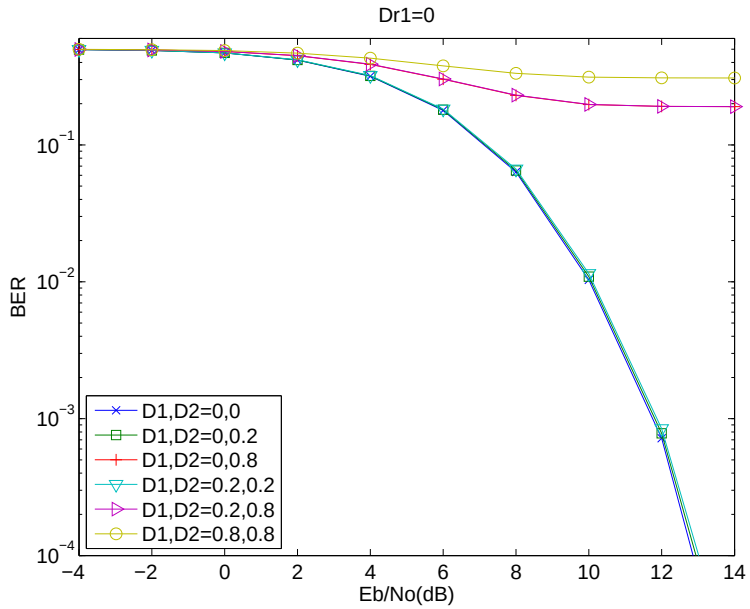

Figure 3.8: BER at S_1 in a DNC system with time synchronization error for different values of E_b/N_0 (x-axis) and D_1 and D_2 (as labeled). ($D_{r1} = 0$, $A_{a1} = 1$, $A_{a2} = 1$)

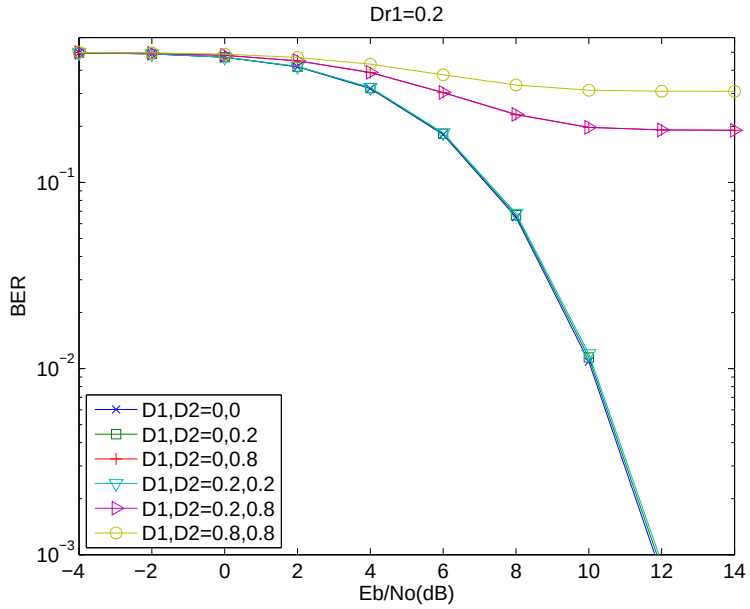

Figure 3.9: BER at S_1 in a DNC system with time synchronization error for different values of E_b/N_0 (x-axis) and D_1 and D_2 (as labeled).($D_{r1} = 0.2$, $A_{a1} = 1$, $A_{a2} = 1$)

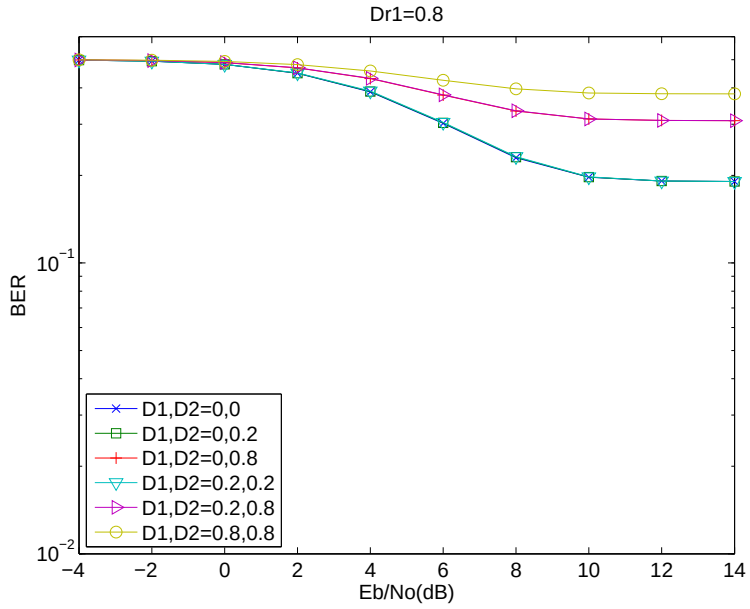

Figure 3.10: BER at S_1 in a DNC system with time synchronization error for different values of E_b/N_0 (x-axis) and D_1 and D_2 (as labeled). ($D_{r1} = 0.8$, $A_{a1} = 1$, $A_{a2} = 1$)

3.4.3 Effect of Unequal Link Quality

In order to describe the effects of unequal link quality, the BER performance with different values of A_{a1} and A_{a2} is investigated. Therefore, the received $(E_b/N_0)_{s1r}$ from S_1 to R, the received $(E_b/N_0)_{s2r}$ from S_2 to R, and the received $(E_b/N_0)_{rs1}$ from R to S_1 are assumed to be different. Note that due to the symmetry of the channel, $(E_b/N_0)_{s1r}$ and $(E_b/N_0)_{rs1}$ have the same value.

Three sets of $(E_b/N_0)_{s1r}$ are compared: $(E_b/N_0)_{s1r}$= 0 dB, 6 dB, 10 dB. The BER performance of equal link quality, which means $(E_b/N_0)_{s2r} = (E_b/N_0)_{s1r}$, is shown in Figs. 3.11-3.13. In Figs. 3.14-3.16, the BER performance of $(E_b/N_0)_{s2r} = (E_b/N_0)_{s1r}$+3 dB is shown. The values shown in the x-axis are $(E_b/N_0)_{s1r}$. Based on these figures, we note the following:

- In Figs. 3.11-3.13, while we vary one parameter among D_1, D_2, D_{r1} and fix the other two to be zero, the BER performance for equal link quality for the three figures is the same because the received E_b/N_0 value of all three links is the same. In other words, the delay of any link between S_1 to R, S_2 to R and R to S_1 have equal influence on BER performance in terms of equal link quality.

- Comparing Fig. 3.14 with Fig. 3.16, these two figures are the same. In other words, D_1 and D_{r1} have equal influence on BER performance since the received E_b/N_0 is the since $(E_b/N_0)_{s1r}$ equals to $(E_b/N_0)_{rs1}$.

- When $(E_b/N_0)_{s2r}$ is greater than $(E_b/N_0)_{s1r}$, D_1 has more influence on the BER performance than D_2. For example, in Fig. 3.14, the maximum D_1 is 0.2 in order to achieve a BER less than $8 * 10^{-3}$ for $(E_b/N_0)_{s1r} = 10$ dB and $D_2 = 0$. On the other hand, in Fig. 3.15, the maximum D_2 is 0.32 in order to achieve a BER less than $8 * 10^{-3}$ for $(E_b/N_0)_{s1r} = 10$ dB and $D_1 = 0$.

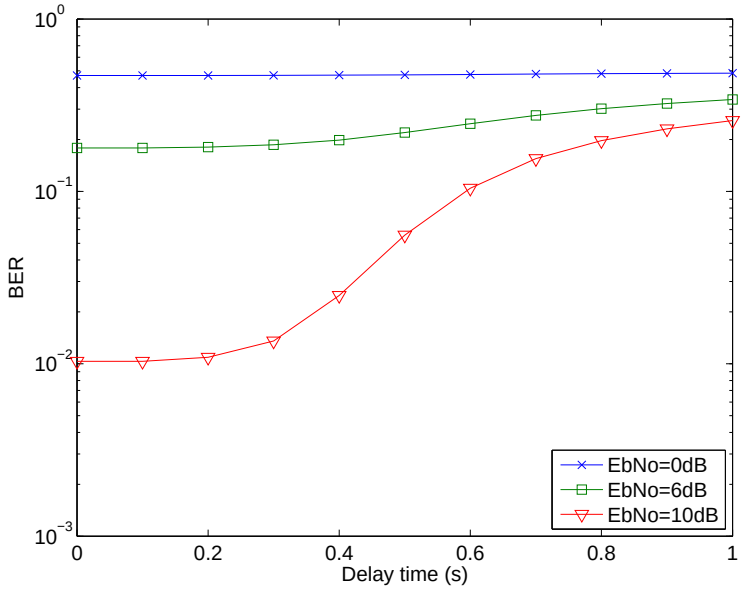

Figure 3.11: BER at S_1 in a DNC system with time synchronization error for different values of D_1 (x-axis) and $(E_b/N_0)_{s1r}$ (as labeled). ($D_2 = 0$, $D_{r1} = 0$, $(E_b/N_0)_{s2r} = (E_b/N_0)_{s1r}$)

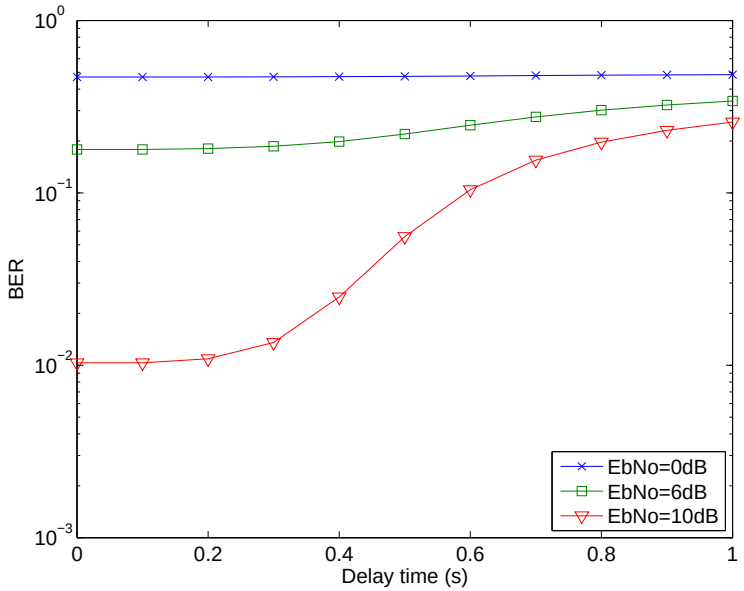

Figure 3.12: BER at S_1 in a DNC system with time synchronization error for different values of D_2 (x-axis) and $(E_b/N_0)_{s1r}$ (as labeled). ($D_1 = 0$, $D_{r1} = 0$, $(E_b/N_0)_{s2r} = (E_b/N_0)_{s1r}$)

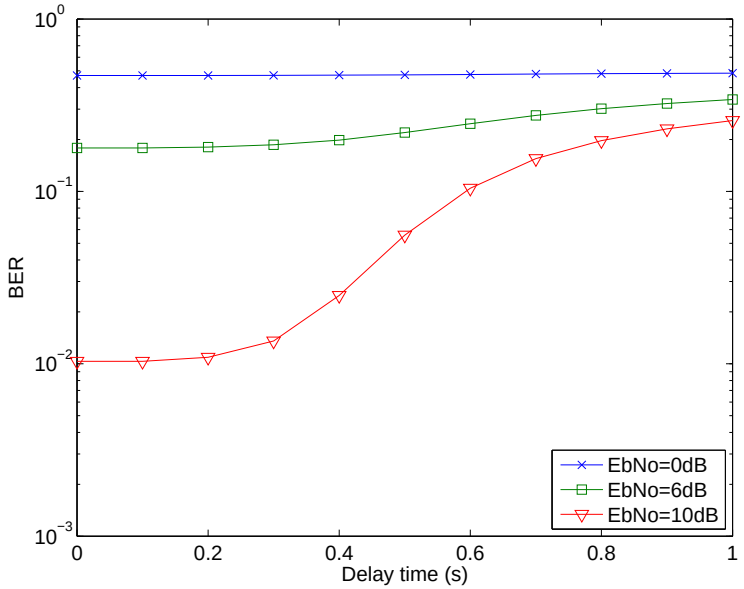

Figure 3.13: BER at S_1 in a DNC system with time synchronization error for different values of D_{r1} (x-axis) and $(E_b/N_0)_{s1r}$ (as labeled). ($D_1 = 0$, $D_2 = 0$, $(E_b/N_0)_{s2r} = (E_b/N_0)_{s1r}$)

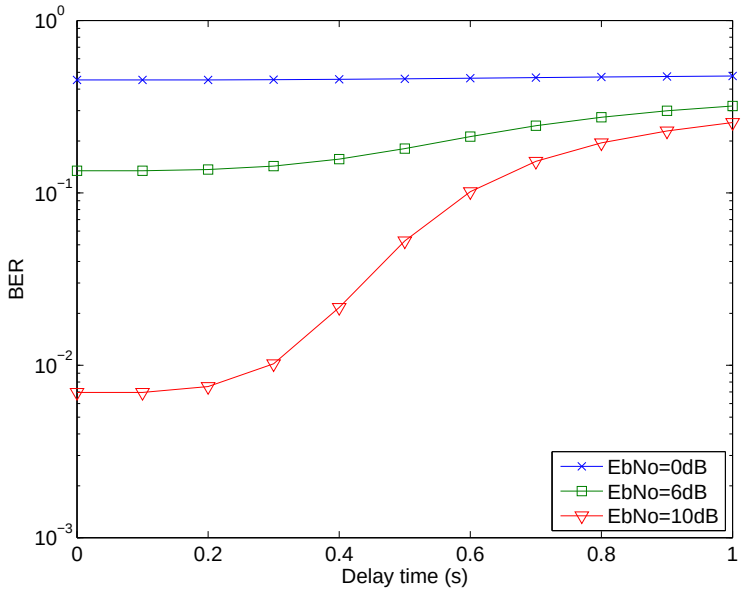

Figure 3.14: BER at S_1 in a DNC system with time synchronization error for different values of D_1 (x-axis) and $(E_b/N_0)_{s1r}$(as labeled). ($D_2 = 0$, $D_{r1} = 0$, $(E_b/N_0)_{s2r} = (E_b/N_0)_{s1r} + 3$ dB)

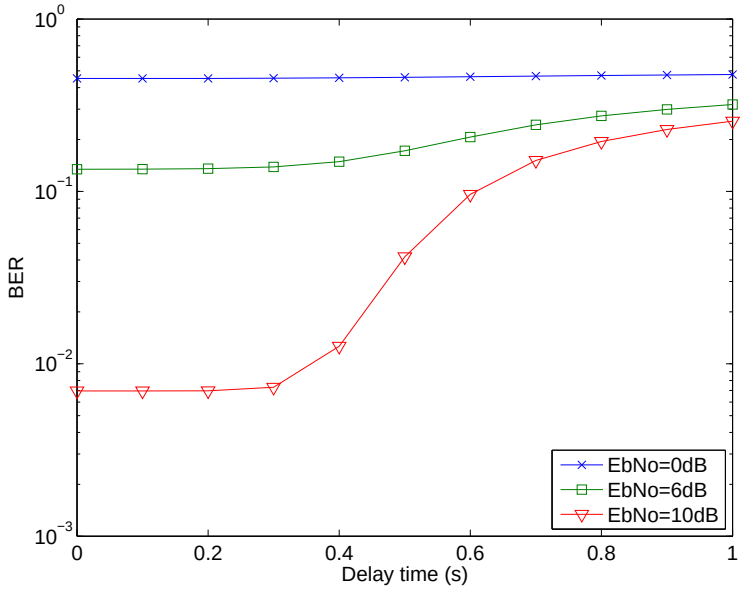

Figure 3.15: BER at S_1 in a DNC system with time synchronization error for different values of D_2 (x-axis) and $(E_b/N_0)_{s1r}$ (as labeled). ($D_1 = 0$, $D_{r1} = 0$, $(E_b/N_0)_{s2r} = (E_b/N_0)_{s1r} + 3$ dB)

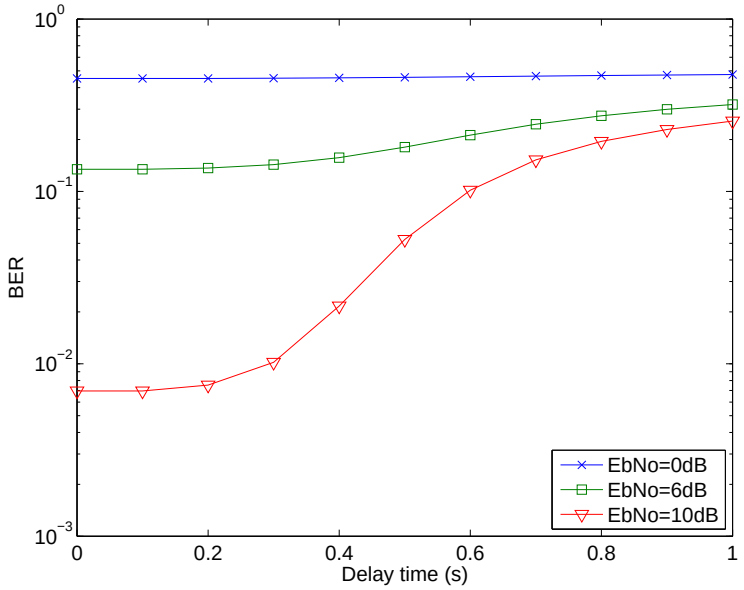

Figure 3.16: BER at S_1 in a DNC system with time synchronization error for different values of D_{r1} (x-axis) and $(E_b/N_0)_{s1r}$ (as labeled). ($D_1 = 0$, $D_2 = 0$, $(E_b/N_0)_{s2r} = (E_b/N_0)_{s1r} + 3$ dB)

3.5 Optimal Non-coherent Detection of FSK signals in a PNC System

In this section, we discuss the non-coherent detection of FSK signals in a PNC system with time synchronization errors. We begin our study by deriving the optimal non-coherent detector. Then the BER performance is evaluated via simulation due to the complexity of determining the pdf of the decision variable. Due to the symmetry of the communication flows in the two opposite directions, only the BER performance at S_1 is discussed. The results are also applicable to that of S_2.

As described in the system model, the transmission in a PNC system consists of two phases: the transmission from S_1 to R and the transmission from S_2 to R in the first time slot, and the transmission from R to S_1 (or S_2) in the second time slot. Therefore, a bit error occurs at S_1 if one of the following two events happens:

1. A bit error occurs in the estimate of $\hat{a}[n]$ after the first time slot and no bit error occurs in the link from R to S_1 in the second time slot.

2. No bit error occurs in the estimate of $\hat{a}[n]$ after the first time slot and a bit error occurs in the link from R to S_1 in the second time slot.

That is, the BER at S_1, after the second time slot, is equal to

$$Pe_{S_1} = Pe_{rs1}(1 - Pe_r) + (1 - Pe_{rs1})Pe_r, \tag{3.42}$$

where Pe_{rs1} is the BER at S_1 of the transmission from R to S_1 (second time slot) and Pe_r is the BER at R after $\hat{a}[n]$ is decoded (first time slot).

The optimal receiver for binary non-coherent FSK signals [48] is used to decode the signal received at S_1 in the second time slot. For the signal received at R in the first time slot, an optimal detector for non-coherent BFSK in a PNC system is used. We derive it based on the

detector of binary non-coherent CPFSK in a PNC system proposed in [25]. Note that when deriving the optimal detector, the timing error is assumed to be zero for all links. After the optimal detector is presented, we discuss the effect of time synchronization error on the BER performance via simulation.

The equivalent low-pass signal waveforms transmitted by S_1, S_2, or R is

$$s(t) = \sqrt{\frac{1}{T}} \sum_{k=0}^{N-1} e^{2\pi \Delta f(a[k]+1)t} g(t - kT). \tag{3.43}$$

The received signal $r(t)$ at R is

$$r(t) = A_{a1} s_1(t) e^{j\phi_1} + A_{a2} s_2(t) e^{j\phi_2} + z(t), \tag{3.44}$$

where $z(t) = n_c(t) + j n_s(t)$ is the additive Gaussian noise and

$$s_1(t) = \sqrt{\frac{1}{T}} \sum_{k=0}^{N-1} e^{2\pi \Delta f(a_1[k]+1)t} g(t - kT), \tag{3.45}$$

$$s_2(t) = \sqrt{\frac{1}{T}} \sum_{k=0}^{N-1} e^{2\pi \Delta f(a_2[k]+1)t} g(t - kT). \tag{3.46}$$

For the optimal detector, the decision rule of the detector at R is

$$\Lambda(\hat{a}[n]) \underset{\hat{a}[n]=0}{\overset{\hat{a}[n]=1}{\gtrless}} 0, \tag{3.47}$$

where $\Lambda(\hat{a}[n])$ is the log-likelihood ratio given by

$$\begin{aligned} \Lambda(\hat{a}[n]) &= log \frac{P(\hat{a}[n]=1|\mathbf{y})}{P(\hat{a}[n]=0|\mathbf{y})} \\ &= log \frac{P(XOR(a_1[n],a_2[n])=1|\mathbf{y})}{P(XOR(a_1[n],a_2[n])=0|\mathbf{y})} \\ &= log \frac{P(a_1[n]=0,a_2[n]=1|\mathbf{y})+P(a_1[n]=1,a_2[n]=0|\mathbf{y})}{P(a_1[n]=0,a_2[n]=0|\mathbf{y})+P(a_1[n]=1,a_2[n]=1|\mathbf{y})}, \end{aligned} \tag{3.48}$$

where $\mathbf{y} = [y^U \; y^L]$ is the sampled output vector after the received signal is passed through the receiver shown in Fig. 3.17.

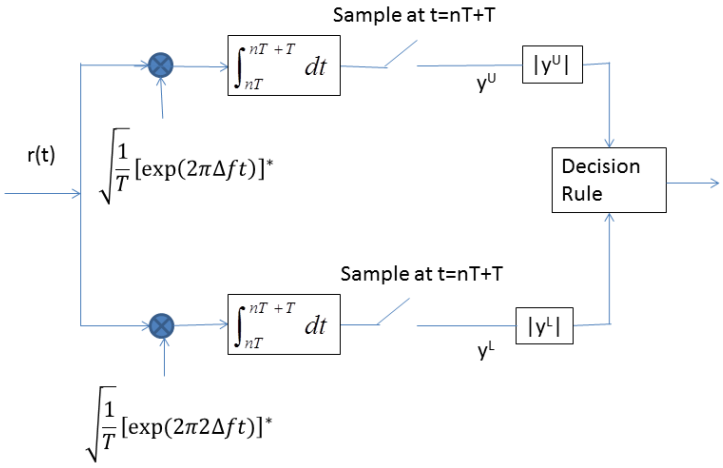

Figure 3.17: Optimal receiver of binary orthogonal baseband FSK signals in a PNC system.

When $a_1[n] = 0, a_2[n] = 1$, the output of the correlators at the sampling instant are given by [23]

$$\begin{aligned}
&y^U = \int_{nT}^{nT+T} r(t)\sqrt{\tfrac{1}{T}}e^{-2\pi\Delta ft}g(t-nT)dt \\
&= A_{a1}\int_{nT}^{nT+T} s_1(t)e^{j\phi_1}\sqrt{\tfrac{1}{T}}e^{-2\pi\Delta ft}g(t-nT)dt + A_{a2}\int_{nT}^{nT+T} s_2(t)e^{j\phi_2}\sqrt{\tfrac{1}{T}}e^{-2\pi\Delta ft}g(t-nT)dt \\
&+ \int_{nT}^{nT+T} n_c(t)\sqrt{\tfrac{1}{T}}e^{-2\pi\Delta ft}g(t-nT)dt + j\int_{nT}^{nT+T} n_s(t)\sqrt{\tfrac{1}{T}}e^{-2\pi\Delta ft}g(t-nT)dt \\
&= A_{a1}\int_{nT}^{nT+T} \sqrt{\tfrac{1}{T}}\textstyle\sum_{k=0}^{N-1} e^{2\pi\Delta ft}g(t-kT)e^{j\phi_1}\sqrt{\tfrac{1}{T}}e^{-2\pi\Delta ft}g(t-nT)dt \\
&+A_{a2}\int_{nT}^{nT+T} \sqrt{\tfrac{1}{T}}\textstyle\sum_{k=0}^{N-1} e^{2\pi\Delta f2t}g(t-kT)e^{j\phi_2}\sqrt{\tfrac{1}{T}}e^{-2\pi\Delta ft}g(t-nT)dt + n_{uc} + jn_{us} \\
&= A_{a1}e^{j\phi_1}\tfrac{1}{T}\int_{nT}^{nT+T} g(t-nT)g(t-nT)dt + 0 + n_{uc} + jn_{us} \\
&= A_{a1}\cos(\phi_1) + n_{uc} + j(A_{a1}\sin(\phi_1) + n_{us}) = A_{a1}e^{j\phi_1} + n_U,
\end{aligned} \tag{3.49}$$

and

$$\begin{aligned}
y^L &= \int_{nT}^{nT+T} r(t)\sqrt{\tfrac{1}{T}}e^{-2\pi\Delta 2ft}g(t-nT)dt \\
&= A_{a2}\cos(\phi_2) + n_{lc} + j(A_{a2}\sin(\phi_2) + n_{ls}) = A_{a2}e^{j\phi_2} + n_L,
\end{aligned} \tag{3.50}$$

where n_{uc}, n_{us}, n_{lc} and n_{ls} are four independent zero mean Gaussian variables with variance

N_0. By definition, $n_U = n_{uc} + jn_{us}$ and $n_L = n_{lc} + jn_{ls}$.

When $a_1[n] = 1$ and $a_2[n] = 0$, the output of the correlators at the sampling instant are [23]

$$\begin{aligned} y^U &= A_{a2}\cos(\phi_2) + n_{uc} + j(A_{a2}\sin(\phi_2) + n_{us}) = A_{a2}e^{j\phi_2} + n_U, \\ y^L &= A_{a1}\cos(\phi_1) + n_{lc} + j(A_{a1}\sin(\phi_1) + n_{ls}) = A_{a1}e^{j\phi_1} + n_L. \end{aligned} \tag{3.51}$$

When $a_1[n] = 0$ and $a_2[n] = 0$, the output of the correlators at the sampling instant are [23]

$$\begin{aligned} y^U &= A_{a1}\cos(\phi_1) + A_{a2}\cos(\phi_2) + n_{uc} + j(A_{a1}\sin(\phi_1) + A_{a2}\sin(\phi_2) + n_{us}) \\ &= A_{a1}e^{j\phi_1} + A_{a2}e^{j\phi_2} + n_U, \\ y^L &= n_{lc} + jn_{ls} = n_L. \end{aligned} \tag{3.52}$$

When $a_1[n] = 1$ and $a_2[n] = 1$, the output of the correlators at the sampling instant are [23]

$$\begin{aligned} y^U &= n_{uc} + jn_{us} = n_U, \\ y^L &= A_{a1}\cos(\phi_1) + A_{a2}\cos(\phi_2) + n_{lc} + j(A_{a1}\sin(\phi_1) + A_{a2}\sin(\phi_2) + n_{ls}) \\ &= A_{a1}e^{j\phi_1} + A_{a2}e^{j\phi_2} + n_L. \end{aligned} \tag{3.53}$$

For ease of presentation, y^U and y^L are expressed in a general form as

$$\begin{aligned} y^U &= A_U e^{j\theta_U} + n_U, \\ y^L &= A_L e^{j\theta_L} + n_L, \end{aligned} \tag{3.54}$$

where

$$A_U = \begin{cases} A_{a1} & a_1[n] = 0, a_2[n] = 1 \\ A_{a2} & a_1[n] = 1, a_2[n] = 0 \\ |A_{a1}e^{j\phi_1} + A_{a2}e^{j\phi_2}| & a_1[n] = 0, a_2[n] = 0 \\ 0 & a_1[n] = 1, a_2[n] = 1 \end{cases}, \tag{3.55}$$

$$\theta_U = \begin{cases} \phi_1 & a_1[n]=0, a_2[n]=1 \\ \phi_2 & a_1[n]=1, a_2[n]=0 \\ tan^{-1}\left(\frac{A_{a1}\sin(\phi_1)+A_{a2}\sin(\phi_2)}{A_{a1}\cos(\phi_1)+A_{a2}\cos(\phi_2)}\right) & a_1[n]=0, a_2[n]=0 \\ 0 & a_1[n]=1, a_2[n]=1 \end{cases}, \tag{3.56}$$

$$A_L = \begin{cases} A_{a2} & a_1[n]=0, a_2[n]=1 \\ A_{a1} & a_1[n]=1, a_2[n]=0 \\ 0 & a_1[n]=0, a_2[n]=0 \\ |A_{a1}e^{j\phi_1} + A_{a2}e^{j\phi_2}| & a_1[n]=1, a_2[n]=1 \end{cases}, \tag{3.57}$$

and

$$\theta_L = \begin{cases} \phi_2 & a_1[n]=0, a_2[n]=1 \\ \phi_1 & a_1[n]=1, a_2[n]=0 \\ 0 & a_1[n]=0, a_2[n]=0 \\ tan^{-1}\left(\frac{A_{a1}\sin(\phi_1)+A_{a2}\sin(\phi_2)}{A_{a1}\cos(\phi_1)+A_{a2}\cos(\phi_2)}\right) & a_1[n]=1, a_2[n]=1 \end{cases}. \tag{3.58}$$

Assuming that $a_1[n]$ and $a_2[n]$ are independent and equally likely to assume the values 0 and 1, the decision rule using Bayes rule is

$$\Lambda(\hat{a}[n]) = log\frac{p(\mathbf{y}|a_1[n]=0, a_2[n]=1) + p(\mathbf{y}|a_1[n]=1, a_2[n]=0)}{p(\mathbf{y}|a_1[n]=0, a_2[n]=0) + p(\mathbf{y}|a_1[n]=1, a_2[n]=1)}. \tag{3.59}$$

The conditional pdf $p(\mathbf{y}|a_1[n], a_2[n])$ is found by

$$p(\mathbf{y}|a_1[n], a_2[n]) = \frac{1}{2\pi}\int_0^{2\pi}\frac{1}{2\pi}\int_0^{2\pi} p(\mathbf{y}|a_1[n], a_2[n], \phi_1, \phi_2)d\phi_1 d\phi_2, \tag{3.60}$$

by assuming the phases ϕ_1 and ϕ_2 to be independent random variables uniformly distributed between 0 and 2π. Using the fact that $A_U e^{j\theta_U}$ and $A_L e^{j\theta_L}$ are given by the addition of two independent complex-valued, circularly-symmetric Gaussian random variable, we conclude that the phase of $A_U e^{j\theta_U}$ and $A_L e^{j\theta_L}$, which is denoted as θ_u and θ_l as shown in (3.54), are

i.i.d. uniformly distributed over $[0, 2\pi)$ [25]. The amplitude A_U is independent of the phase. As shown in [25], the conditional pdf $p(\mathbf{y}|a_1[n], a_2[n])$ is given by

$$\begin{aligned} p(\mathbf{y}|a_1[n], a_2[n]) &= \tfrac{1}{2\pi^2 N_0} \int_0^{2\pi} exp\left\{-\tfrac{|y^U - A_U e^{j\theta_u}|^2}{N_0}\right\} d\theta_u \\ &\times \tfrac{1}{2\pi^2 N_0} \int_0^{2\pi} exp\left\{-\tfrac{|y^L - A_L e^{j\theta_l}|^2}{N_0}\right\} d\theta_l, \end{aligned} \tag{3.61}$$

where

$$\tfrac{1}{2\pi} \int_0^{2\pi} exp\left\{-\tfrac{|y^U - A_U e^{j\theta_u}|^2}{N_0}\right\} d\theta_u = exp\left\{-\tfrac{|y^U|^2 + A_U^2}{N_0}\right\} I_0\left(\tfrac{2A_U|y^U|}{N_0}\right) \tag{3.62}$$

and

$$\tfrac{1}{2\pi} \int_0^{2\pi} exp\left\{-\tfrac{|y^L - A_L e^{j\theta_l}|^2}{N_0}\right\} d\theta_l = exp\left\{-\tfrac{|y^L|^2 + A_L^2}{N_0}\right\} I_0\left(\tfrac{2A_L|y^L|}{N_0}\right). \tag{3.63}$$

Substituting the four conditional pdfs $p(\mathbf{y}|a_1[n] = 0, a_2[n] = 1)$, $p(\mathbf{y}|a_1[n] = 1, a_2[n] = 0)$, $p(\mathbf{y}|a_1[n] = 0, a_2[n] = 0)$, and $p(\mathbf{y}|a_1[n] = 1, a_2[n] = 1)$ in (3.59), we have

$$\begin{aligned} \Lambda(\hat{a}[n]) &= log\left[e^{-\gamma_1} I_0\left(\tfrac{2|y^U|}{\sqrt{N_0/\gamma_1}}\right) e^{-\gamma_2} I_0\left(\tfrac{2|y^L|}{\sqrt{N_0/\gamma_2}}\right) + e^{-\gamma_1} I_0\left(\tfrac{2|y^U|}{\sqrt{N_0/\gamma_2}}\right) e^{-\gamma_2} I_0\left(\tfrac{2|y^L|}{\sqrt{N_0/\gamma_1}}\right)\right] \\ &- log\left[e^{-\gamma} I_0\left(\tfrac{2|y^U|}{\sqrt{N_0/\gamma}}\right) e^{-\gamma} I_0\left(\tfrac{2|y^L|}{\sqrt{N_0/\gamma}}\right)\right], \end{aligned} \tag{3.64}$$

where $\gamma_i = \frac{A_{ai}^2}{N_0}$ $(i = 1, 2)$ and $\gamma = \frac{A_{a1}^2 + A_{a2}^2}{N_0}$.

3.6 The Effects of System Parameters in a PNC System with Timing Errors

The effects of several system parameters in the performance of the considered PNC system are studied in this section via simulation. To gain insight into the BER performance, we consider the following three system parameters: ranges of timing errors, received E_b/N_0 values, and unequal link quality. Without loss of generality, it is assumed that $T = 1$.

3.6.1 Effect of Timing Errors

We first study the effect of timing errors in a PNC system with non-coherent FSK modulation. The other two system parameters are fixed and are discussed later.

The BER performance of a PNC system with time synchronization errors for different values of D_1, D_2 and D_{r1} is shown in Figs. 3.18-3.23. The received E_b/N_0 values from S_1 to R and from S_2 to R are taken to be 10 dB. Based on these figures, we note the following:

- As seen in Fig. 3.20, when the time synchronization error increases, the BER performance of the considered PNC system is greatly degraded, as expected.
- The BER performance of the considered PNC system gets significantly worse when time synchronization error is greater than 0.5 (i.e. $D_1 > 0.5$, $D_2 > 0.5$ and $D_{r1} > 0.5$). As shown in Figs. 3.21-3.23, the BER for any combination of values of D_1 and D_2 is greater than 0.01.

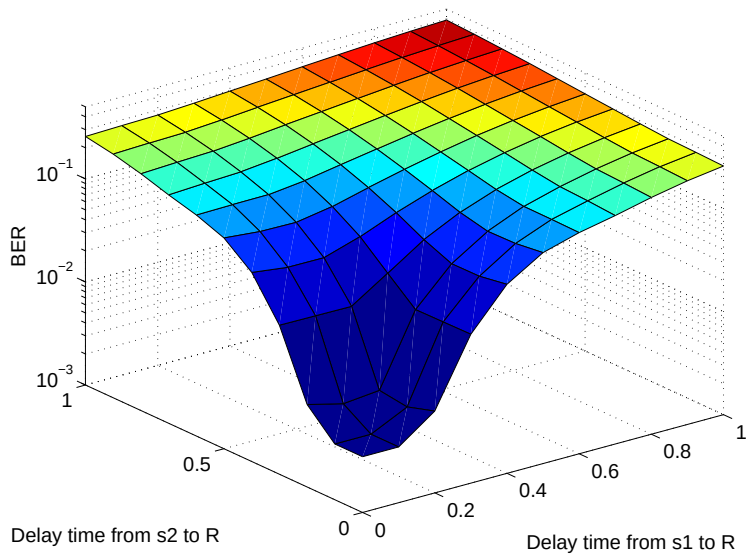

Figure 3.18: BER at S_1 in a PNC system with time synchronization error for different values of D_1 (x-axis) and D_2 (y-axis). ($D_{r1} = 0$, $A_{a1} = 1$, $A_{a2} = 1$, $E_b/N_0 = 10$ dB)

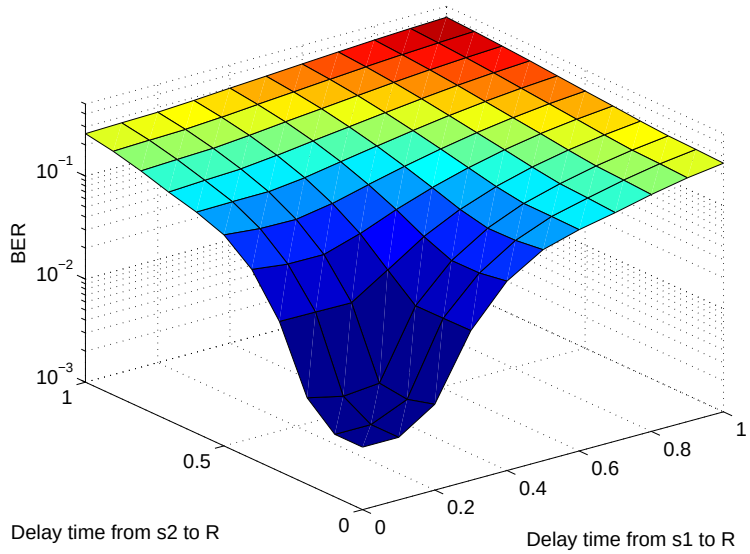

Figure 3.19: BER at S_1 in a PNC system with time synchronization error for different values of D_1 (x-axis) and D_2 (y-axis). ($D_{r1} = 0.2$, $A_{a1} = 1$, $A_{a2} = 1$, $E_b/N_0 = 10$ dB)

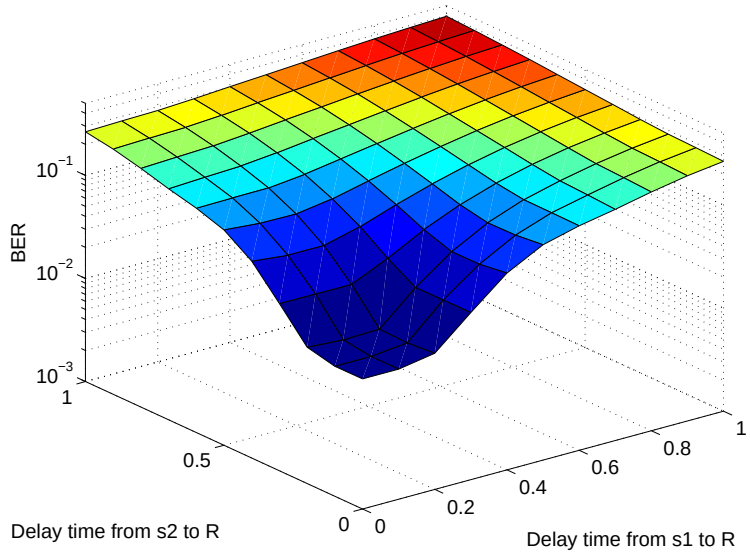

Figure 3.20: BER at S_1 in a PNC system with time synchronization error for different values of D_1 (x-axis) and D_2 (y-axis). ($D_{r1} = 0.4$, $A_{a1} = 1$, $A_{a2} = 1$, $E_b/N_0 = 10$ dB)

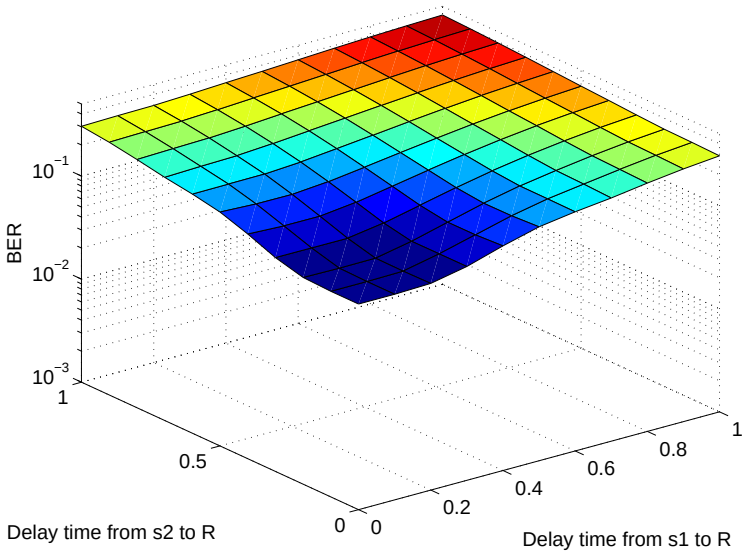

Figure 3.21: BER at S_1 in a PNC system with time synchronization error for different values of D_1 (x-axis) and D_2 (y-axis). ($D_{r1} = 0.6$, $A_{a1} = 1$, $A_{a2} = 1$, $E_b/N_0 = 10$ dB)

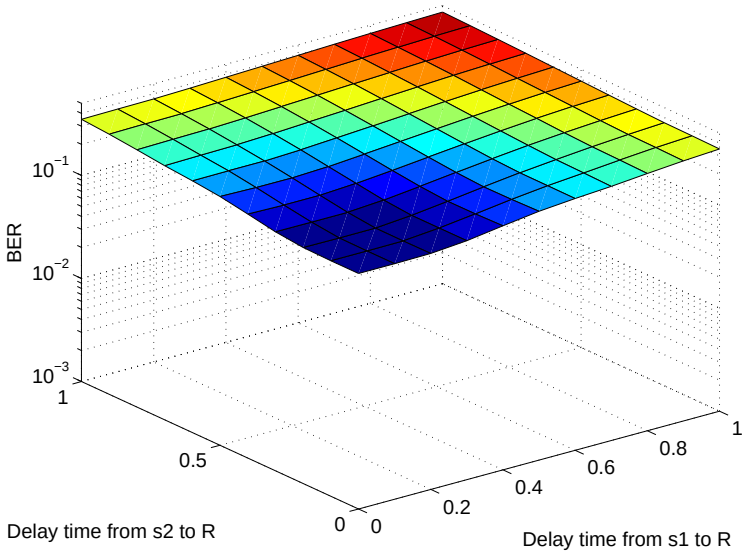

Figure 3.22: BER at S_1 in a PNC system with time synchronization error for different values of D_1 (x-axis) and D_2 (y-axis). ($D_{r1} = 0.8$, $A_{a1} = 1$, $A_{a2} = 1$, $E_b/N_0 = 10$ dB)

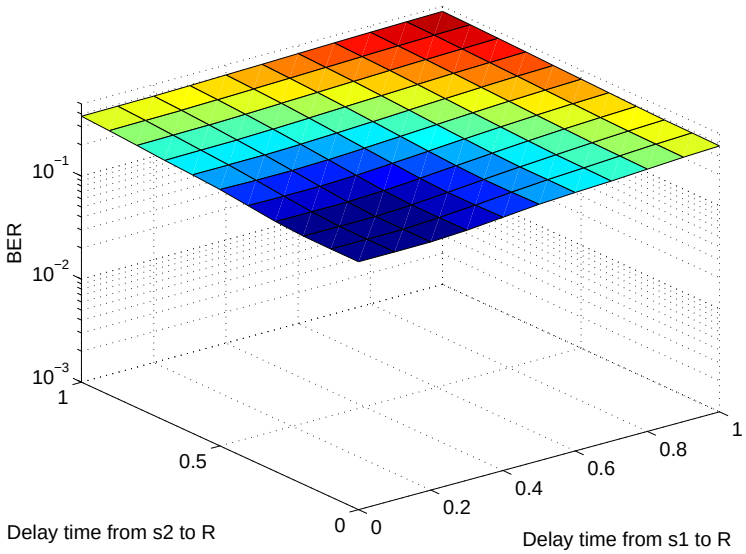

Figure 3.23: BER at S_1 in a PNC system with time synchronization error for different values of D_1 (x-axis) and D_2 (y-axis). ($D_{r1} = 1.0$, $A_{a1} = 1$, $A_{a2} = 1$, $E_b/N_0 = 10$ dB)

3.6.2 Effect of Received E_b/N_0

In order to describe the effects of the received E_b/N_0, the received E_b/N_0 is varied from -4 dB to 14 dB. In this subsection, equal link quality ($A_{a1} = 1$ and $A_{a2} = 1$) is assumed.

In Figs. 3.24-3.26, the BER performance for different values of E_b/N_0, D_1, and D_2 in a PNC system with time synchronization errors are given. In Fig. 3.24, it is assumed that $D_{r1} = 0$. In Fig. 3.25, it is assumed that $D_{r1} = 0.2$. In Fig. 3.26, it is assumed that $D_{r1} = 0.8$. Based on these figures, we note the following:

- As observed in Figs. 3.24-3.26, when the time synchronization error is large in any of the link from S_1 to R, S_2 to R or R to S_1, i.e. when $D_1 = 0.8$, $D_2 = 0.8$ or $D_{r1} = 0.8$, a significant decrease in BER is observed for all values of E_b/N_0.

- Comparing Fig. 3.25 with Fig. 3.9, when $D_1 \leq 0.2$, $D_2 \leq 0.2$ or $D_{r1} \leq 0.2$, the BER performance of PNC with time synchronization errors is better than that of DNC. For example, in Fig. 3.25, the required E_b/N_0 to achieve a BER of 10^{-3} is 11 dB for

$D_{r1} = 0.2$, $D_1 = 0$ and $D_2 = 0$ while in Fig. 3.9, the required E_b/N_0 to achieve a BER of 10^{-3} is 12 dB for $D_{r1} = 0.2$, $D_1 = 0$ and $D_2 = 0$.

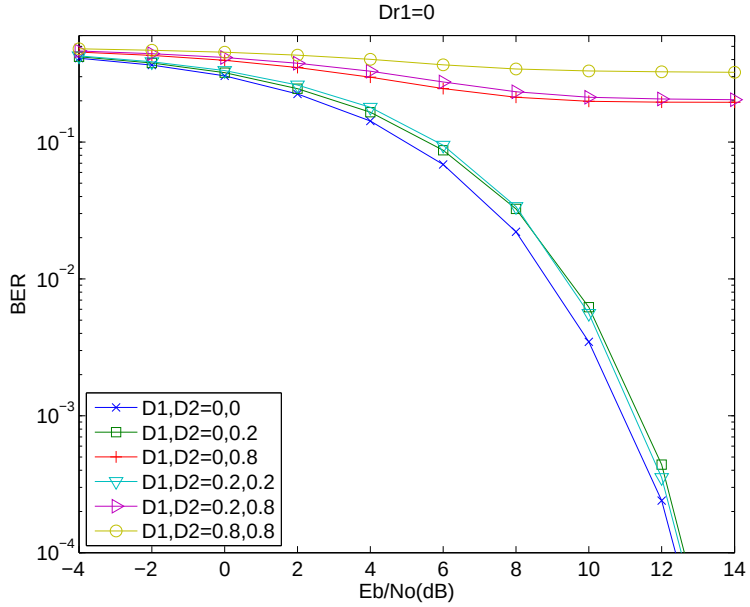

Figure 3.24: BER at S_1 in a PNC system with time synchronization error for different values of E_b/N_0 (x-axis) and D_1 and D_2 (as labeled). ($D_{r1} = 0$, $A_{a1} = 1$, $A_{a2} = 1$)

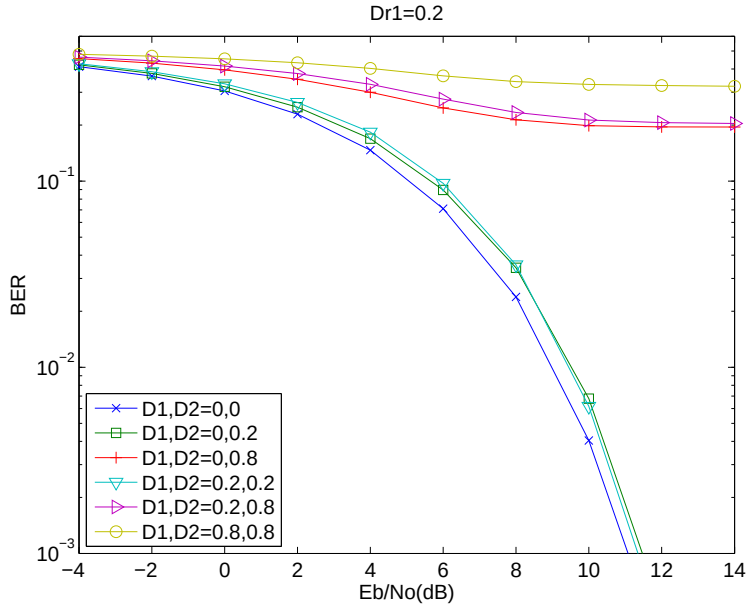

Figure 3.25: BER at S_1 in a PNC system with time synchronization error for different values of E_b/N_0 (x-axis) and D_1 and D_2 (as labeled).($D_{r1} = 0.2$, $A_{a1} = 1$, $A_{a2} = 1$)

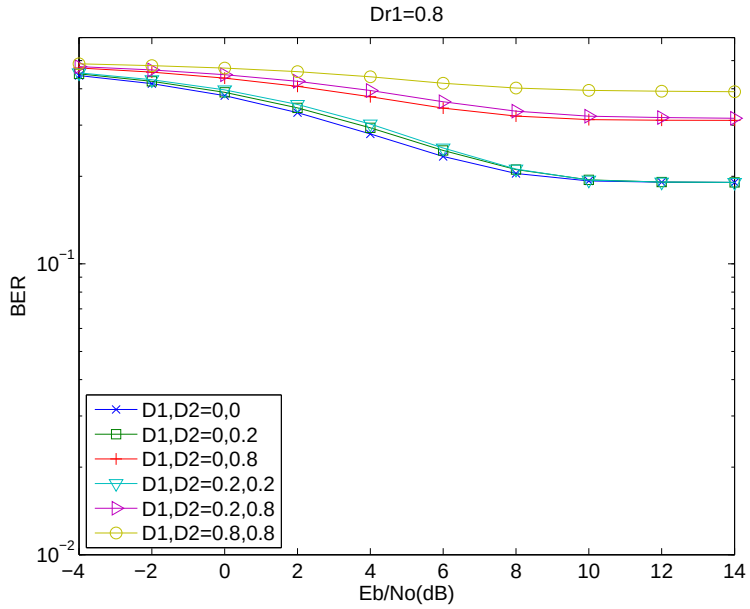

Figure 3.26: BER at S_1 in a PNC system with time synchronization error for different values of E_b/N_0 (x-axis) and D_1 and D_2 (as labeled). ($D_{r1} = 0.8$, $A_{a1} = 1$, $A_{a2} = 1$)

3.6.3 Effect of Unequal Link Quality

In order to describe the effects of unequal link quality, the BER performance with different values of A_{a1} and A_{a2} is investigated. Therefore, the received $(E_b/N_0)_{s1r}$ from S_1 to R, the received $(E_b/N_0)_{s2r}$ from S_2 to R, and the received $(E_b/N_0)_{rs1}$ from R to S_1 can be different. Note that due to the symmetry of the channel, $(E_b/N_0)_{s1r}$ and $(E_b/N_0)_{rs1}$ are the same.

Three values of $(E_b/N_0)_{s1r}$ are used: $(E_b/N_0)_{s1r}$ =0 dB, 6 dB, 10 dB. In Figs. 3.27-3.29, the BER performance of equal link quality, which means $(E_b/N_0)_{s2r} = (E_b/N_0)_{s1r}$, is shown. In Figs. 3.30-3.32, the BER performance of $(E_b/N_0)_{s2r} = (E_b/N_0)_{s1r}$+3 dB is shown. The values shown in the x-axis is $(E_b/N_0)_{s1r}$. Based on these figures, we note the following:

- In Figs. 3.27 and 3.28, when we fix D_{r1} and vary either D_1 or D_2, and fix the other to zero, the BER performance for equal link quality for the two figures is the same because the received E_b/N_0 value of all three links is the same. In other words, the delay of any link between S_1 to R and S_2 to R have equal influence on the final BER

performance.

- The BER performance is more sensitive to D_1 than to D_{r1} with equal link quality. In Fig. 3.27, D_2 and D_{r1} are fixed to zero and D_1 is varied. The maximum D_1 to achieve a BER lower than $5 * 10^{-3}$ is 0.18. In Fig. 3.29, D_1 and D_2 are fixed to zero and D_{r1} is varied. The maximum D_{r1} to achieve a BER lower than $5 * 10^{-3}$ is 0.25.

- Similarly, the BER performance is more sensitive to D_1 or D_2 than D_{r1} with unequal link quality. For example, in Fig. 3.30, D_2 and D_{r1} are fixed to zero and D_1 is varied. The maximum D_1 to achieve a BER lower than $5 * 10^{-3}$ is 0.12. In Fig. 3.31, D_1 and D_{r1} are fixed to zero and D_2 is varied. The maximum D_2 to achieve a BER lower than $5 * 10^{-3}$ is 0.21. In Fig. 3.32, D_1 and D_2 are fixed to zero and D_{r1} is varied. The maximum D_{r1} to achieve a BER lower than $5 * 10^{-3}$ is 0.25.

- When $(E_b/N_0)_{s2r}$ is greater than $(E_b/N_0)_{s1r}$, the BER performance is more sensitive to D_1 than D_2. For example, in Fig. 3.30, D_2 and D_{r1} are fixed to zero and D_1 is varied. The maximum D_1 to achieve a BER lower than $5 * 10^{-3}$ is 0.12. In Fig. 3.31, D_1 and D_{r1} are fixed to zero and D_2 is varied. The maximum D_2 to achieve a BER lower than $5 * 10^{-3}$ is 0.21.

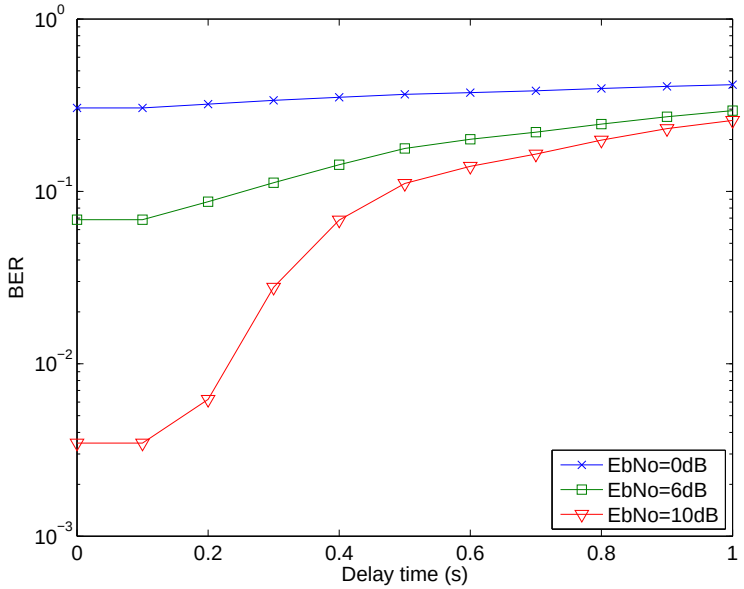

Figure 3.27: BER at S_1 in a PNC system with time synchronization error for different values of D_1 (x-axis) and and $(E_b/N_0)_{s1r}$ (as labeled). ($D_2 = 0$, $D_{r1} = 0$, $(E_b/N_0)_{s2r} = (E_b/N_0)_{s1r}$)

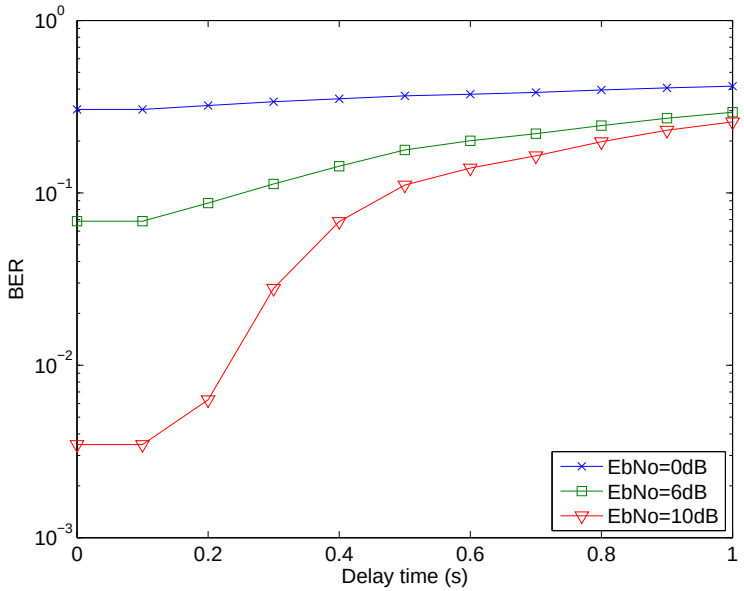

Figure 3.28: BER at S_1 in a PNC system with time synchronization error for different values of D_2 (x-axis) and and $(E_b/N_0)_{s1r}$ (as labeled). ($D_1 = 0$, $D_{r1} = 0$, $(E_b/N_0)_{s2r} = (E_b/N_0)_{s1r}$)

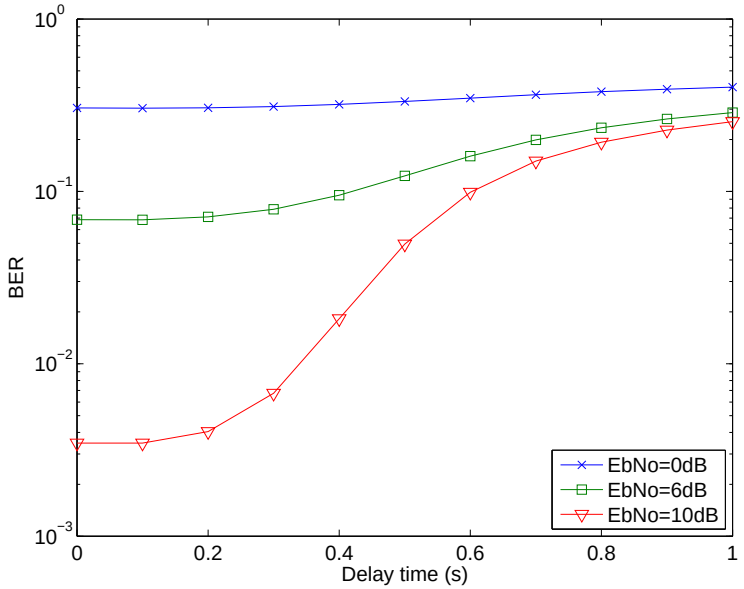

Figure 3.29: BER at S_1 in a PNC system with time synchronization error for different values of D_{r1} (x-axis) and and $(E_b/N_0)_{s1r}$ (as labeled). ($D_1 = 0$, $D_2 = 0$, $(E_b/N_0)_{s2r} = (E_b/N_0)_{s1r}$)

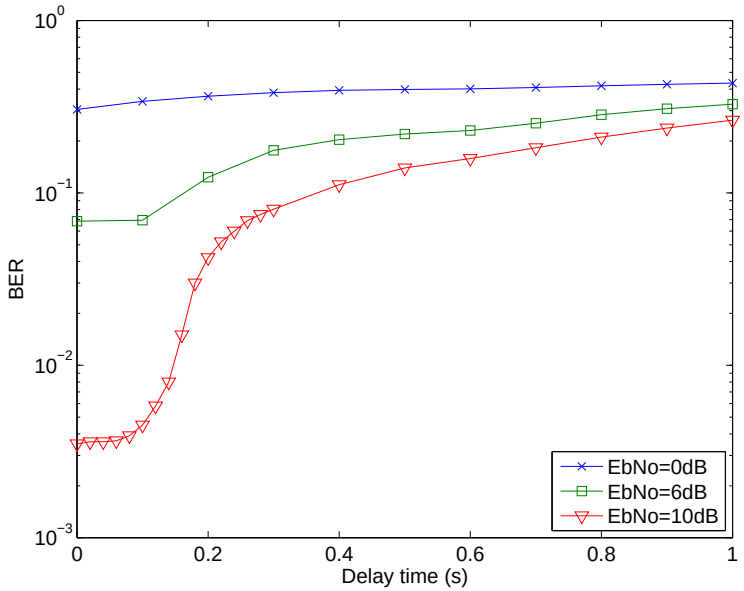

Figure 3.30: BER at S_1 in a PNC system with time synchronization error for different values of D_1 (x-axis) and and $(E_b/N_0)_{s1r}$(as labeled). ($D_2 = 0$, $D_{r1} = 0$, $(E_b/N_0)_{s2r} = (E_b/N_0)_{s1r}$+3 dB)

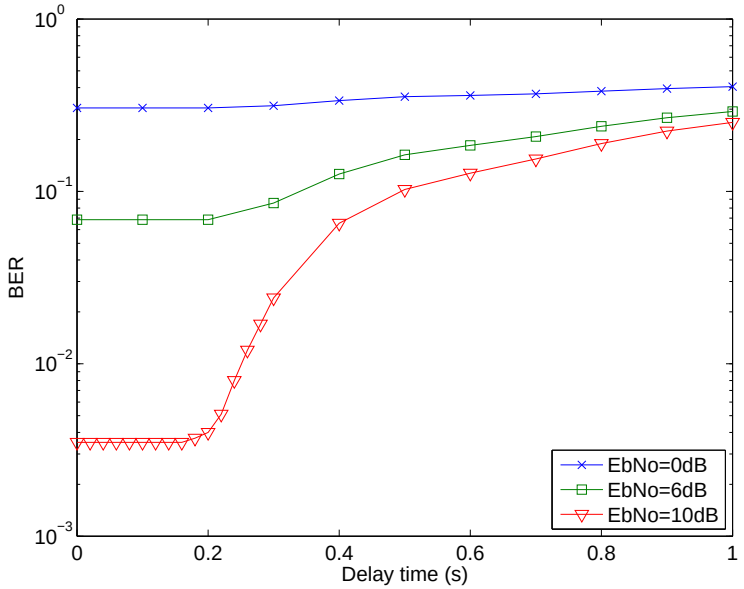

Figure 3.31: BER at S_1 in a PNC system with time synchronization error for different values of D_2 (x-axis) and and $(E_b/N_0)_{s1r}$ (as labeled). ($D_1 = 0$, $D_{r1} = 0$, $(E_b/N_0)_{s2r} = (E_b/N_0)_{s1r}$+3 dB)

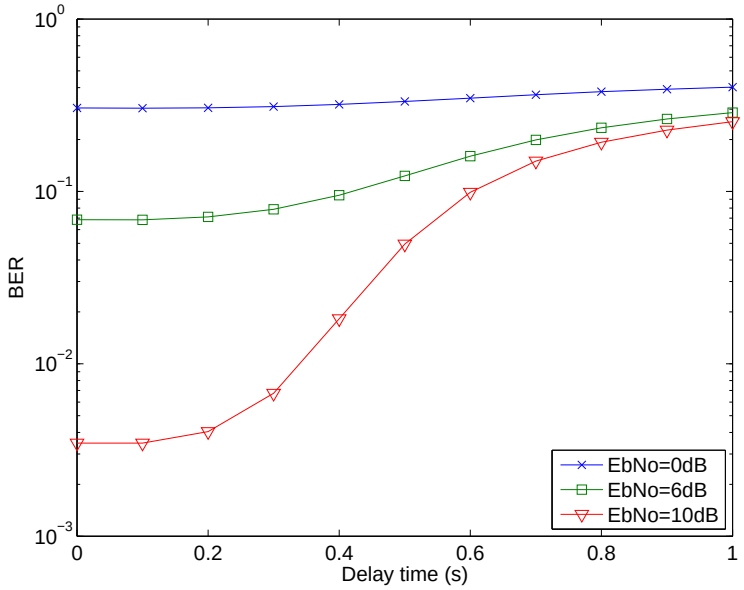

Figure 3.32: BER at S_1 in a PNC system with time synchronization error for different values of D_{r1} (x-axis) and and $(E_b/N_0)_{s1r}$ (as labeled). ($D_1 = 0$, $D_2 = 0$, $(E_b/N_0)_{s2r} = (E_b/N_0)_{s1r}$+3 dB)

3.7 Conclusions

In this chapter, we first analyzed the effect of timing errors on the BER performance of a DNC system with an optimal detector for non-coherent FSK signals. Using this analysis as a benchmark, we investigated the effect of timing errors on the BER performance of a PNC system with an optimal detector for non-coherent FSK signals. The main goal of this chapter was to understand the effects of timing errors, received E_b/N_0, and unequal link quality on the BER performance of DNC and PNC systems. From this study, we noted that:

- The BER performance of the considered DNC system is more sensitive to time synchronization errors on the link with worse quality.
- Similarly, the BER performance of the considered PNC system is more sensitive to time synchronization errors of the link with worse quality between S_1 to R and S_2 to R.
- The BER performance of the considered PNC system is more sensitive to time synchronization errors of the source to relay links than that of the relay to source link with both equal and unequal link quality.

Chapter 4

Value and Cost of Cognition For Resource Allocation Algorithms with Ideal and Non-ideal MAC Protocols

4.1 Introduction

CR is a radio that is aware of the spectrum environment, can learn from its environment, and adjust its transmission parameters for reliable transmission and efficient utilization of the radio spectrum [14]. The term "cognitive radio" was first introduced by Mitola in 1999 [27]. For a comprehensive review of the history of CR, the reader is referred to [28] and [14]. When used in an opportunistic/dynamic spectrum access scenario [29], CRs are able to "...determine which portions of the spectrum are available and detect the presence of licensed users when a user operates in a licensed band", "...select the best available channel", "...coordinate access to this channel with other users", and "...vacate the channel when a licensed user is detected" [30]. As a cognitive radio has the capability to select the best available channels, the next challenge is to efficiently allocate resources. In this work, we are

interested in the value and cost of cognition of different resource allocation algorithms.

In our work, resource allocation algorithms in OFDMA CR-based ad hoc networks are considered. Due to the infrastructureless nature of ad hoc networks, distributed resource allocation algorithms are investigated. A survey on distributed resource allocation algorithms suitable for such networks is provided in [31]. Also, a list of work on distributed algorithms based on the use of game theory [54] is given in [55].

Orthogonal frequency division multiplexing (OFDM) is an attractive technology for CR systems [56], [57] due to "...its flexibility in dynamically allocating radio resources to multiple users and its ability to reduce interference between adjacent subcarriers" [41]. Orthogonal frequency division multiple access (OFDMA) is "an extension of OFDM that exploits multiuser diversity and consequently, resource allocation, consisting of efficient subcarrier and power allocation, is essential in taking advantage of the benefits of OFDMA" [31]. Surveys of resource allocation algorithms for OFDMA networks are provided in [31], [58].

In CR-based ad hoc networks, given the variety of spectrum opportunities with different bandwidth and channel states, CRs first select channels and then perform power allocation. CRs select transmission channels by using a "pricing" function, which can be the channel "quality" (quantified in terms of signal-to-noise-plus-interference-ratio) [32]-[34], interference temperature [35]-[37], or some other pricing factor [38]-[40]. After the channels are selected, power is allocated with the goal of meeting the SINR requirement while minimizing interference to possible PUs. In [41], a distributed algorithm was proposed for allocating power and bits in multiuser OFDM-based wireless systems. Grace, Tozer, and Burr proposed that each link increase by using a function of the ratio of its initial observed interference and some predetermined interference threshold [35]. The subcarriers are allowed to be simultaneously shared by multiple users, and both the iterative water-filling algorithm and equal power allocation are considered. With a waterfilling power allocation algorithm [42]-[45], more power is allocated to better channels with low noise levels, so that the sum of data rates in channels is maximized [46]. It is shown in [47] that a water-filling algorithm can reach the optimal

allocation of power for a single user with a fixed allocation of subcarriers.

Three resource allocation algorithms with different levels of channel knowledge are proposed in the context of a CR-based ad hoc network. The value and cost of cognition of these algorithms are studied in terms of achieved effective data rate, power consumption, number of times that channel estimation and adaptations are performed, and convergence time when channel adaptation are necessary. Both an ideal MAC protocol and a non-ideal MAC protocol (dedicated control channel) are considered.

The system model is presented in Section 4.2. The proposed algorithms are described in Section 4.3. Simulation results and analysis on resource allocation algorithms are given in Section 4.4. A non-ideal MAC protocol scheme (DCC) is described in Section 4.5. In Section 4.6, the performances of the resource allocation algorithms with ideal and DCC protocols are compared. Finally, conclusions are drawn in Section 4.7.

4.2 System Model

In the proposed system model, the usable spectrum is divided into N orthogonal frequency channels with equal bandwidth B. U CR user pairs are randomly distributed in a given area. All CR user pairs have the same target data rate requirement of R_{target}. In order to achieve the data rate requirement, each CR user pair adaptively adjusts its transmission channels and transmission power by using a given resource allocation algorithm. Each CR user pair can only transmit in a fixed number of channels. The goal is to keep the sum of the data rates in each channel equal to R_{target} (it might be lower than R_{target} due to high interference levels, for example). Each CR can transmit with maximum total power P_{MAX} over all of its subchannels. Multiple CR user pairs are allowed to access the same channel, which might bring unwanted interference to other pairs. Multiple CR user pairs are also allowed to use the same control channel simultaneously as long as the SINR requirement for exchanging control information is met.

An M-QAM system is assumed. The maximum modulation order supported is $M_{max} = 2^{kmax}$, where k_{max} is the maximum number of bits/symbol supported by the users. The signal-to-interference-plus-noise ratio ($SINR_{req}$) required to achieve the target symbol error probability (SEP) is approximately given by [48]

$$SINR_{req} = \frac{M-1}{3}\left[Q^{-1}\left(\frac{SEP_{target}}{4}\right)\right]^2, \tag{4.1}$$

where M is the modulation order and $Q^{-1}(.)$ is the inverse Q function.

Perfect channel estimation and symmetric channels are assumed. Each channel has the same thermal noise floor. Signals transmitted through different channels experience independent and identically distributed Rayleigh fading. Using a path loss model, the received signal power is given by [53]

$$P_R = c_0 \frac{\alpha^2}{d_l^2} P_T, \tag{4.2}$$

where P_R is the received signal power, P_T is the transmitted signal power, c_0 is a constant $c_0 = \left(\frac{c}{4\pi f}\right)^2$, c is the speed light, f is the carrier frequency, d_l is the link distance, and α is the channel gain.

Two power allocation schemes are considered in our work, which are water-filling algorithm and equal power allocation algorithm. It is well-known that water-filling algorithm is the optimal solution to distributed a fixed total transmission power to a set of M additive white Gaussian noise (AWGN) channels, each of which may have a different noise power level [47]. The basic idea is that more power is allocated to channels with low noise levels and no power is allocated to channels on which the noise power exceeds a certain threshold (water level). In our system model, the interference from other CR users is modeled as Gaussian noise, which is an assumption commonly found in the literature [59]. Therefore, although we assume that all channels have the same noise level, the noise pulse interference level is acturally different. As shown in [44], the transmission power P_n using water-filling algorithm in the n-th ($n = 1, ..., M$) transmission channel of a CR user pair with a fixed total transmission

power P_{total} (P_{total} is initialized as P_{MAX}) is

$$P_n = \left[c_0 - T_n^{-1}\right]^+, \text{ where } [x]^+ = \begin{cases} x & \text{for } x > 0 \\ 0 & \text{else} \end{cases} \tag{4.3}$$

where the "water level" c_0 must be chosen such that $\sum_{n=1}^{M} P_n = P_{total}$, and T_n is defined as

$$T_n = \frac{|H_n|^2}{\sigma_n^2}, n = 1, ..., M, \tag{4.4}$$

where H_n is the channel gain coefficient of the n-th channel and σ_n^2 is the variance of the Gaussian noise.

Therefore, the data rate achieved in the n-th channel is given by

$$R_n = log_2\left(1 + \frac{3SINR_n}{\left[Q^{-1}(SEP_{target}/4)\right]^2}\right), \tag{4.5}$$

where $SINR_n$ is the SINR on the n-th channel. If $R_{total} = \sum_{n=1}^{M} R_n$ is smaller than R_{target}, then $P_{total} = P_{MAX}$ and the CR user pair transmits at maximum power. Otherwise, P_{total} is minimized under the constraint that $\sum_{n=1}^{M} R_n = R_{target}$.

For equal power allocation, the total transmission is equally distributed among all the transmission channels of a CR user pair. That is, the transmission power P_n in the n-th ($n = 1, 2, ..., M$) transmission channel of a CR user pair with a fixed total transmission power P_{total} is

$$P_n = \frac{P_{total}}{M}. \tag{4.6}$$

4.3 Description of the Proposed Allocation Algorithms

Before we analyze the value and cost of cognition of different resource allocation algorithms in a CR-based ad hoc network, three allocation algorithms A, B and C with different levels

of knowledge of channel states are proposed. In allocation algorithm A, channels are selected randomly and the power (and data rate) to be used in each channel is equally distributed. In allocation algorithm B, channels are selected randomly and a water-filling strategy is used for the allocation of the transmission power and data rate to be used in each channel. It should be noted that the SINR of the selected channels are estimated in order to perform the water-filling algorithm. Consequently, allocation algorithm B has a higher overhead than allocation algorithm A. In allocation algorithm C, channels are selected based on SINR and a water-filling strategy is used to allocate the transmission power and data rate to be used in each channel. The numbers of channels are chosen as 3, 6 and 12 channels for each user. If the target data rate is not satisfied, the different allocation algorithms adaptively adjust their channel assignment and power allocation, as explained next.

We begin the description of these three proposed allocation algorithms by first defining several terms which will be used in the descriptions that follows:

Effective data rate Effective data rate is the average number of bits transferred per second from a CR transmitter and accepted as valid by a CR receiver. Valid means the BER of the received bits is greater than some threshold; otherwise these bits are treated as error bits and the effective data rate is assumed to be zero.

The worse channel It is the channel with the lowest SINR among a group of channels.

The best channel It is the channel with the highest SINR among a group of channels.

In the allocation algorithm A, the current channels that do not meet the target data rate (for example, due to high interference) will be substituted. For example, each user selects z channels. If the target data rate in any channel is not satisfied in x channels among all the current channels, a CR user pair will randomly select x new channels and substitute them with the x old channels. However, since the x new channels are chosen randomly, it is possible that the target date rate is still not satisfied. In this case, a CR user pair will randomly select new channels in the next time slot again for those channels which do

not meet the target data rate. Note that the transmission power is always the maximum transmission power for allocation algorithm A.

In the allocation algorithm B, if the total target data rate is not satisfied, one new channel is randomly chosen and its SINR is estimated. In order to check whether using this new channel will improve the total effective data rate, channel estimations are also performed on all the channels currently in use by the CR user pair, and the worse channel among these channels will be substituted with the new channel if the new randomly chosen channel has a higher SINR than the *worst* channel. If not, channels are not substituted. If the total target date rate is still not satisfied after performing power allocation, a CR user pair continues to choose another new channel in the same time slot and repeats the same substitution procedure. This substitution procedure can be done at most z times, where z is the number of channels that each user transmits on. In other words, the maximum number of new channels allowed to be selected in one time slot is the total number of channels that one user transmits on.

In the allocation algorithm C, if the total target data rate is not met, channel estimation is performed on all the available channels and the best channel is selected. If this channel has not been selected by the CR user pair, the worst channel among the channels of a CR user pair will be substituted with this channel if this channel is better. If not, no channel substitution is performed in this time slot. If the total target date rate is still not satisfied after performing power allocation algorithms on the new set of current channels, the worst channel among the current channels will be substituted with the second best channel among all the channels if this channel is better and has not been used. This substitution procedure is performed at most z times, where z is the number of channels that each user transmits on.

4.4 Performance Analysis: Ideal MAC

In this section, an ideal MAC scheme, in which all the service requests are accepted and there is no collision on the control channel, is assumed. The numerical values used for the simulation are: number of available channels is 50, the area where users are randomly distributed is a square area of 200-by-200 meters, the target date rate for each user is R_{target} = 12kbps, the maximum transmission power for each user is 1W and the carrier frequency f for c_0 in (4.2) is 900MHz. To gain insight into the system performance, we consider the following three metrics: percentage of users reaching the target data rate, average effective data rate, and average power consumption.

4.4.1 Value of Cognition for Different Resource Allocation Algorithms

The percentage of users reaching the target data rate and the average effective data rate when allocation algorithms A, B and C are employed are shown in Fig. 4.1 for three numbers of channels per CR user pair. It is found that the algorithm with the higher effective data rate also has the highest percentage of users reaching the target data rate.

An interesting result is worth noting in Fig. 4.1(a)(b). For allocation algorithm A, when the number of users is smaller than 4 users, whether the number of channels for each user is 3, 6 or 12, the performance of percentage of users reaching the target data rate and the effective data rate is 100%. As the number of users increases for allocation algorithm A, fewer channels employed by each user are preferred, which is a behavior previously observed in [59]. This is due to the fact that the system is interference-limited when a large number of users are present and the system is noise-limited when the number of users is small. When the system is interference-limited, the best scenario would be the one in which each user would access orthogonal channels - in this case, the closest transmission model to this "ideal" scenario is the case in which users transmit on three channels only. For allocation

algorithm B and allocation algorithm C, the same result is observed as shown in Fig. 4.1.

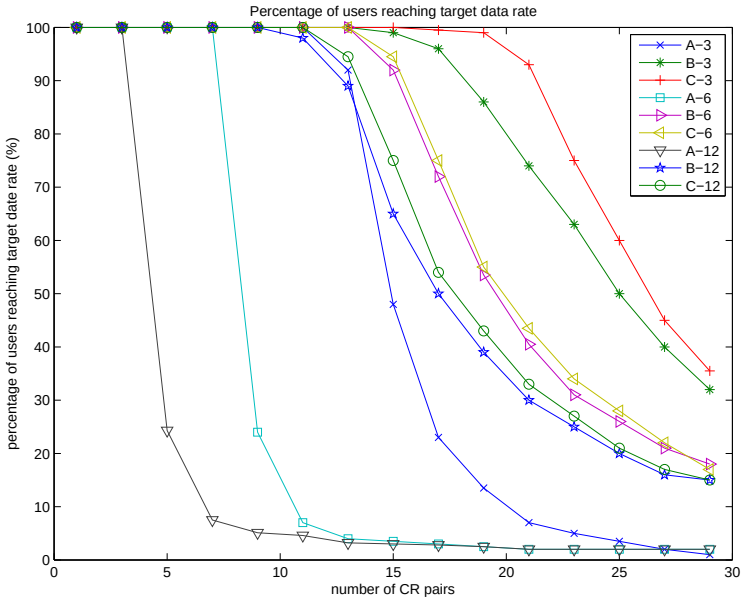

(a) Percentage of users reaching target data rate

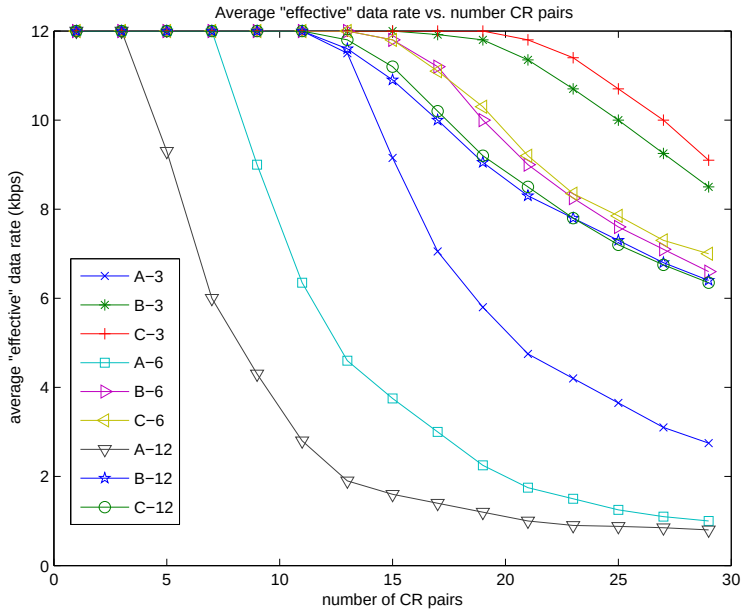

(b) Average effective data rate

Figure 4.1: Percentage of users reaching target data rate and average effective data rate for allocation algorithms A, B and C. The number of channels that one user employed for allocation algorithms A, B, and C is labeled as: A-3, A-6, A-12, B-3, B-6, B-12, C-3, C-6, and C-12. For example, A-3 means the number of channels that one user employed for allocation algorithm A is 3.

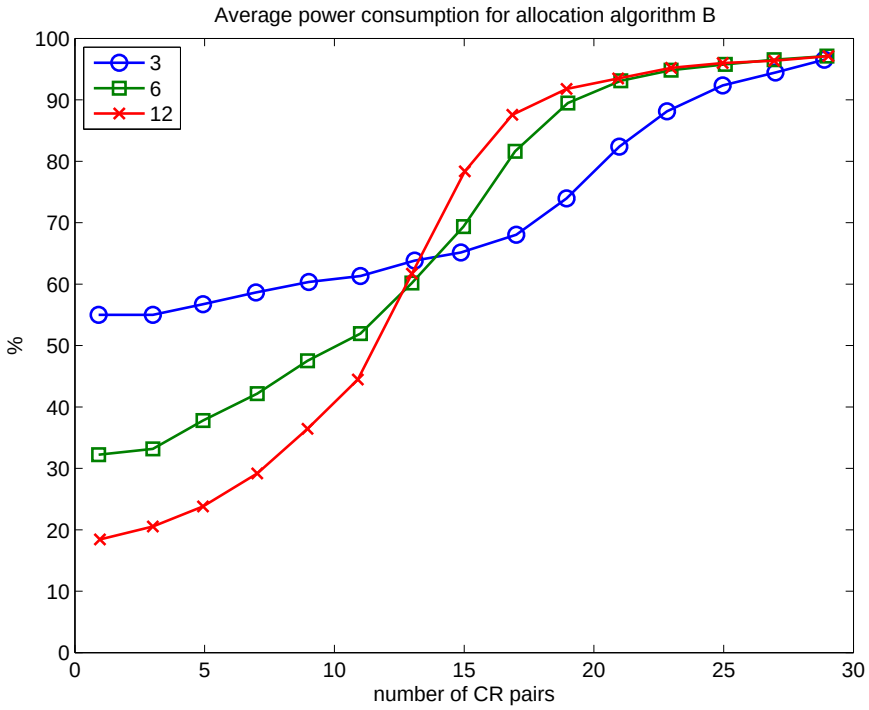

(a) Allocation algorithm B

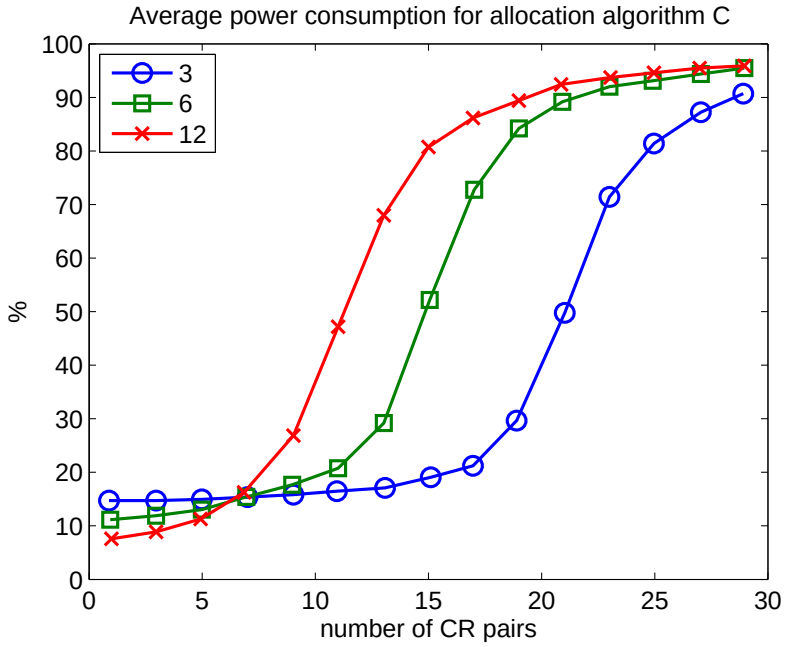

(b) Allocation algorithm C

Figure 4.2: Average power consumption. The average transmission power is shown as a percentage of the maximum transmission power. The number of channels that one user transmits on is labeled as: 3 (channels), 6 (channels), and 12 (channels).

As shown in Fig. 4.1, allocation algorithm B achieves a significantly higher effective data rate and percentage of users reaching the target data rate than algorithm A for all three numbers of channels per user. This is because algorithm B has a higher level of *awareness* of the channels, meaning that old channels are only substituted with new randomly chosen channels if the new channels have better "quality" (quantified in terms of SINR) than the old ones. Additionally, power is allocated proportionally to the SINR of a given channel by using water-filling algorithm. Therefore, the total effective data rate is greatly increased.

In Fig. 4.1, algorithm C achieves a higher data rate and percentage of users reaching the target data rate compared with algorithm B for all three numbers of channels per user. This is because algorithm C has a higher level of *awareness* than algorithm B. Algorithm C selects new channels by using their estimated SINR values.

The average power consumption per user of allocation algorithms B and C is given in Fig. 4.2. Note the average power consumption of allocation algorithm A is always P_{MAX}. In terms of the average power consumption per user, algorithm C consumes less transmission power than algorithm B for all three numbers of channels that one user transmits.

For allocation algorithm B, it is noted that when the system is noise-limited (when the number of CR pairs is small), the power consumption for 12 channels per CR user pair is the lowest compared with that for 3 and 6 channels per CR user pair. When the interference level increases due to the increase of number of CR user pairs in the system, fewer channels employed by each user are preferred. When the system is interference-limited, the scenario consuming least power is the case in which users transmit on three channels only. For allocation algorithm C, the same result is observed.

4.4.2 Cost of Cognition for Different Resource Allocation Algorithms

The average number of channel adaptations (number of channel changes) per time slot per CR user pair for algorithms A, B and C is shown in Figs. 4.3-4.5 for 6 channels and different numbers of CR user pairs.

From these figures, it is first noted that the number of channel adaptations increases when the number of users is large, especially for allocation algorithm A. Further, the low level of *awareness* of allocation algorithm A results in high cost of number of channel adaptations. Allocation algorithm B has lower cost in terms of channel adaptation than algorithm A, as seen by comparing Figs. 4.3 and 4.4. Also, by comparing Figs. 4.4 and 4.5, it is seen that algorithm C has slightly lower cost than algorithm B. For example, the average numbers of adaptations per user are 5.7, 3.3, and 2 for 29 CR user pairs in a network in the 2nd time slot for allocation algorithms A, B, and C, respectively.

As seen in Fig. 4.3, after 100 time slots, for allocation algorithm A, the number of adaptation does not converge to zero when the number of CR user pairs is greater than 5, which means the users are always making channel adaptations. For allocation algorithms B and C, as shown in Figs. 4.4 and 4.5, the number of adaptation converges to zero after 100 time slots for all numbers of CR user pairs. This is because allocation algorithms B and C have higher levels of *awareness* than allocation algorithm A. Allocation algorithm A selects the "new" channels randomly. Allocation algorithm B substitutes with new randomly selected channel only if they have better "quality". Allocation algorithm C estimates all the channels before choosing new channels. Also, the water-filling algorithm in allocation algorithms B and C will adaptively "fill" the chosen channels and it is more likely to achieve a higher data rate than algorithm A.

However, when a CR needs to substitute channels in allocation algorithms B and C, it first need to estimate the SINR of the channels. In order to compare the cost of algorithms B

and C, the average numbers of channel estimations for algorithms B and C are compared in Figs. 4.6(a) and (b). Since allocation algorithm A does not estimate the channel, its estimation number is zero. Channel estimations are performed when the total target data rate is not met, and there will be no channel adaptations if no better channels are found after channel estimations. Note that although algorithm C has a slightly higher data rate than algorithm B in Fig. 4.1, and approximately the same number of adaptations in Figs. 4.4 and 4.5, its number of channel estimations is more than 4 times greater than algorithm B.

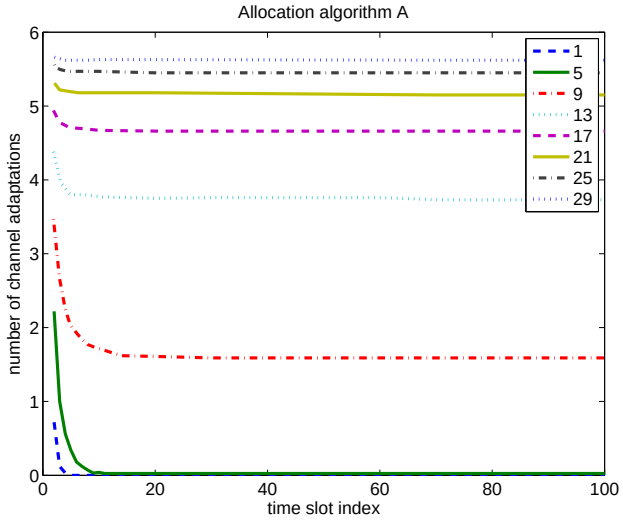

Figure 4.3: The average number of channel adaptations for algorithms A over 100 time slots. The number of channels that each CR user pair transmits on is 6. Number of CR user pairs is labeled as: 1, 5, 9...29.

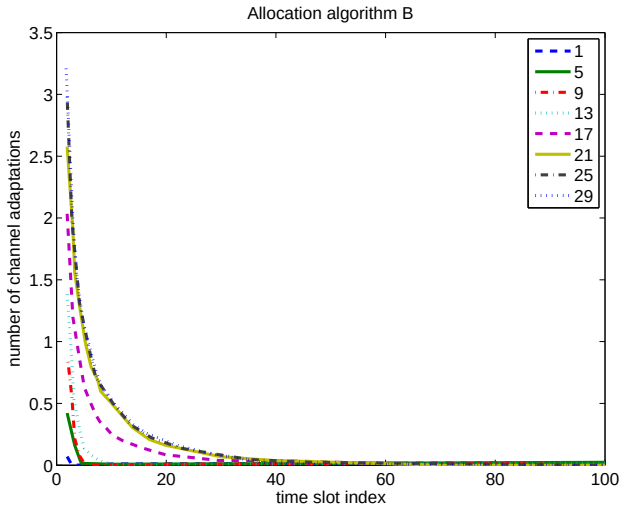

Figure 4.4: The average number of channel adaptations for algorithms B over 100 time slots. The number of channels that each CR user pair transmits on is 6. Number of CR user pairs is labeled as: 1, 5, 9...29.

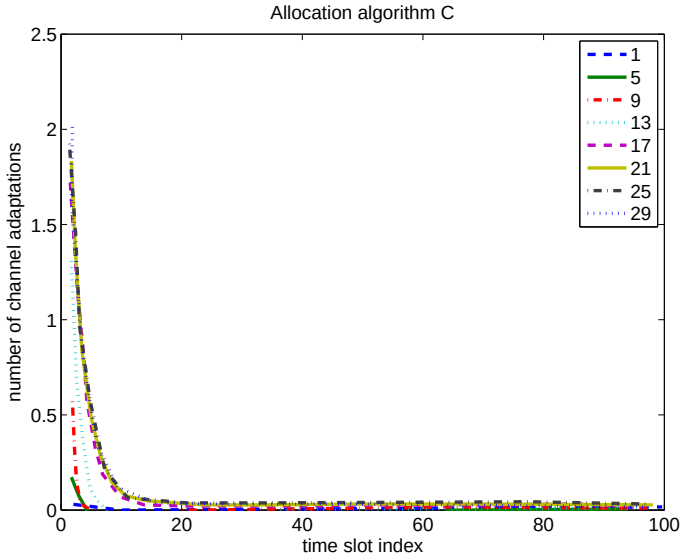

Figure 4.5: The average number of channel adaptations for algorithms C over 100 time slots. The number of channels that each CR user pair transmits on is 6. Number of CR user pairs is labeled as: 1, 5, 9...29.

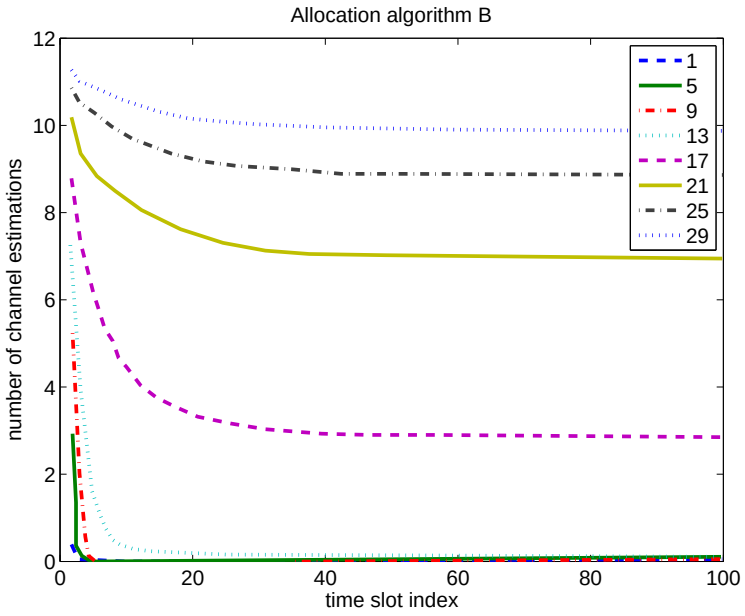

(a) Allocation algorithm B

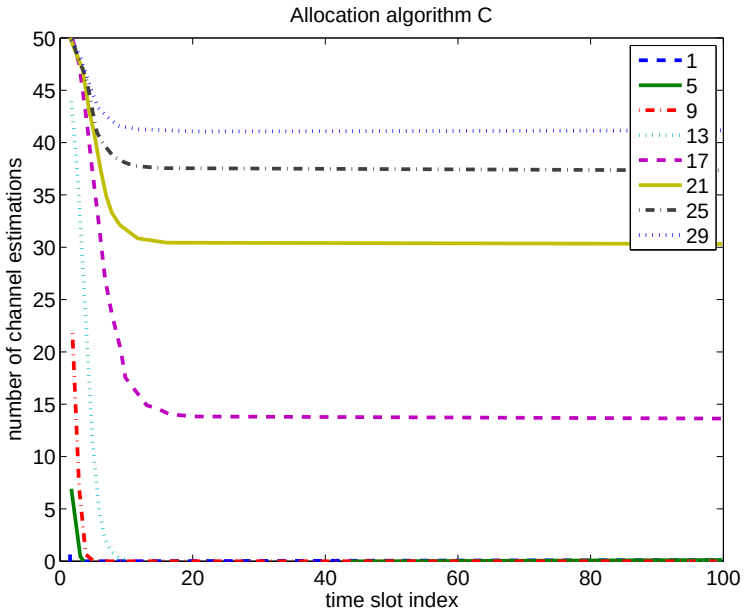

(b) Allocation algorithm C

Figure 4.6: Average number of channel estimations with 6 channels for algorithms B and C. Number of CR user pairs is labeled as: 1, 5, 9... 29.

4.4.3 The Primary User (PU) Detection Event

The network overhead when a PU is detected on one or more channels currently being used by a given CR is considered in this subsection. When a PU is detected, CR user pairs should stop transmitting on those channels and immediately vacate them. Two cases of primary user detection are studied. In the first case, a PU is detected on 5 channels in the 50-th time slot. The numbers of channel adaptations for allocation algorithms A, B and C are shown in Figs. 4.7-4.9, respectively. The numbers of channel estimations for allocation algorithms B and C are shown in Figs. 4.10 and 4.11, respectively. In the second case, a PU is detected on 20 channels in the 50-th time slot. The numbers of channel adaptations for allocation algorithms A, B and C are shown in Figs. 4.12-4.14, respectively. The numbers of channel estimations for allocation algorithms B and C are shown in Figs. 4.15 and 4.16, respectively.

As shown in Figs. 4.7-4.9, allocation algorithm A has the highest adaptation cost, algorithm B has the second highest adaptation cost, and algorithm C has the lowest adaptation cost when a PU is detected. For example, the average numbers of adaptations per user are 5.7, 0.7, and 0.6 for 29 CR user pairs in a network near the 50-th time slot for allocation algorithms A, B, and C, respectively.

As shown in Figs. 4.10 and 4.11, allocation algorithm C has a higher number of channel estimations than algorithm B when a PU is detected. For example, the average numbers of estimations per user are 10.7 and 48 for 29 CR user pairs in a network near the 50-th time slot for allocation algorithms B and C, respectively.

In Fig. 4.7, the number of channel adaptations for algorithm A grows at the 50-th time slot when the number of channels per user is greater than or equal to 9. This is because fewer channels are available and the interference level is therefore increased. In Figs. 4.8 and 4.9, the number of channel adaptations required for algorithm B and C drops close to zero after a few time slots. Note that it takes algorithm B approximately twice the time to converge compared with allocation algorithm C. The fast convergence is a very important feature in an ad-hoc network. If intentional interference occurs in the network, algorithm C recovers more

quickly than algorithm B. A faster convergence of algorithm C compared with algorithm B is also observed in Figs. 4.10 and 4.11. In Figs. 4.10 and 4.11, the number of channel estimations increase after the PU detection event because the interference level increases due to loss of channels. It takes algorithm B approximately twice the time to converge compared with algorithm C. Note for both algorithm B and algorithm C, the convergence time increases with the number of CR user pairs. When there are even fewer channels available in the network, the difference between algorithms A, B and C is more obvious, as illustrated in Figs. 4.12-4.16.

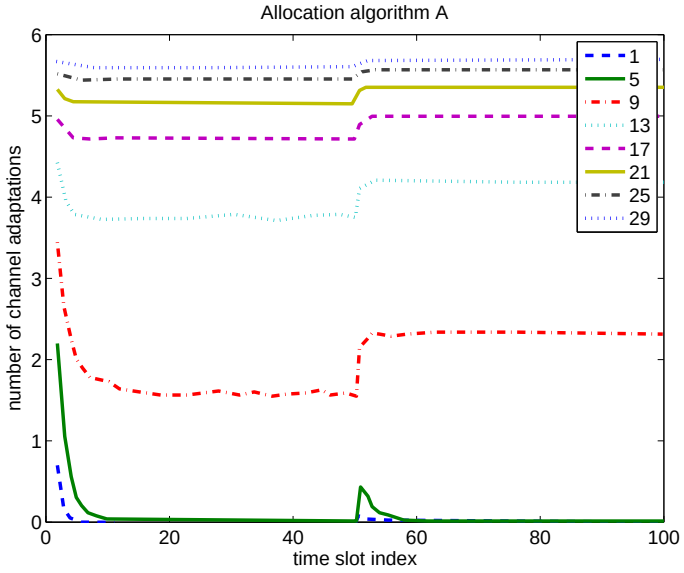

Figure 4.7: Average number of channel adaptations per user for allocation algorithm A after a PU is detected on 5 channels in the 50th time slot. Each CR user pair transmits on 6 channels. Number of CR user pairs is labeled as: 1, 5, 9... 29.

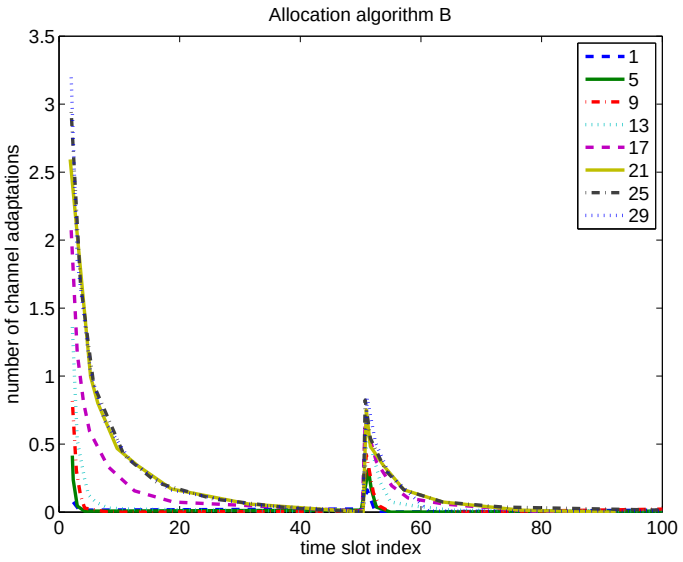

Figure 4.8: Average number of channel adaptations per user for allocation algorithm B after a PU is detected on 5 channels in the 50th time slot. Each CR user pair transmits on 6 channels. Number of CR user pairs is labeled as: 1, 5, 9... 29.

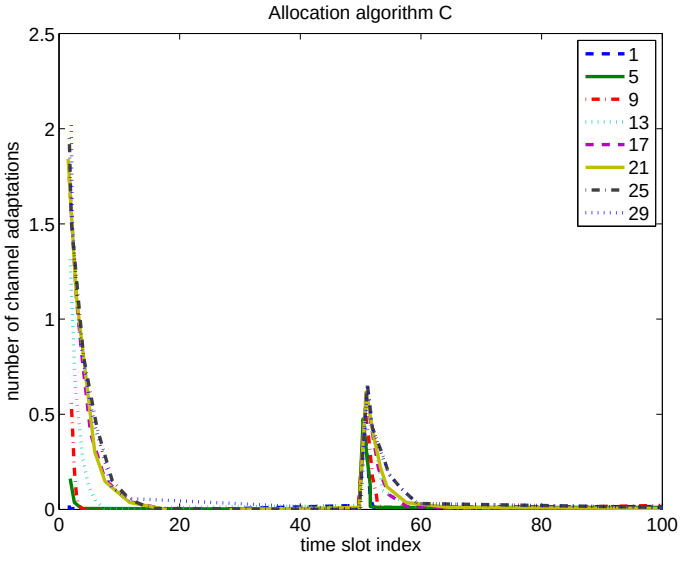

Figure 4.9: Average number of channel adaptations per user for allocation algorithm C after a PU is detected on 5 channels in the 50th time slot. Each CR user pair transmits on 6 channels. Number of CR user pairs is labeled as: 1, 5, 9... 29.

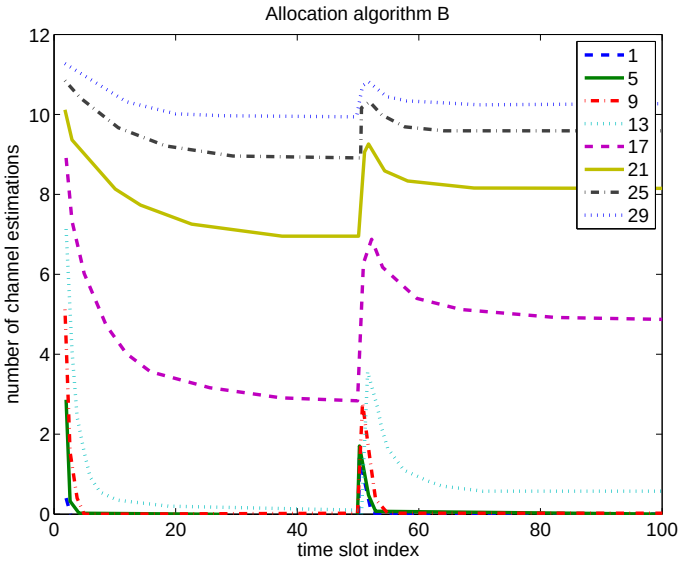

Figure 4.10: Average number of channel estimations per user for allocation algorithm B after a PU is detected on 5 channels in the 50th time slot. Each CR user pair transmits on 6 channels. Number of CR user pairs is labeled as: 1, 5, 9...29.

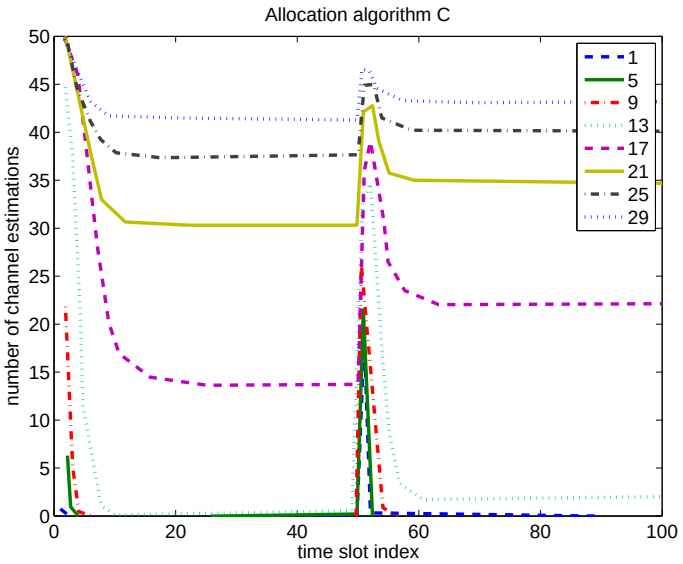

Figure 4.11: Average number of channel estimations per user for allocation algorithm C after a PU is detected on 5 channels in the 50th time slot. Each CR user pair transmits on 6 channels. Number of CR user pairs is labeled as: 1, 5, 9...29.

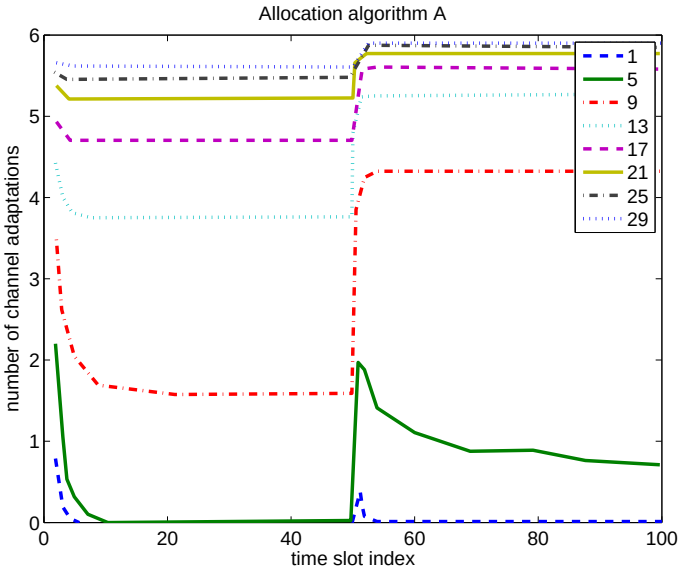

Figure 4.12: Average number of channel adaptations per user for allocation algorithm A after a PU is detected on 20 channels in the 50th time slot. Each CR user pair transmits on 6 channels. Number of CR user pairs is labeled as: 1, 5, 9...29.

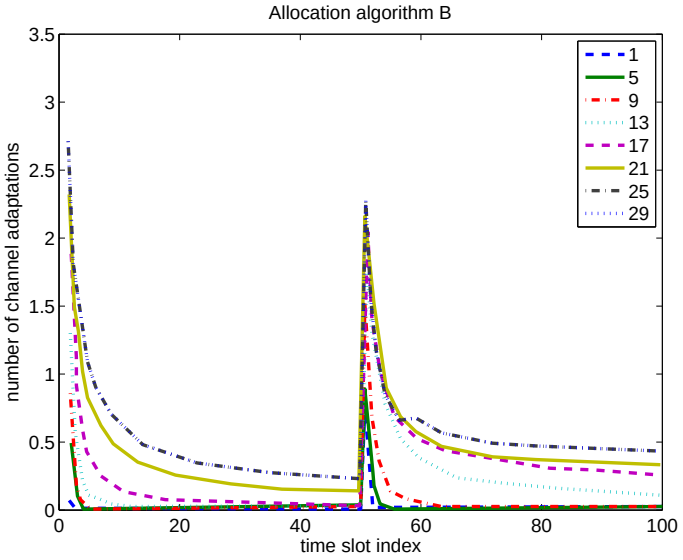

Figure 4.13: Average number of channel adaptations per user for allocation algorithm B after a PU is detected on 20 channels in the 50th time slot. Each CR user pair transmits on 6 channels. Number of CR user pairs is labeled as: 1, 5, 9...29.

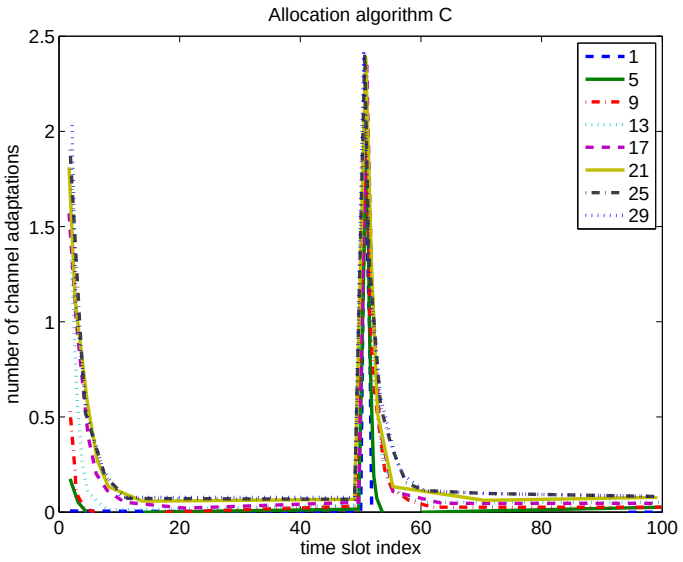

Figure 4.14: Average number of channel adaptations per user for allocation algorithm C after a PU is detected on 20 channels in the 50th time slot. Each CR user pair transmits on 6 channels. Number of CR user pairs is labeled as: 1, 5, 9...29.

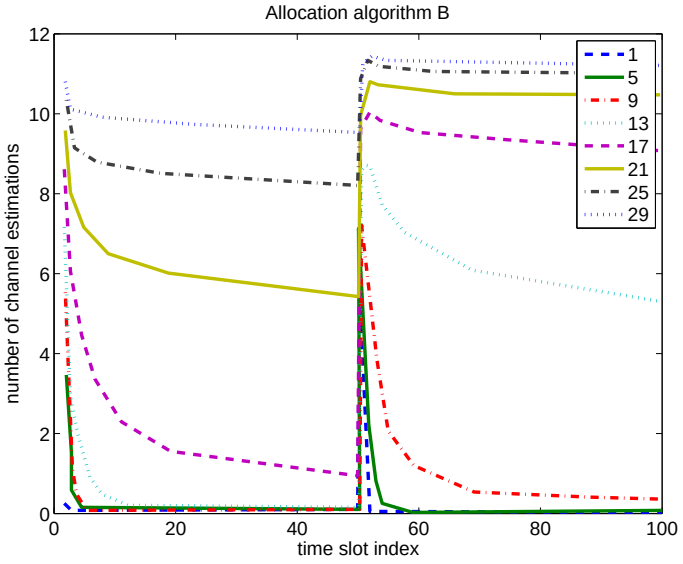

Figure 4.15: Average number of channel estimations per user for allocation algorithm B after a PU is detected on 20 channels in the 50th time slot. Each CR user pair transmits on 6 channels. Number of CR user pairs is labeled as: 1, 5, 9...29.

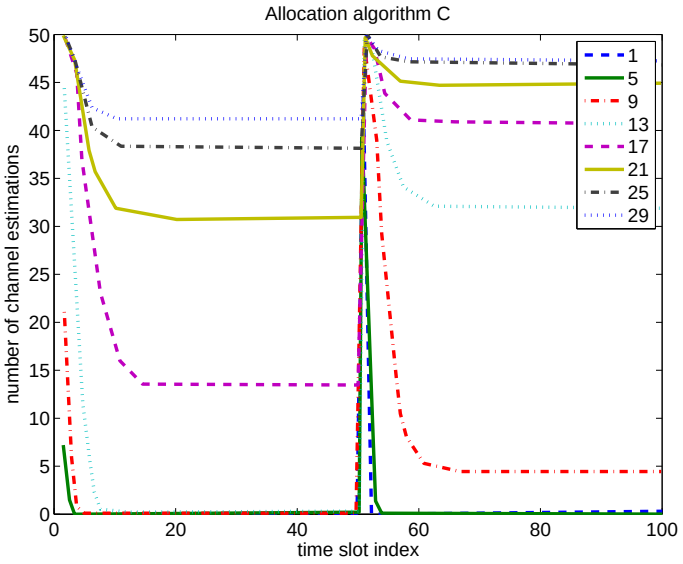

Figure 4.16: Average number of channel estimations per user for allocation algorithm C after a PU is detected on 20 channels in the 50th time slot. Each CR user pair transmits on 6 channels. Number of CR user pairs is labeled as: 1, 5, 9...29.

4.5 Dedicated Control Channel (DCC)

For a non-ideal MAC protocol, a CR user pair has to wait for a period of time, which is called as "delay time" in this thesis, when the control channel is busy. The delay time is assumed to be uniformly distributed between $t_{Delay} - t_{RTSCTS}$ and $t_{Delay} + t_{RTSCTS}$, where t_{Delay} is the average delay time and t_{RTSCTS} is the transmission of RTS and CTS packets. The dedicated control channel protocol is a simple MAC protocol which is easy to design and understand. One fixed channel is reserved to be the control channel. When a CR is idle, it listens to the control channel. In order to establish a connection, as well as to adjust transmission parameters, the following procedure is used: the transmitter tunes to the control channel and sends a RTS. If the corresponding receiver hears the RTS, it will send a CTS on the control channel, and then the two radios exchange the necessary control information (such as channels to be used) to start a new transmission. If the control channel is busy, the

transmitter delays its service request by a random number of time slots.

4.6 Performance Analysis: DCC

The average delay time t_{delay} with DCC, which is the time a CR user pair will wait when control channel is busy, is set to three different values: 200, 400 and 700 mini-time-slots. (1 time slot is equal to 1000 mini-time-slots.) It is assumed that it takes t_{RTSCTS}, which is taken to be 200 mini-time slots in this section, to exchange the CTS and a RTS packets.

In Figs. 4.17-4.19, the percentages of users reaching the target data rate for allocation algorithms A, B and C with DCC protocol are compared with that obtained when using an ideal MAC protocol, respectively. In Figs. 4.20-4.22, the average effective data rate of the three algorithms are compared. In Figs. 4.23 and 4.24, the average power consumption of the three algorithms are compared.

Let's first compare allocation algorithm B with algorithm C. It is shown in Figs. 4.18, 4.19, 4.21 and 4.22 that both the percentage of users reaching the target data rate and the average effective data rate of DCC is smaller than the ideal case for allocation algorithms B and C. Note that for the curves corresponding to DCC, allocation algorithm B has lower percentage of users reaching the target data rate and lower average effective data rate than algorithm C, but algorithm B consumes more power than algorithm C. In addition, in terms of average delay time t_{delay} for algorithm B and C, increasing average delay time t_{delay} slightly reduces the performance. The average delay time t_{delay} of 200 mini-time-slots performs the best among all three sets of delay time, as expected. Note in Figs. 4.23 and 4.24 that the power consumption of algorithms B and C with DCC is lower than ideal MAC since some users have stopped transmitting for a delay time when the control channel is busy.

Allocation algorithm A performs better when a DCC is considered when compared to the ideal case. This is directly related to the allocation strategy of algorithm A. Allocation algorithm A randomly chooses the new channels and its number of channel adaptations

does not converge to zero with some numbers of CR user pairs. When t_{delay} increases, there are fewer users in transmission who are sharing the same channels. Therefore, better performance is achieved when t_{delay} is equal to 700 mini-time-slots.

For algorithm C, when the number of CR user pairs increases, the interference level also increases, and the control channel has a heavier load. The power consumption in Fig. 4.24 is related to the effective data rate in Fig. 4.22. For example, when the network is noise-limited when the number of CR user pairs is less than 13, the power increases with increasing number of users entering the network. When the network is interference-limited, more users will stop transmission to wait for the control channel. Therefore, the average power consumption drops.

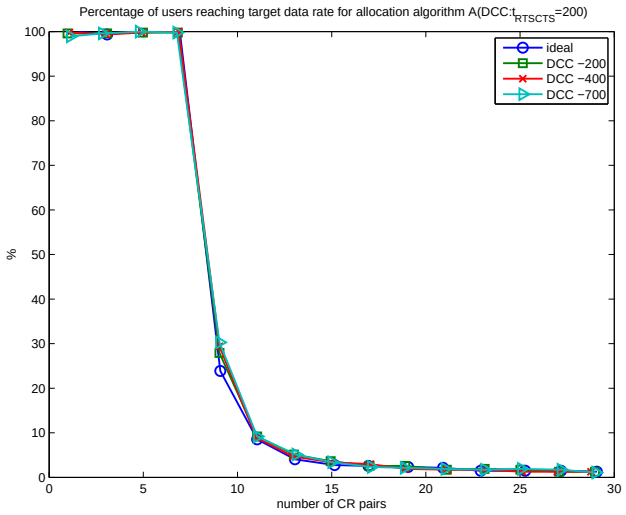

Figure 4.17: Comparison of the percentage of users reaching target data rate of allocation algorithms A of ideal MAC and DCC (t_{RTSCTS}=200 mini-time-slots) with 6 channels per user. Number of CR user pairs is labeled as 1, 3, 5...29. The user will stop transmitting in the current mode if it does not get access to the control channel. t_{delay} is 200, 400 and 700.

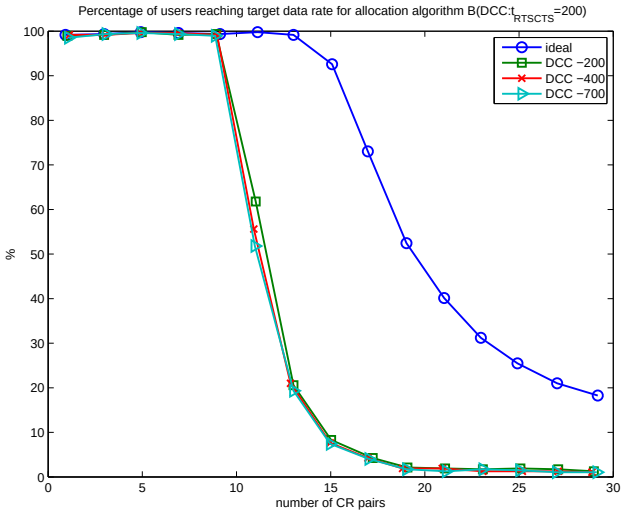

Figure 4.18: Comparison of the percentage of users reaching target data rate of allocation algorithms B of ideal MAC and DCC (t_{RTSCTS}=200 mini-time-slots) with 6 channels per user. Number of CR user pairs is labeled as 1, 3, 5...29. The user will stop transmitting in the current mode if it does not get access to the control channel. t_{delay} is 200, 400 and 700.

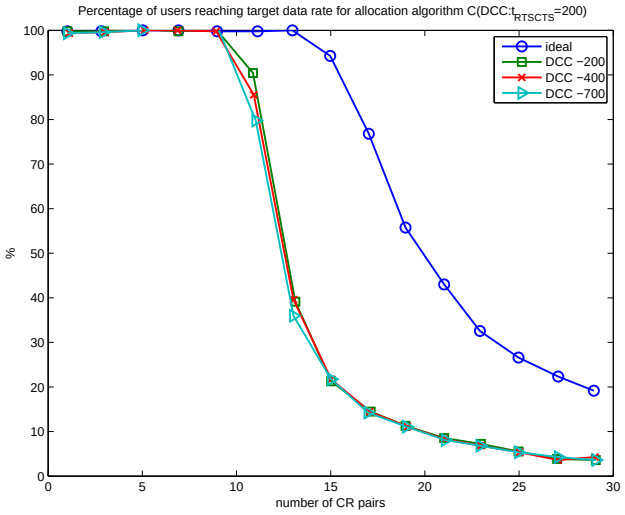

Figure 4.19: Comparison of the percentage of users reaching target data rate of allocation algorithms C of ideal MAC and DCC (t_{RTSCTS}=200 mini-time-slots) with 6 channels per user. Number of CR user pairs is labeled as 1, 3, 5...29. The user will stop transmitting in the current mode if it does not get access to the control channel. t_{delay} is 200, 400 and 700.

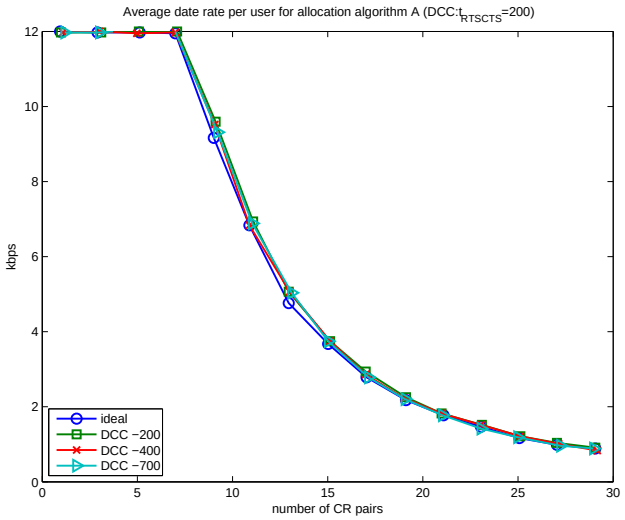

Figure 4.20: Comparison of the average data rate of users reaching target data rate of allocation algorithms A of ideal MAC and DCC (t_{RTSCTS}=200 mini-time-slots) with 6 channels per user. Number of CR user pairs is labeled as 1, 3, 5...29. The user will stop transmitting in the current mode if it does not get access to the control channel. t_{delay} is 200, 400 and 700.

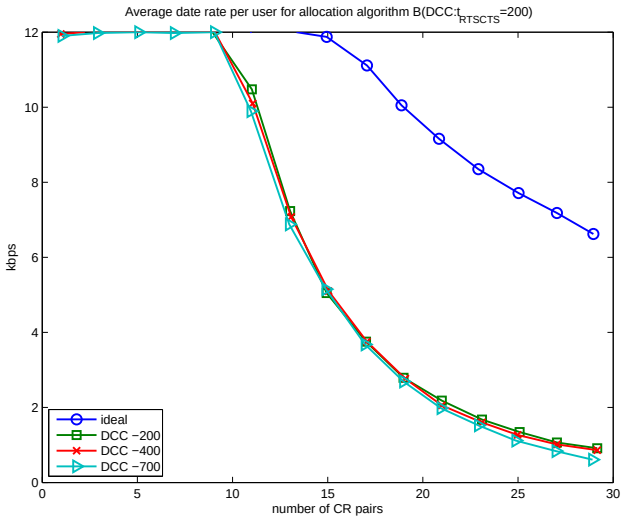

Figure 4.21: Comparison of the average data rate of users reaching target data rate of allocation algorithms B of ideal MAC and DCC (t_{RTSCTS}=200 mini-time-slots) with 6 channels per user. Number of CR user pairs is labeled as 1, 3, 5...29. The user will stop transmitting in the current mode if it does not get access to the control channel. t_{delay} is 200, 400 and 700.

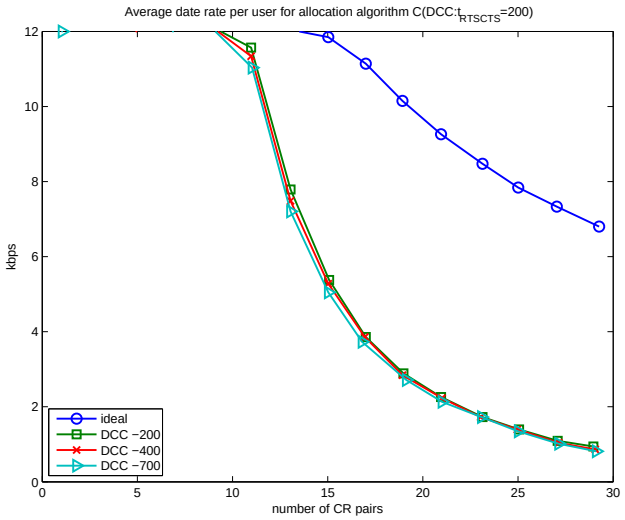

Figure 4.22: Comparison of the average data rate of users reaching target data rate of allocation algorithms C of ideal MAC and DCC (t_{RTSCTS}=200 mini-time-slots) with 6 channels per user. Number of CR user pairs is labeled as 1, 3, 5...29. The user will stop transmitting in the current mode if it does not get access to the control channel. t_{delay} is 200, 400 and 700.

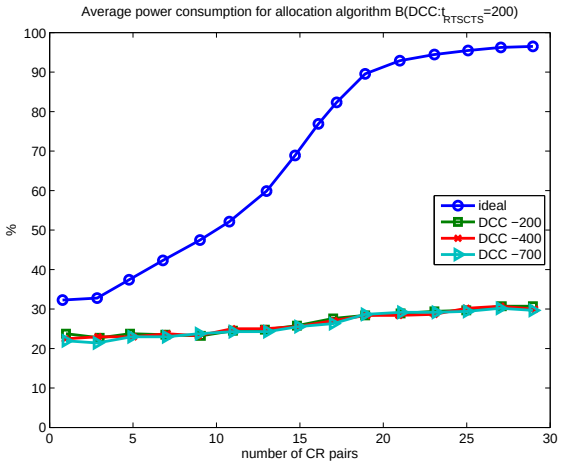

Figure 4.23: Comparison of the average power consumption of users reaching target data rate of allocation algorithms B of ideal MAC and DCC (t_{RTSCTS}=200 mini-time-slots) with 6 channels per user. The average transmission power is shown as a percentage of the maximum transmission power. Number of CR user pairs is labeled as 1, 3, 5...29. The user will stop transmitting in the current mode if it does not get access to the control channel. t_{delay} is 200, 400 and 700.

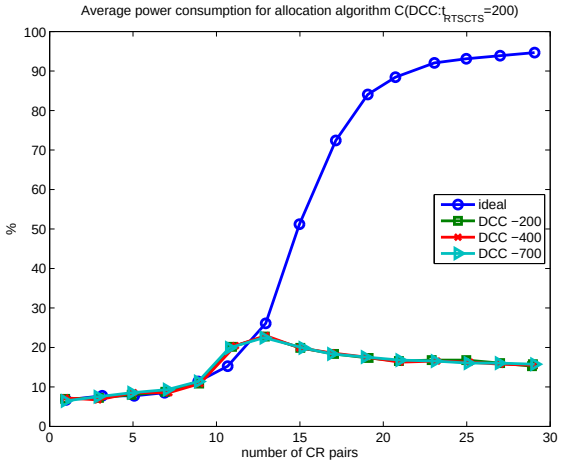

Figure 4.24: Comparison of the average power consumption of users reaching target data rate of allocation algorithms C of ideal MAC and DCC (t_{RTSCTS}=200 mini-time-slots) with 6 channels per user. The average transmission power is shown as a percentage of the maximum transmission power. Number of CR user pairs is labeled as 1, 3, 5...29. The user will stop transmitting in the current mode if it does not get access to the control channel. t_{delay} is 200, 400 and 700.

4.7 Conclusions

In this chapter, the value and cost of cognition of three resource allocation algorithms with different levels of channel knowledge in a CR-based ad hoc network was evaluated. Both an ideal MAC protocol and a non-ideal MAC protocol (DCC) were considered. The percentage of users reaching target data rate, effective data rate, power consumption, number of times that channel adaptations and estimations are performed, and convergence time were compared. Additionally, the convergence time of different resource allocation algorithms when channel adaptations are necessary was investigated.

From our simulation results and analysis, we conclude that

- A resource allocation algorithm with a higher level of *awareness* results in better performance gain and number of channel adaptations, but greater cost in terms of number

of channel estimations. A resource allocation algorithm with a higher level of channel knowledge converges quicker when channel adaptations are necessary. These conclusions are true for both ideal MAC protocol and non-ideal MAC protocol.

- In terms of the number of channel adaptations required to convergence when a PU is detected, it typically takes algorithm C less than half of the number of channel adaptations required by algorithm B.

- For all values of average delay time, allocation algorithm A performs better with DCC protocol, showing higher percentage of users reaching the target data rate, higher average effective data rate, and lower average power consumption. This behavior is a result of the fact that when the average delay time increases, there are fewer users in transmission who share the same channels. This makes the control channel less crowded and improves the overall system performance.

- For algorithms B and C, increasing the average delay time slightly reduces their performance, as expected.

Chapter 5

Concluding Remarks

This thesis addressed the effects of channel estimation and time synchronization errors on the performance of different network coding schemes and the value and cost of cognition of various resource allocation algorithms in CR-based ad hoc networks.

In the first part of this work, the effects of channel estimation and time synchronization errors on two network coding algorithms were analyzed. We proposed a network coding scheme based on a decode-and-forward relay with different numbers of users. The maximum-likelihood detector for different numbers of users was derived. We found that the gain provided by the considered network coding scheme is significant (1) for small number of users and (2) when the quality of the relay link is better than that of the direct link. In addition, the effects of imperfect channel estimation on the proposed scheme were examined. It was shown that potential performance improvement resulting from the proposed scheme could be negated by the effect of channel estimation errors. In addition, the effects of time synchronization errors on the BER performance of DNC and PNC systems with non-coherent FSK modulation was analyzed. The effects of received E_b/N_0 and unequal link quality were investigated. We found that the DNC and PNC schemes are very sensitive to timing errors in the link with worse quality.

In the second part of the work, we investigated the value and cost of cognition for three different resource allocation algorithms which have different levels of channel knowledge in a CR-based ad hoc network. Three resource allocation algorithms with different levels of channel knowledge were proposed, and the trade-off between performance gain and cost was given. For these three algorithms, the percentage of users reaching target data rate, effective data rate, power consumption, number of times that channel adaptations and estimations are performed, and convergence time were obtained and compared. Additionally, the convergence time of different resource allocation algorithms when channel adaptations are necessary (due to the appearance of a PU, for example) was investigated. Results showed that a resource allocation algorithm with a higher level of channel knowledge results in better performance gain, but greater cost in terms of number of channel estimations. Also, a resource allocation algorithm with a higher level of channel knowledge converges quicker when channel adaptations are necessary.

Bibliography

[1] R. Ahlswede, C. Ning, S.-Y. Li, and R. Yeung, "Network information flow," *IEEE Trans. Inf. Theory*, vol. 46, pp. 1204 –1216, Jul. 2000.

[2] S.-Y. Li, R. Yeung, and C. Ning, "Linear network coding," *IEEE Trans. Inf. Theory*, vol. 49, pp. 371–381, Feb. 2003.

[3] T. Ho, R. Koetter, M. Medard, D. R. Karger, and M. Effros, "The benefits of coding over routing in a randomized setting," in *IEEE Int. Symp. Inf. Theory*, p. 442, Jun.-Jul. 2003.

[4] R. Koetter and M. Medard, "Beyond routing: an algebraic approach to network coding," in *Proc. IEEE 21st Ann. Joint Conf. Computer Commun. Societies*, vol. 1, pp. 122–130, 2002.

[5] T. Ho, M. Medard, R. Koetter, D. Karger, M. Effros, J. Shi, and B. Leong, "A random linear network coding approach to multicast," *IEEE Trans. Inf. Theory*, vol. 52, pp. 4413 –4430, Oct. 2006.

[6] S. Zhang, S. C. Liew, and P. P. Lam, "Physical-layer network coding," in *ACM MobiComm*, pp. 358–365, 2006.

[7] S. Katti, S. Gollakota, and D. Katabi, "Embracing wireless interference: Analog network coding," in *ACM Sigcomm*, pp. 397–408, 2007.

[8] Q.-T. Vien, L.-N. Tran, and E.-K. Hong, "Network coding-based retransmission for relay aided multisource multicast networks," *EURASIP J. Wireless Commun. and Netw.*, 2011.

[9] S. Sharma, Y. Shi, J. Liu, Y. T. Hou, and S. Kompella, "Is network coding always good for cooperative communications?," *Proc. IEEE Int. Conf. Computer Commun.*, vol. vol., no., pp. 1–9, 2010.

[10] Y. Wu, P. A. Chou, and S. Y. Kung, "Information exchange in wireless networks with network coding and physical-layer broadcast," Tech. Rep. MSR-TR-2004-78, Microsoft Research, Redmond, 2004.

[11] S. Zhang, S. C. Liew, and H. Wang, "Synchronization analysis in physical layer network coding," *ArXiv e-prints*, vol. abs/1001.0069, 2010.

[12] D. Maduike, H. D. Pfister, and A. Sprintson, "Design and implementation of physical-layer network-coding protocols," in *43rd Asilomar Conf. Signals, Syst., and Comput.*, pp. 781 –787, Nov. 2009.

[13] L. Lu, S. C. Liew, and S. Zhang, "Optimal decoding algorithm for asynchronous physical-layer network coding," *ArXiv e-prints*, vol. abs/1105.0155, 2011.

[14] S. Haykin, "Cognitive radio: brain-empowered wireless communications," *IEEE J. Sel. Areas Commun.*, vol. 23, pp. 201–220, Feb. 2005.

[15] J. Mo, H.-S. So, and J. Walrand, "Comparison of multichannel MAC protocols," *IEEE Trans. Mobile Comput.*, vol. 7, pp. 50 –65, Jan. 2008.

[16] J. Kleinberg and E. Tardos, *Algorithm Design*. Boston: Pearson Education, 2005.

[17] J. Liu, D. Goeckel, and D. Towsley, "Bounds on the throughput gain of network coding in unicast and multicast wireless networks," *IEEE J. Sel. Areas Commun.*, vol. 27, pp. 582 –592, Jun. 2009.

[18] S. Zhang, S. C. Liew, and L. Lu, "Physical layer network coding schemes over finite and infinite fields," in *IEEE Clobal Telecomm. Conf.*, pp. 1–6, Nov. 2008.

[19] Y. H. amd D. Goeckel, Z. Ding, D. Towsley, and K. K. Leung, "Achievable rates for network coding on the exchange channel," in *IEEE Military Commun. Conf.*, pp. 1–7, Oct. 2007.

[20] H. Wang, X. Xia, and Q. Yin, "A linear analog network coding for asynchronous two-way relay networks," *IEEE Trans. Wireless Commun.*, vol. 9, pp. 3630 –3637, Dec. 2010.

[21] H. Gacanin and F. Adachi, "The performance of network coding at the physical layer with imperfect self-information removal," *EURASIP J. Wireless Commun. and Netw.*, 2010.

[22] K. Yasami and A. Abedi, "Effect of channel estimation error on performance of physical layer network coding," in *IEEE Consum. Commun. Netw. Conf.*, pp. 973 –974, Jan. 2011.

[23] J. H. Sorensen, R. Krigslund, P. Popovski, T. Akino, and T. Larsen, "Physical layer network coding for FSK systems," *IEEE Commun. Lett.*, vol. 13, pp. 597 –599, Aug. 2009.

[24] S. Moon and C. Ling, "A new noncoherent decoder for wireless network coding," *ArXiv e-prints*, vol. abs/1012.5956, 2010.

[25] M. C. Valenti, D. Torrieri, and T. Ferrett, "Noncoherent physical-layer network coding using binary CPFSK modulation," in *IEEE Military Commun. Conf.*, pp. 1 –7, Oct. 2009.

[26] T. Ferrett, M. C. Valenti, and D. Torrieri, "Receiver design for noncoherent digital network coding," in *IEEE Military Commun. Conf.*, pp. 2096 –2101, Nov. 2010.

[27] I. Mitola, J. and J. Maguire, G.Q., "Cognitive radio: making software radios more personal," *IEEE Pers. Commun.*, vol. 6, pp. 13 –18, Aug. 1999.

[28] B. Fette, *Cognitive Radio Technology*. New York: Newnes, 2006.

[29] Federal Communications Commission,, "Unlicensed operation in TV broadcast bands and additional spectrum for unlicensed devices below 900MHz and in the 3GHz band," tech. rep., Docket 10-174, Washington, DC, Sept. 2010.

[30] I. F. Akyildiz, W.-Y. Lee, M. C. Vuran, and S. Mohanty, "NeXt generation/dynamic spectrum access/cognitive radio wireless networks: A survey," *Comput. Netw.*, vol. 50, pp. 2127 – 2159, 2006.

[31] E. Yaacoub and Z. Dawy, "A survey on uplink resource allocation in OFDMA wireless networks," *IEEE Commun. Surveys Tutorials*, vol. PP, no. 99, pp. 1 –16, 2011.

[32] Q. Qi, L. B. Milstein, and D. R. Vaman, "Cognitive radio based multi-user resource allocation in mobile ad hoc networks using multi-carrier CDMA modulation," *IEEE J. Sel. Areas Commun.*, vol. 26, pp. 70 –82, Jan. 2008.

[33] G. J. Foschini and Z. Miljanic, "A simple distributed autonomous power control algorithm and its convergence," *IEEE Trans. Veh. Technol.*, vol. 42, pp. 641 –646, Nov. 1993.

[34] C. Zhong, C. Li, L. Yang, and Z. He, "Dynamic resource allocation for the downlink of multi-cell systems with full spectral reuse," *Int. Conf. Neural Networks and Signal Process*, pp. 173 –177, Jun. 2008.

[35] D. Grace, T. Tozer, and A. Burr, "Reducing call dropping in distributed dynamic channel assignment algorithms by incorporating power control in wireless ad hoc networks," *IEEE J. Sel. Areas Commun.*, vol. 18, pp. 2417 –2428, Nov. 2000.

[36] M. Hong, J. Kim, H. Kim, and Y. Shin, "An adaptive transmission scheme for cognitive radio systems based on interference temperature model," *5th IEEE Consumer Commun. and Netw. Conf.*, pp. 69 –73, Jan. 2008.

[37] S. Ahmad, J. Deaton, U. Shukla, R. Irwin, L. DaSilva, and A. MacKenzie, "A comparison of channel assignment techniques with power control in ad hoc networks," *Proc. 18th Int. Conf. Computer Commun. and Networks*, pp. 1 –6, Aug. 2009.

[38] F. Wang, M. Krunz, and S. Cui, "Price-based spectrum management in cognitive radio networks," *IEEE J. Sel. Topics Signal Process*, vol. 2, pp. 74 –87, Feb. 2008.

[39] C. Y. Wong, R. Cheng, K. Lataief, and R. Murch, "Multiuser OFDM with adaptive subcarrier, bit, and power allocation," *IEEE J. Sel. Areas Commun.*, vol. 17, pp. 1747 –1758, Oct. 1999.

[40] E. Yaacoub and Z. Dawy, "Achieving the nash bargaining solution in OFDMA uplink using distributed scheduling with limited feedback," *Int. J. of Electronics and Commun. AEUE (Elsevier)*, vol. 65, pp. 320–330, 2011.

[41] Y. Zhang and C. Leung, "A distributed algorithm for resource allocation in OFDM cognitive radio systems," *IEEE Trans. Veh. Technol.*, vol. 60, pp. 546 –554, Feb. 2011.

[42] Z. Shen, J. G. Andrews, and B. L. Evans, "Optimal power allocation in multiuser OFDM systems," *IEEE Global Commun. Conf.*, vol. 1, pp. 337 – 341, Dec. 2003.

[43] Z. Shen, J. G. Andrews, and B. L. Evans, "Adaptive resource allocation in multiuser OFDM systems with proportional rate constraints," *IEEE Trans. Wireless Commun.*, vol. 4, pp. 2726 – 2737, Nov. 2005.

[44] G. Munz, S. Pfletschinger, and J. Speidel, "An efficient waterfilling algorithm for multiple access OFDM," *IEEE Global Commun. Conf.*, vol. 1, pp. 681 – 685, Nov. 2002.

[45] D. Zhang, Y. Xu, and Y. Cai, "A high efficiency algorithm of power and bit allocation for OFDMA systems," *Int. Conf. Wireless Commun. Netw. and Mobile Comput.*, pp. 85 –88, Sep. 2007.

[46] W. Yu and J. M. Cioffi, "Constant-power waterfilling: Performance bound and low-complexity implementation," *IEEE Trans. Commun.*, vol. 54, pp. 23–28, Jan. 2006.

[47] R. G. Gallager, *Information Theory and Reliable Communication*. John Wiley & Sons, 1968.

[48] J. G. Proakis, *Digital Communications*. McGraw-Hill New York, 4 ed., 2001.

[49] H. Cheon and D. Hong, "Effect of channel estimation error in OFDM-based WLAN," *IEEE Commun. Lett.*, vol. 6, pp. 190 –192, May. 2002.

[50] R. You, H. Li, and Y. Bar-Ness, "Diversity combining with imperfect channel estimation," *IEEE Trans. Commun.*, vol. 53, pp. 1655 – 1662, Oct. 2005.

[51] S. Takaoka, H. Gacanin, and F. Adachi, "Impact of imperfect channel estimation on OFDM/TDM performance," in *IEEE 61st Veh. Technol. Conf.*, vol. 1, pp. 442–446, May. 2005.

[52] B. Gedik and M. Uysal, "Impact of imperfect channel estimation on the performance of amplify-and-forward relaying," *IEEE Trans. Wireless Commun.*, vol. 8, pp. 1468 –1479, Mar. 2009.

[53] T. S. Rapport, *Wireless Communications Principles and Practice*. Pearson Education, 2 ed., 2004.

[54] V. Srivastava, J. Neel, A. B. MacKenzie, R. Menon, L. A. DaSilva, J. E. Hicks, J. H. Reed, and R. P. Gilles, "Using game theory to analyze wireless ad hoc networks," *IEEE Commun. Surv. Tutorials*, vol. 7, pp. 46–56, Fourth Quarter 2005.

[55] J. Huang, R. Berry, and M. Honig, "Distributed interference compensation for wireless networks," *IEEE J. Sel. Areas Commun.*, vol. 24, pp. 1074 – 1084, may 2006.

[56] H. Mahmoud, T. Yucek, and H. Arslan, "OFDM for cognitive radio: merits and challenges," *IEEE Wireless Commun.*, vol. 16, pp. 6 –15, April 2009.

[57] T. Weiss and F. Jondral, "Spectrum pooling: an innovative strategy for the enhancement of spectrum efficiency," *IEEE Commun. Mag.*, vol. 42, pp. S8 – 14, Mar. 2004.

[58] S. Sadr, A. Anpalagan, and K. Raahemifar, "Radio resource allocation algorithms for the downlink of multiuser OFDM communication systems," *IEEE Commun. Surveys Tutorials*, vol. 11, pp. 92 –106, 2009.

[59] H. S. Dhillon, *Optimal Sum-rate of Multi-band MIMO Interference Channel*. PhD thesis, Virginia Polytechnic Institute and State University, 2010.